[FEFE]-HYDROGENASE SUBSTRATE TRANSPORT MECHANISMS AND INVESTIGATION OF ALGAL HYDROGEN METABOLISM

By

Adam Cornish

A DISSERTATION

Submitted to
Michigan State University
In partial fulfillment of the requirements
For the degree of

DOCTOR OF PHILOSOPHY

Biochemistry and Molecular Biology

2012

ABSTRACT

[FEFE]-HYDROGENASE SUBSTRATE TRANSPORT MECHANISMS AND INVESTIGATION OF ALGAL HYDROGEN METABOLISM

By

Adam Cornish

The global population has recently exceeded 7 billion people and the demand for energy continues to expand as the number of industrialized countries grows. Currently, the energy economy is dominated by the utilization of polluting and non-renewable fossil fuels. Both the collection and use of petroleum-based fuels is destructive to the environment and is not sustainable over a long time-scale, which justifies the investigation into the development of renewable, alternative fuels. Of the various fuels that have been proposed, molecular hydrogen (H_2) in particular holds great promise as a clean-burning fuel capable of supplementing the current energy economy, especially as the combustion of H_2 generates only water vapor as by-product. H_2 can be generated via a number of chemical processes, but current H_2 technologies either require fossil fuels as inputs or are energy-inefficient. The biological production of H_2, however, has garnered a great deal of interest because microorganisms are able to drive H_2 synthesis using energy derived from both light and dark fermentative metabolisms. This manner of production does not depend on mining non-renewable resources and microbes can be cultured at the industrial scale without competing with arable land needed for agriculture.

H_2 evolution in these microorganisms is dependent on nitrogenases and/or hydrogenases, enzymes which utilize unique metal centers for catalysis. Hydrogenases

have been of particular interest for industrial-scale H_2 production because these enzymes are found in a diverse array of organisms and require only protons and electrons as substrates. In particular, [FeFe]-hydrogenases have very high turnover numbers and catalysis can be coupled to photosynthesis. Unfortunately, these enzymes are inactivated by molecular oxygen (O_2), and a number of studies have therefore attempted to engineer O_2-tolerant hydrogenases. However, engineering enzymes to introduce optimal qualities has been impeded by an incomplete understanding of the overall reaction mechanism.

Substrate (protons, electrons, and H_2) transport is essential to hydrogenase activity, yet relatively little information is available regarding the intraprotein transport of substrate in [FeFe]-hydrogenase. I focused my investigation on identifying and testing pathways important for substrate transport between the enzyme surface and the active site in the *Clostridium pasteurianum* [FeFe]-hydrogenase. I have elucidated a key pathway for proton transport and confirmed that two iron-sulfur clusters are essential in an electron transfer relay, contributing to the overall characterization of [FeFe]-hydrogenase activity.

Green algae utilize [FeFe]-hydrogenases to catalyze H_2 production using reducing equivalents derived from photosynthesis and these enzymes are an integral component of anaerobic metabolism in these microalgae. I explored the H_2 production capabilities of a multicellular green alga, *Volvox carteri*, and characterized two hydrogenases likely responsible for this activity. In addition, a unique hydrogenase gene cluster discovered within the *Volvox carteri* genome provided interesting hints into the origin of [FeFe]-hydrogenase in green algae.

To my mother, father, and sister, for supporting me through
both the good and the bad times.

To Michael, for being my partner in life,
and for loving duckies.

ACKNOWLEDGEMENTS

First and foremost, I would like to thank my excellent mentor, Dr. Eric Hegg, for his guidance and encouragement throughout the course of my PhD studies. It has been his great ideas, his willingness to let me fail when I needed to, and his ability to set me back on the right path that I have arrived to this point in my career. Thank you, Eric.

I want to thank all past and current members of the hydrogenase team. Many thanks to Katrin for her enthusiasm and technical skills. Thanks to Saundra for helping me grow as mentor and for all of the coffee, and to Robin for being so passionate about science. Thanks to Travis, who is far more responsible for his scientific development than I am, and a big thank you to Adam T., for learning what a 1:1000 dilution is.

I also have to express my appreciation for the entire Hegg lab and their persistent ability to ignore what I say and understand what I mean. Emily, Hui, Vaidy and others, you've made this lab a great place to work.

I'd like to give a very special thank you to Dr. Changcheng Xu, who first encouraged me in the world of scientific research, and Dr. Christoph Benning, who continues to put out papers with my name on them.

Thank you to all of my science friends (Dorothy Tappenden, Chris Buehl, and Eric Carter) and my "real-life" friends (Kristi Tilford, Tiffany Leusby, and everyone at Animosity). You made my time outside of lab so much more sane.

I give sincere thanks to the members of my guidance committee: Drs.Robert Hausinger, Charles Hoogstraten, Gemma Reguera, and Shelagh Ferguson-Miller. Their advice and direction were integral to my success through my PhD.

Most of all, I want to thank the Department of Biochmemistry and Molecular Biology, as well as Michigan State University, for giving me the opportunity to study and grow in a fantastic learning environment.

TABLE OF CONTENTS

LIST OF TABLES

LIST OF FIGURES

LIST OF ABBREVIATIONS

AA	amino acid
BLAST	basic local alignment search tool
BSA	bovine serum albumin
BV	benzyl viologen
CD	circular dichroism
CpI	*Clostridium pasteurianum* [FeFe]-hydrogenase
DdH	*Desulfovibrio desulfuricans* [FeFe]-hydrogenase
Fe_d	distal iron of [FeFe]-hydrogenase H-cluster
DTMA	dithiomethylamine
DTME	dithiomethylether
E_a	activation energy
EDTA	ethylenediaminetetraacetic acid
EPR	electron paramagnetic resonance
ESEEM	electron spin echo envelope modulation
Hmd	H_2-forming methylene-H_4MPT dehydrogenases
H_{ox}	oxidized form of the [FeFe]-hydrogenase
H_{red}	reduced form of the [FeFe]-hydrogenase
HYSCORE	hyperfine sub-level correlation
k_{cat}	catalytic rate constant
kDa	kilodalton
K_i	inhibition constant

k_{obs}^{rel}	normalized rate of activity
LB	lysogeny broth
NCBI	National Center for Biotechnology Information
NTA	nitriloacetic acid
methenyl-H_4MPT$^+$	methenyltetrahydromethanopterin
methylene-H_4MPT	methylenetetrahydro-methanopterin
MV	methyl viologen
PCR	polymerase chain reaction
PETF	plastidic ferredoxin
PSI	photosystem I
PSII	photosystem II
QM/MM	quantum mechanical and molecular mechanics calculations
ROS	reactive oxygen species
RT-PCR	reverse transcription polymerase chain reaction
SAM	*S*-adenosyl methionine
SVM	standard *Volvox* medium
YNP	Yellowstone National Park

CHAPTER 1

Introduction

A Sustainable Fuel Economy

In June of 2012, the Arctic lost ~1 million square miles of ice (four times the area of Texas), which is the largest loss of ice in June in the satellite record (1). That month also marked the June with the highest globally-averaged land surface temperature on record (1.93 ˚F above the average), and these are only two of many climate-related records being broken in 2012 (2). A strong correlation can be deduced between the temperature reports, the disappearance of arctic ice mass, and the fact that the United States this year alone has released ~7 million metric tons of carbon dioxide (CO_2) into the atmosphere (3). Climate change is a reality and, recognizing that the rate of greenhouse gas emissions is increasing with each passing year (3), alternative energy options need to be investigated and pursued.

Currently, primary global fuel sources are petroleum-derived products (gasoline, diesel, jet fuel, etc), and the processes of extraction, preparation, and combustion of these products have negative impacts upon the global environment (4, 5). Even if fuels made from petroleum were environmentally safe to process and utilize, petroleum is still a finite resource—every gallon of gasoline burned is a gallon that has been converted into CO_2 and is contributes an additional burden onto the carbon cycle. Petroleum resources must be mined as current stores are consumed, and while isolating crude oil is a process that can reap large rewards (high yields of oil), it also comes at great risk (high yields of oil into the ocean), as exemplified by the Deepwater Horizon oil spill of 2010. Unfortunately, the economic costs of oil spills do not always directly affect the

price of gasoline at the pump, and this price is often misleading, because it does not take into account public health or environmental risks. If these hidden costs were included in the price of gas, the cost per gallon could be far greater than it is currently (6, 7, 8).

Natural gas, coal, and ethanol are a few of the available alternative energy carriers that supplement petroleum-based fuels (9, 10). Unfortunately, these fuels share similar problems with crude oil and petroleum, especially as natural gas and coal generate CO_2, a potent greenhouse gas, upon combustion. Natural gas and coal must still be mined and extracted from the earth, often through hydraulic fracking (natural gas) and mountaintop removal mining (coal), all of which cause intense geological stress, damaging the environment, and often contaminating groundwater (11, 12, 13). The production of ethanol has a less immediate impact upon the environment, but does compete with local agriculture, as the majority of ethanol produced is derived from staple crops such as potatoes, sugar cane, and corn (14). Although “cleaner” in some ways than petroleum, these fuels also struggle with environmental impacts and long-term sustainability.

Another alternative fuel is diatomic hydrogen (H_2), which has many ideal properties and has the potential to supplement currently existing transportation fuels. H_2 is the most abundant molecule in the solar system, has a high energy density per unit mass, and generates only water as a by-product of combustion (Reaction 1). Unfortunately, the light weight of H_2 allows it to escape Earth’s gravity, resulting in atmospheric concentrations of roughly only 1 ppm H_2, yet atomic hydrogen is extremely abundant on the planet’s surface in the form of hydrocarbons and water. Steam

reforming of either natural gas or coal is currently the most common method for collecting H_2 but requires extremely high temperatures, generates carbon monoxide (CO) as a by-product, and has the other aforementioned problems associated with natural gas (15). Several methods of direct electrolysis can be used to generate gaseous O_2 and H_2 from liquid water without the formation of hazardous by-products, but implementation of this technology is impeded by high costs and expensive material requirements (16, 17). Microorganisms also have the capability to generate H_2 without the use of fossil fuels and many of these organisms are able to couple the fermentation of sugars or energy derived from sunlight to H_2 synthesis (18, 19). Significantly, this biological production of H_2 does not require arable land, thus avoiding competition with modern agriculture (20) and providing rationale for the use of biological H_2 production.

$$H_2 + 1/2\ O_2 \rightarrow H_2O_{(g)} \qquad \text{(Reaction 1)}$$

Hydrogen in Biology

The role of H_2 in organismal metabolism must be understood before utilizing these microorganisms for large-scale H_2 production. Although H_2 exists at ~1 ppm, it is often an important component of the microbial lifecycle (21, 22). On early Earth, relatively high concentrations of H_2 were likely present and this small molecule could have played an integral part in many beginning biological functions (23). Today, H_2 serves an essential function in the metabolism of many microbes, acting as both an energy carrier and an endpoint of proton reduction, with recent evidence suggesting that

H_2 may also have a role in pathogen survival during infection (22, 24).

A variety of bacteria and cyanobacteria produce H_2 as an obligate by-product of nitrogen (N_2) fixation (21, 25, 26). Catalyzed by nitrogenase, the theoretical stoichiometry of the reaction involves consumption of 16 ATP molecules for every two molecules of ammonia and one molecule of H_2 produced (Reaction 2), but reactions utilizing more ATP or generating greater than stoichiometric amounts of H_2 have been reported. (27, 28, 29, 30). Due to the oxygen-sensitivity of nitrogenase, some filamentous cyanobacteria form heterocysts—microoxic differentiated cells—allowing for both nitrogen fixation and H_2 formation under aerobic conditions (21, 31).

$$N_2 + 8\ H^+ + 8\ e^- + 16\ ATP \rightarrow 2\ NH_3 + H_2 + 16\ ADP + 16\ P_i \qquad \text{(Reaction 2)}$$

Under anaerobiosis, H_2 formation can be coupled to sugar fermentation, to anoxygenic photosynthesis, or to the oxidation of metals (22, 32, 33). To sustain ATP and NADH production under microoxic conditions, microbes degrade organic molecules via anaerobic respiration, generating electrons which are usually funneled into the respiratory electron chain (34). Lacking the typical terminal electron acceptor (O_2), excess electrons derived during anaerobiosis can be channeled into proton reduction (Reaction 3) to generate H_2 (35). This process eliminates buildup of largely negative reduction potentials, effectively decreasing formation of damaging radical species.

$$2\ H^+ + 2\ e^- \rightarrow H_2 \qquad \text{(Reaction 3)}$$

Anaerobic protists and pathogenic fungi are also able to evolve H_2, coupling proton reduction to ATP synthesis utilizing mitochondria-like organelles called hydrogenosomes (36, 37, 38). Under anaerobiosis, these organelles produce H_2 during the conversion of pyruvate to CO_2 and acetyl-CoA, ultimately leading to ATP formation via succinyl coenzyme A synthetase (39). Hydrogenosome-containing organisms release H_2 and acetate as by-products, which can then be utilized by other microbes in the community.

H_2 molecules diffuse easily through cell membranes, representing a loss or gain of electrons as H_2 passes between microbes and carrying electrons with them. A number of organisms utilize H_2 uptake enzymes under anaerobiosis to gain electrons to drive anabolic processes. Cyanobacteria are able to take up H_2 to regain “wasted” electrons that were channeled into H_2-production during N_2 fixation, effectively recycling electrons for further ammonia production (40, 41). Bacteria and algae which evolve H_2 during fermentation often grow syntrophically with a variety of organisms (e.g., Knallgas bacteria) which are then able to take up exogenous H_2, utilizing the electrons from H_2 to power CO_2 fixation and basic anabolic metabolism (42, 43, 44).

H_2 uptake can also be important in the conversion of CO_2 to methane in methanogenic archaea, where the H_2 often acts as an integral component in multiple steps of the process. The decomposition of H_2 to protons is fundamental in driving a Na^+/H^+ antiporter, which then regenerates the Na^+ gradient essential to methyl-group transfer (45). Electrons derived from H_2 are used to reduce ferredoxin, and these electrons are then donated to generate the first compound in methane synthesis, formyl-methanofuran (46). Essential to intermediary steps, hydrides from H_2 are added

to both methenyltetrahydromethanopterin (methenyl-H_4MPT^+) and methylenetetrahydro-methanopterin (methylene-H_4MPT) (45, 47), further demonstrating the important role of H_2 in methanogen metabolism.

Pathogenic bacteria have been shown to utilize H_2 to increase survival during infection. To colonize the intestine, pathogens must first endure the low pH levels (pH 2-2.5) of acid in the stomach. Recently, *Escherichia coli* has been shown to deacidify highly acidic media via proton uptake and subsequent reduction to H_2, effectively increasing the local pH and enhancing acid resistance (48). H_2 metabolism may also be important in the response of pathogenic bacteria to oxidative stress, antibiotic treatments, and macrophage attack. Microbial and cellular H_2 production has been linked with resistance to oxidative stress induced by antibiotics and human immune cells (24, 49, 50), especially in regards to OH•, a highly cytotoxic ROS (51).

Industrial Hydrogen Production

Biological H_2 production has the potential to supplement and bolster current technologies using renewable and/or non-polluting raw materials. A broad range of microbes (e.g., green algae, cyanobacteria, sugar-reducing thermophilic bacteria) are able to couple anaerobic photosynthetic or fermentative processes to H_2 production (22). For industrial biological H_2 production, ideal microorganisms would need to be amenable to large-scale culturing using nutrient-rich waste water (52, 53). At the end of their lifecycles, H_2-producing organisms can be harvested for agricultural feedstocks or used in the manufacture of other biofuels, such as bioethanol or biodiesel (54, 55).

Finally, a biological system selected for industrial H_2 production needs to require few material inputs, utilize genetically tractable organisms, and be able to produce large quantities of H_2.

One popular approach for large-scale H_2 production involves supplying anaerobically-cultured bacteria with inexpensive fermentable carbon sources. A variety of sugars can be utilized to drive H_2 formation during fermentation, principally depending on the identity of the microbe (22, 56, 57). Glycerol is one candidate to feed into fermentative H_2-production, as this 3-carbon product is an obligate waste material generated during biodiesel refinement, which has increased the availability of glycerol and sharply decreased its price on the global market (58, 59). Another candidate is lignocellulosic biomass (e.g., corn stover), which is a popular substrate within the industrial agricultural complex, providing another source of sugars which could be used for fermentative biohydrogen production (60, 61), although bioethanol remains the principal focus of cellulosic biofuel research (62).

Another approach to biological H_2 production is the use of microalgae—organisms which utilize photosynthesis to either directly or indirectly drive H_2 synthesis. A standard method for this synthesis involves alternating between light and dark cycles, allowing these organisms to undergo oxygenic photosynthesis—fixing CO_2 and storing reducing equivalents as starch—followed by anaerobic respiration and concomitant production of H_2 (19, 63). Unfortunately, all H_2-synthesizing enzymes are extremely O_2-sensitive and require anaerobic conditions for maximal activity, which presents difficulties during oxygenic photosynthesis (35, 64). To circumvent this O_2 sensitivity, sulfur deprivation has been utilized in the green alga *Chlamydomonas reinhardtii*,

eliminating photosystem II activity and allowing non-oxygenic photosynthesis to drive H_2 production under microoxic conditions (65, 66).

Hydrogen-Forming Enzymes

As already discussed, organisms have developed a large toolset for the production of H_2 from metabolic, organic, and photosynthetic sources. Key enzymes in these reactions are nitrogenase and hydrogenase, enzymes which utilize unique organometallic active sites to catalyze the production of H_2 (19). A detailed understanding of the enzymes, metabolic processes, and organisms involved in generating molecular hydrogen is essential to build and sustain efficient biological H_2-synthesis technologies.

Nitrogenases are complex metalloenzymes which form H_2 as a catalytic by-product during N_2 fixation and, like all H_2-forming enzymes, nitrogenases are inactivated by O_2. There are three primary classes of nitrogenase based on the active site composition, but the molybdenum (Mo)-nitrogenase is the best characterized of these enzymes. The iron (Fe) protein of Mo-nitrogenase is a dimer that is bridged by a [4Fe4S] cluster, and each subunit contains one MgATP-binding site. The Mo-nitrogenase is composed of two Fe proteins and the tetrameric $\alpha_2\beta_2$ molybdenum iron (MoFe) protein, which contains two P-clusters ($[Fe_8S_7]$) and two FeMoco ($[MoFe_7S_9C]$) cofactors per nitrogenase (27, 28). Recent targeted substitution experiments have generated nitrogenase variants which still evolve H_2 but lack N_2-fixation activity, effectively separating these two processes from one another (67).

Hydrogenases are enzymes which catalyze both proton reduction and H_2 oxidation at an organometallic active site (22, 32, 68). Protons for this reaction are supplied by water, whereas the electrons needed for reduction are derived from fermentation or photosynthesis and are shuttled to the hydrogenase via a variety of physiological carriers (e.g., ferredoxin, NAD(P)H, cytochrome c_3) (22, 69, 70, 71, 72). As noted previously, these enzymes are rapidly inactivated by O_2 and are therefore primarily active in organisms during anaerobic metabolism (73, 74, 75). The catalytic turnover of H_2 in hydrogenase can be ~1000-fold greater than that of nitrogenase and, importantly, hydrogenases are ATP-independent and can be directly linked to photosynthesis, providing a rationale for using these enzymes in industrial-scale H_2 production (18). Like nitrogenases, hydrogenases are classified according to the metal composition of their respective active sites: [FeFe], [NiFe], and [Fe] (22, 76, 77, 78, 79).

[FeFe]-hydrogenases are bidirectional enzymes, although preferential H_2 evolution has been observed for some organisms *in vivo* (80). The [FeFe]-hydrogenase active site (H-cluster) is composed of a cysteine-coordinated [4Fe4S] cubane cluster connected by a proteinaceous thiolate ligand to a unique diiron sub-cluster ($[2Fe]_H$) (Figure 1.1A). This $[2Fe]_H$ is further ligated by two cyanide (CN^-) and three carbon monoxide (CO) molecules, as well as a non-proteinaceous dithiolate ligand, and proper assembly of the cluster requires three accessory proteins (76, 77). Encoded by the *hydA* gene, this class of enzyme is primarily encoded in the genomes of sulfate- or metal-reducing bacteria, hyperthermophilic bacteria, and parasitic anaerobes. Genes encoding hydrogenase are also found in eukaryotic genomes, such as green algae, anaerobic protozoans, and fungi (22, 81).

Figure 1.1. **Structures of the active sites found in the three different classes of hydrogenases.** A) Structural representation of the [FeFe]-hydrogenase active site, emphasizing the diiron cluster and associated ligands. The identity of X is proposed to be a nitrogen atom, although oxygen and carbon atoms remain possibilities. B) Structural representation of the [NiFe]-active site coordinated by four proteinaceous cysteine thiolates. C) Structural representation of the [Fe]-hydrogenase iron guanylyl pyridone cofactor; a water molecule is modeled in the "open" coordination site of the cofactor.

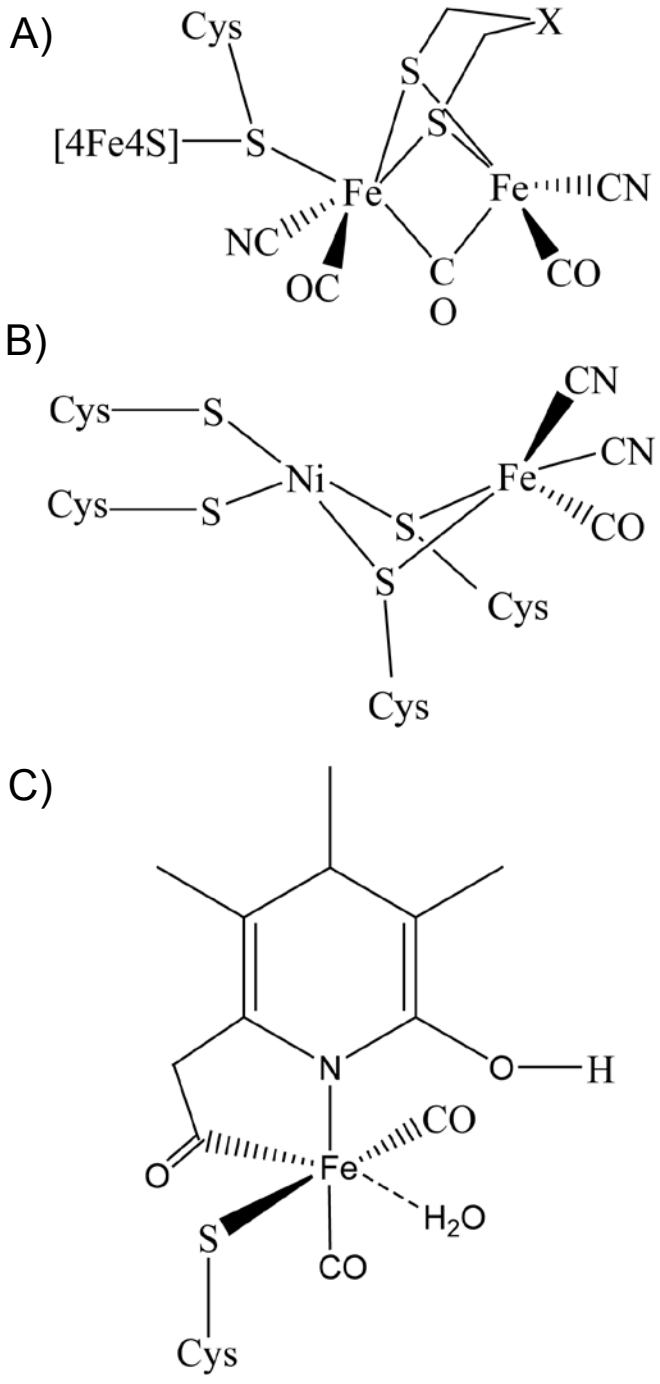

[NiFe]-hydrogenases compose the largest group of known H_2-reactive enzymes and contain the greatest diversity of enzymes, many of which participate in H_2 evolution, H_2 uptake, and/or regulatory functions. The [NiFe]-hydrogenase active site is best described as a nickel-iron center coordinated by four proteinaceous cysteine thiols, with one CO and two CN^- molecules ligating the iron atom (Figure 1.1B) (78, 82, 83). [NiFe]-hydrogenases are multimers, but the essential core structure is a heterodimer composed of a large catalytic subunit and a smaller subunit containing three iron-sulfur clusters involved in electron transfer to the active site (78, 84). [NiFe]-hydrogenases can be further classified into five distinct subclasses according to protein sequence: I) Membrane-localized H_2-uptake enzymes involved in oxidizing H_2 to feed electrons into anaerobic respiration, IIa) Soluble uptake enzymes which are often associated with H_2 recycling during nitrogen-fixation, IIb) H_2-sensing enzymes which regulate the gene expression of H_2-uptake enzymes, III) Cytoplasmic bidirectional enzymes which are NAD(P)H/$NAD(P)^+$-dependent, and IV) Membrane-bound H_2-evolving enzymes composed of six or more subunits (22). Examples of each of these subclasses can be found in a great variety of bacteria, whereas only subclasses IIa and III are utilized by cyanobacteria, and archaeal hydrogenases only fit within subclasses I, III, and IV (22). This great diversity of [NiFe]-hydrogenases is associated with increased complexity in maturation, requiring a minimum of seven assembly proteins for proper active site assembly and insertion (85).

[Fe]-hydrogenases are formally known as H_2-forming methylene-H_4MPT dehydrogenases (Hmd) and catalyze reversible hydride transfer onto methenyl-H_4MPT^+. In nature, these hydrogenases are utilized by methanogenic archaea to

catalyze a step in the conversion of CO_2 to methane, specifically the conversion of methenyl-H_4MPT^+ to methylene-H_4MPT (86). A three-dimensional crystal structure of Hmd reveals a single catalytic iron atom that is at the center of an iron guanylyl pyridone cofactor (FeGP cofactor). The iron atom is octahedral and is ligated by two CO molecules, the nitrogen and an acyl carbon of a pyridinol ring, a cysteinyl thiolate, and an "open" site (modeled with a water molecule) (Figure 1.1C) (79, 87). Two putative maturases may be important for Hmd active site assembly, but the assembly mechanism remains uncharacterized (88). Although of great interest for its role in CO_2 reduction to methane, Hmd is not an ideal catalyst for large-scale H_2 production, as the H_2 evolution activity would be dependent on methane oxidation (47, 86).

Phylogenetic analyses of the hydrogenase classes, in conjunction with active site composition and coordination environment, strongly suggest distinct evolutionary origins for all three enzymes (81). Additionally, the maturation machinery is specific to each class, requiring 3, 7-13, or 2 active-site assembly proteins for [FeFe]-, [NiFe-], and [Fe]-hydrogenase, respectively (22, 85, 88, 89). This finding lends further support to the hypothesis that these enzymes are the result of convergent evolution, explaining the existence of unique properties observed between the enzyme classes (81).

A great deal of research has focused on the [FeFe]- and [NiFe]-hydrogenases for large-scale production of H_2, as the only direct substrates for this reaction are protons and electrons. In comparison to [FeFe]-hydrogenase, a greater diversity of [NiFe]-hydrogenases has been discovered, including relatively O_2-insensitive enzymes like the [NiFeSe]-hydrogenase, which replaces an active site cysteinyl ligation with a selenium atom (90). Still, most of these [NiFe]-hydrogenases are not ideal for H_2 formation due to

a catalytic bias for H_2 oxidation over proton reduction under physiological conditions (19, 91). [NiFe]-hydrogenase active site assembly is also very complex and many of these hydrogenases are membrane-bound (22, 85). Conversely, [FeFe]-hydrogenases have some properties which are ideal for H_2 production. For instance, the maximal catalytic turnover of several characterized HydA proteins is 2-3 orders of magnitude greater than the highest-producing [NiFe]-hydrogenases (91, 92), and the maturation of [FeFe]-hydrogenase is comparatively simple (93). Additionally, [FeFe]-hydrogenases are soluble proteins that can be readily expressed, characterized, and used industrially without the concerns that accompany membrane-bound enzymes (94, 95, 96).

The [FeFe]-hydrogenase Active Site

The active sites of [FeFe]-hydrogenases from *Clostridium pasteurianum* (CpI) and *Desulfovibrio desulfuricans* (DdH) are remarkably similar when observed by x-ray crystallography, but differ in coordination of the distal iron (Fe_d) (76, 77). The Fe_d is proposed to be the site of proton reduction as the H-cluster cycles between oxidized and reduced forms (H_{ox} and H_{red}) (97, 98). In the CpI structure (presumed H_{ox} state), Fe_d is in an octahedral coordination environment with two carbon monoxide ligands (terminal and bridging), a terminal cyanide ligand, a terminally-bound water molecule, and two thiolate sulfurs from the dithiolate ligand (76). The DdH structure (H_{red} state) lacks the terminally-bound water molecule observed in the CpI Fe_d (octahedral geometry), leaving open an a coordination site where H_2 is proposed to bind (77, 99). Due to limitations in x-ray crystallography, the identity of the bridging dithiolate ligand

was initially proposed to be propanedithiolate, but subsequent electron paramagnetic resonance (EPR) experiments and density functional theory calculations indicate that dithiomethylamine (DTMA) or dithiomethylether (DTME) are more likely (100, 101, 102). Utilizing either a bridging nitrogen or oxygen atom (DTMA and DTME, respectively), this dithiolate ligand could be involved in proton transfer to the distal iron site (102, 103), as proposed by quantum mechanical and molecular mechanics (QM/MM) simulations (104, 105). These observations indicate that the unique [FeFe]-hydrogenase active site is ideally poised to participate in the reversible reduction of protons to H_2.

The $[2Fe]_H$ of the H-cluster is an organometallic complex that does not form spontaneously and requires assembly before insertion into the apo-enzyme (89). A suite of maturation proteins (HydE, HydF, and HydG) are essential in the synthesis of $[2Fe]_H$, although the mechanism of this assembly and insertion remains to be fully elucidated (Figure 1.2). Homologous to GTPases, HydF both hydrolyzes GTP and acts as a scaffold for $[2Fe]_H$ biosynthesis, although this activity is not dependent on GTP-hydrolysis (106, 107). HydG, a radical *S*-adenosyl methionine (SAM) enzyme, catalyzes the conversion of L-tyrosine to CO and CN^- ligands for attachment to the diiron cluster (108, 109, 110). Similar to HydG, HydE also has radical SAM enzyme activity and, although the role of this enzyme in $[2Fe]_H$ assembly remains to be elucidated, HydE is hypothesized to be involved in synthesis of the bridging dithiolate ligand (111, 112). A recently solved crystal structure reveals a surface-exposed channel for insertion of $[2Fe]_H$ and shows that the active site [4Fe4S] cluster is present before insertion (93, 106, 112). [FeFe]-hydrogenase activity is dependent on proper insertion and assembly of the $[2Fe]_H$, as no appreciable activity is observed without a complete H-cluster (113,

114).

Figure 1.2. **Proposed mechanism for H-cluster assembly by the maturation proteins HydE, HydF, and HydG.** The HydF protein is proposed to act as a scaffold, ligating a [2Fe2S] cluster which will form the core of the $[2Fe]_H$. HydE is proposed to synthesize and attach the dithiolate ligand, while HydG has been shown to catalyze the synthesis of the CO and CN^- ligands. Both HydE and HydG can associate with HydF and attach the ligands to $[2Fe]_H$ in any order, although only one assembly factor binds to HydF at a time. Once the H-cluster is fully synthesized, the active site can be transferred to the apo-hydrogenase by HydF.

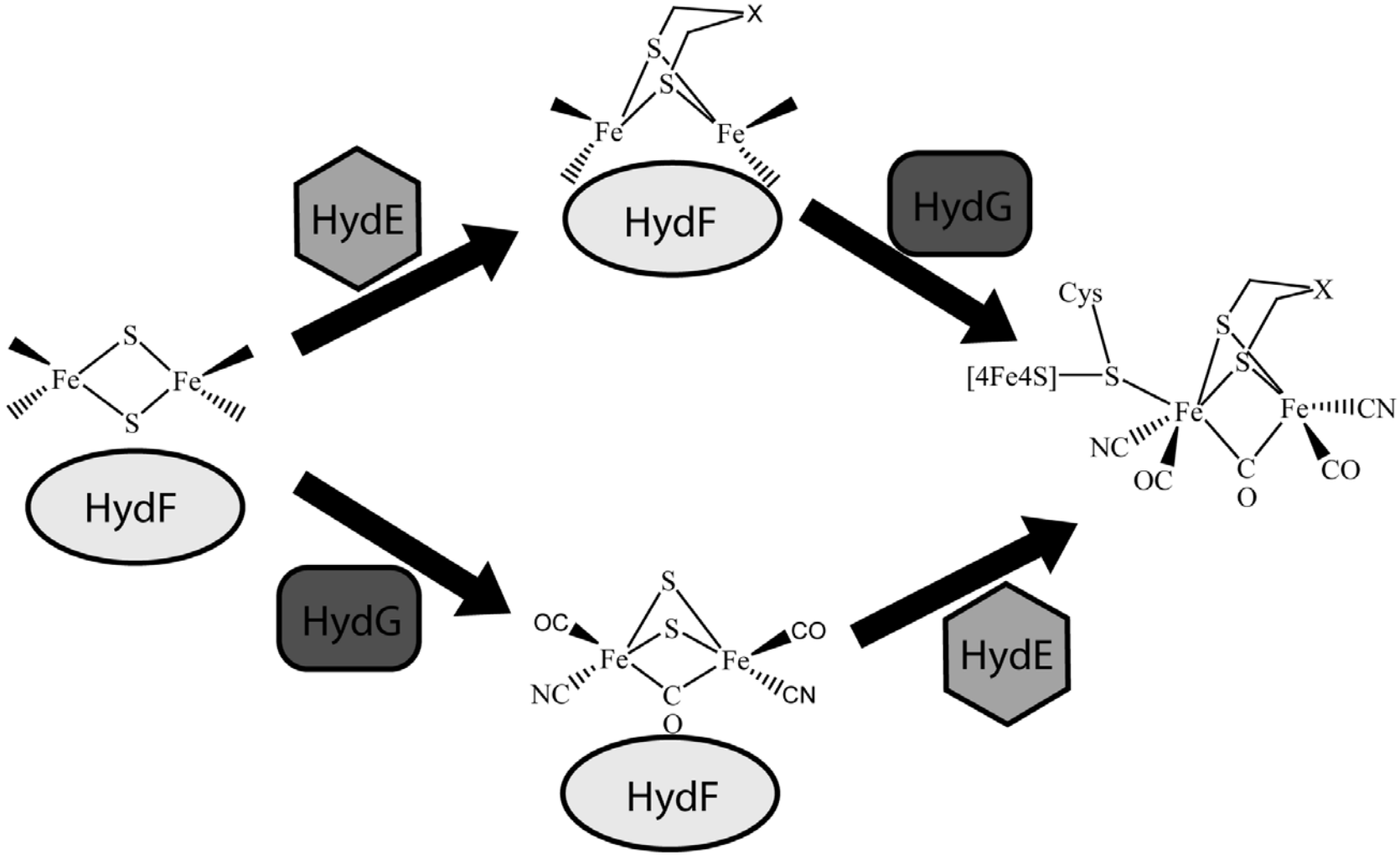

The H-cluster of HydA is irreversibly inactivated in the presence of O_2, effectively eliminating hydrogenase activity under aerobiosis, although some reports indicate O_2-insensitivity when in the H_{ox} state, possibly due to full-occupancy of the distal iron coordination sphere (115, 116). The primary hypothesis for this inactivation is attachment of O_2 to the distal iron, leading to the formation of ROS, which then can directly attack the cubane cluster, culminating in complete degradation of the active site (64, 73, 117). DFT calculations have modeled several gas channels within HydA for H_2 and O_2 diffusion, which could be targets for engineering to decrease O_2-based inactivation (118, 119). Supporting this rationale, previous investigation of a [NiFe]-hydrogenase indicate that narrow gas channels may contribute to O_2-insensitivity, while still allowing for diffusion of the much smaller H_2 molecule (120). Unfortunately, subsequent mutagenesis studies have not succeeded in significantly improving insensitivity to O_2 for either [NiFe]- or [FeFe]-hydrogenases (75).

In addition to O_2-inactivation, [FeFe]-hydrogenase can be reversibly inhibited by several other small molecules, providing more methods to probe the mechanisms of hydrogenase activity. A potent inhibitor of H_2 uptake activity, CO tightly binds to the distal iron of the H-cluster, occluding both H_2- and O_2-binding and rendering CO-bound HydA insensitive to O_2-based inactivation (64, 121, 122). CO is often used to model O_2 diffusion in the enzyme, as it is a small diatomic molecule that can be labeled (123). In contrast to CO, formaldehyde specifically inhibits H_2 evolution activity more strongly than H_2 uptake activity and is thought to bind the partially reduced H-cluster at either the distal iron or dithiolate bridge, preventing proton-transfer (124, 125). In addition to diatomic gaseous molecules, divalent metal cations (e.g., Cd^{2+} ,Cd^{2+}, Hg^{2+}, Zn^{2+})

have also been reported to impair hydrogenase activity (126, 127). Sequestered ~20 Å within the enzyme, the active site metal atoms are unlikely to be exchanged with these cations, and, while early reports suggested that this inhibition was specific to electron transfer (126).

Substrate Transport

[FeFe]-hydrogenase activity is dependent on both the intermolecular and intramolecular transport of protons, electrons, and H_2. While transport of these substrates is essential to enzymatic activity, the majority of [FeFe]-hydrogenase research has focused on either optimizing catalytic turnover or understanding and decreasing O_2-based inactivation (118, 128, 129, 130). Research focused on engineering improved hydrogenases is of great importance, but this work has been hindered by an incomplete understanding of substrate transport mechanisms within the enzyme.

When the first two crystal structures of [FeFe]-hydrogenases were solved, two potential proton transfer pathways were hypothesized based on amino acid sequence conservation, hydrogen-bonding capabilities, and relative distances within the structure (131). Intramolecular protein transfer is typically achieved via hydrogen-bonding networks between protonatable amino acid side-chains and water residues (132, 133). Recently, QM/MM studies on the CpI and DdH hydrogenases provided computational evidence that residues of a putative proton pathway (Figure 1.3) could accept protons from solvent and may form a hydrogen-bonding network extending from the enzyme

surface to the active site (104). To determine the absolute role of these residues in proton transfer, however, direct experimental evidence is required.

Figure 1.3. **Putative proton transport pathway.** A theorized proton transfer relay composed of four conserved amino acids and a modeled water molecule that connect the enzyme surface to the H-cluster. For interpretation of the references to color in this and all other figures, the reader is referred to the electronic version of this dissertation.

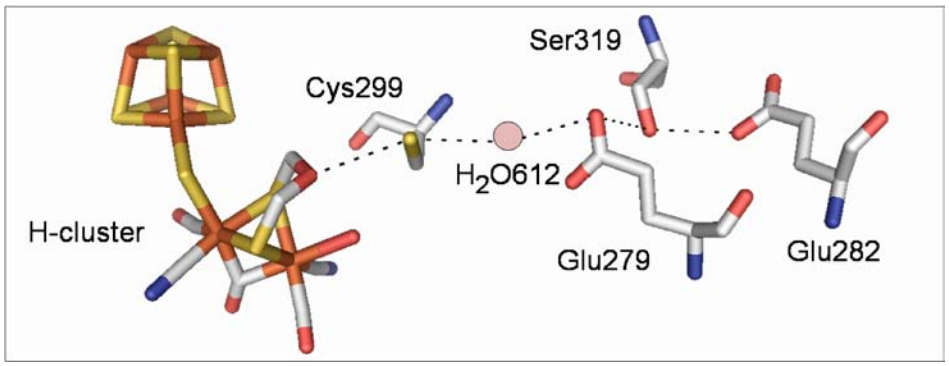

Intermolecular transport of electrons to/from [FeFe]-hydrogenase is accomplished through interactions with physiological electron carriers, and these interactions are dependent on the nature of the hydrogenase. [FeFe]-hydrogenases can differ in the number of both subunits and iron-sulfur cluster-binding domains, as described in detail by Meyer (81). Sulfate- and metal-reducing bacteria donate electrons from cytochrome c_3 to dimeric hydrogenases to mediate formation of a chemiosmotic gradient in the periplasm (134, 135, 136). The *Acetobacterium woodii* bifurcating tetrameric hydrogenase couples H_2 oxidation to the reduction of NADH and ferredoxin in a 1:1 ratio (overcoming the endergonic H_2-based ferredoxin reduction) and effectively feeding energy into CO_2-fixation (72). In green algae, photosynthetically-derived electrons are transferred to the monomeric hydrogenase from a plastidic ferredoxin (PETF), directly linking photosynthesis to H_2 production (71). The interactions between hydrogenase and PETF have been investigated computationally, and the results suggest that the association is mediated largely by electrostatic interactions (137). Similar to algal hydrogenases, monomeric bacterial hydrogenases also accept electrons from ferredoxin to drive H_2 production during dark fermentation (138). The interplay between physiological electron donors and H_2-reactive enzymes appears to be dependent on the structural organization of the hydrogenase, and may imply a positive correlation between subunit composition, number of iron-sulfur clusters, and reactivity with electron carriers.

Intramolecular electron transfer in [FeFe]-hydrogenases is presumed to be accomplished via electron transfer relays composed of iron-sulfur clusters and the relay present in M3 HydA architecture is the most prevalent among sequenced

hydrogenases. The basic M3 architecture is hypothesized to constitute a functional electron transfer relay (76) and is composed of four iron-sulfur cluster-binding domains (F-domains) that are observed in ~75% of sequenced [FeFe]-hydrogenases. A [2Fe2S] cluster and two [4Fe4S] clusters are ligated by a typical four cysteine thiolate-coordination in three F-domains (designated FS2, FS4A, and FS4B, respectively). The fourth domain (FS4C) uses a histidine and triple cysteine linkage to coordinate a third cubane cluster, which is similar to the distal iron-sulfur cluster in the [NiFe]-hydrogenase electron transfer relay (139). Intriguingly, the proposed electron transfer relay in the *C. pasteurianum* enzyme branches past FS4B, potentially terminating at either the FS4C or the FS2 cluster (Figure 1.4). Earlier reports have hypothesized that these two clusters could serve to modulate the reduction potential of the enzyme for interaction with electron carriers, provide specific binding-sites for electron donors, or act as different electrons “routes” for proton reduction and H_2 oxidation (131). Due to the prevalence of this putative relay in [FeFe]-hydrogenases, the characterization of its role in hydrogenase activity is essential to understanding the complete catalytic mechanism.

Molecular H_2 transfer to and from the H-cluster is a passive action and does not require direct mediators. Molecular dynamics studies have modeled H_2 diffusion within the enzyme and have indicated multiple potential routes which often overlap with putative O_2 diffusion pathways (140). A single permanent H_2 channel is unlikely to exist, as transient cavities are formed on the nanosecond timescale while the protein undergoes dynamic motion, allowing H_2 molecules to diffuse through the enzyme (119). Recently, mutagenesis studies were utilized to investigate putative channels in the enzyme, but no definitive routes of H_2 diffusion were confirmed (141).

Figure 1.4. **Electron transfer relay of the *C. pasteurianum* [FeFe]-hydrogenase.** The electron transfer pathway is composed of three [4Fe4S] clusters and a [2Fe2S] cluster.

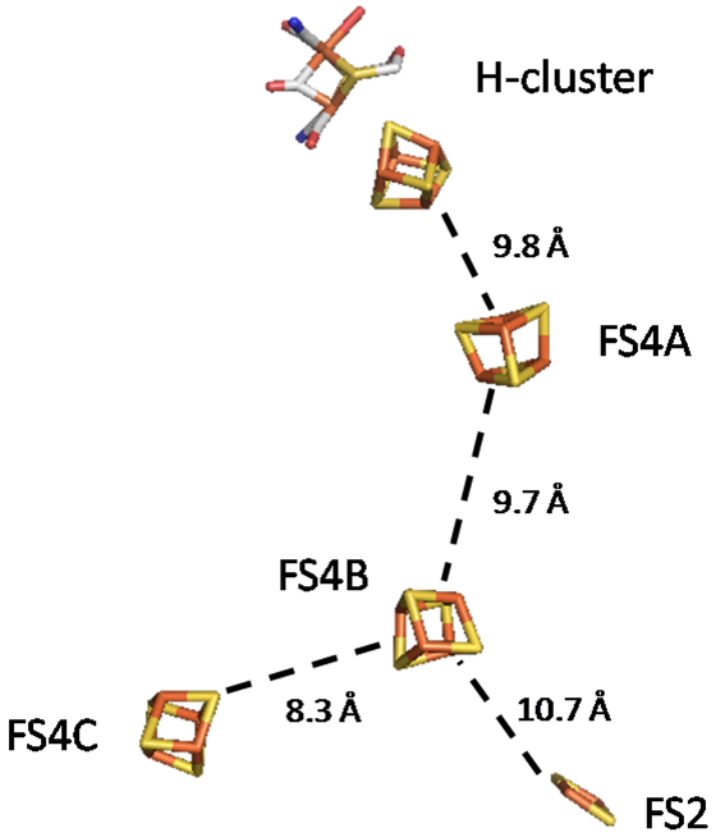

Recent investigations have targeted individual [FeFe]-hydrogenase amino acid residues via substitution to identify roles in O_2 sensitivity, but have had limited success. In particular, Lautier et al. (118) substituted residues within putative gas channels to occlude O_2 from the active site. These substitutions either had no effect on oxygen-sensitivity or sharply impaired hydrogenase activity. Although intriguing, these results are inconclusive in regards to hydrogenase activity without a greater understanding of substrate transport, especially as both studies substituted key residues previously implicated in proton transfer. The elucidation of the proton and electron transport mechanisms is essential in building a comprehensive model for hydrogenase activity, which can then be used for future enzyme engineering and optimization.

[FeFe]-hydrogenase Gene Evolution and Horizontal Gene Transfer

[FeFe]-hydrogenase genes are observed in a broad range of bacteria, green algae, protists, and fungi (22, 81). Prokaryotic in origin, genes encoding the catalytic hydrogenase and assembly proteins (*hyd* genes) are hypothesized to have been acquired by eukaryotes via horizontal gene transfer (35, 81, 95, 142, 143). As gene acquisition via multiple specific gene transfer events into a single genome is improbable, the suite of hydrogenase and maturase genes in eukaryotes was likely acquired as an operon or operon-like cluster from a prokaryotic ancestor. Multiple *hyd* gene clusters can be observed in the genomes of modern-day bacteria (81), providing further evidence for this hypothesis.

Among eukaryotes with known [FeFe]-hydrogenases, green algae contain HYD

proteins with the greatest deviation in protein structure from bacterial homologs. First observed in the *C. reinhardtii* genome, the *hydE* and *hydF* genes (bacterial nomenclature) are absent and are replaced by a fusion gene, *HYDEF* (algal nomenclature) (143). Heterologous expression studies indicate that HYDEF synthesized in a bacterial system is suboptimal for hydrogenase maturation (144), whereas *C. reinhardtii* HYDA can be fully activated using the bacterial HydE, HydF, and HydG suite of proteins (145, 146). This may suggest that, although the mechanism of $[2Fe]_H$ assembly and insertion could differ subtly between organisms, there is probably little discrimination at the level of [FeFe]-hydrogenase identity in relation to maturation.

Most known green algal HYDA proteins lack the F-domains which ligate iron-sulfur clusters proposed to participate in intramolecular electron transfer (147, 148). The physiological significance of this truncation is unknown, although green algal hydrogenase catalytic turnover is among the highest recorded (149). In addition, HYDA is localized to the chloroplast in green algae and accepts electrons from PETF, a ferredoxin associated with photosynthesis (71), suggesting that hydrogenases lacking the N-terminal F-clusters may be optimally poised for accepting photosynthetically-derived electrons. Among green algae studied for hydrogenase activity, only the *Chlorella variabilis* HYDA proteins contain F-domains (150), which may indicate either recent acquisition of the genes or minimal gene restructuring. This question can be further explored once the *C. variabilis* genome has been sequenced, as the presence of the *HYDEF* fusion gene and/or clustering of hyd genes within the genome could indicate evolutionary relationships.

Within most green algae studied for H_2 metabolism at the protein level, two

separate [FeFe]-hydrogenases are present, HYDA1 and HYDA2 (151). A recent report provides evidence of gene duplication, which could explain the presence of these two highly homologous genes (150), although single acquisition of two hydrogenase genes from a gene cluster is still possible. Intriguingly, a unique amino acid domain is conserved among most green algal HYDA sequences, but is absent in *C. variabilis* HYDA sequences, further emphasizing the disparity between these proteins and other green algal hydrogenases.

[FeFe]-hydrogenases have high amino acid sequence homology to nuclear prelamin A recognition factor (NARF) proteins, which are essential for cytoplasmic iron-sulfur cluster biosynthesis (in contrast to mitochondrial synthesis) (36, 152, 153). Known as IOP1/NARFL/NARF in *Homo sapiens* and *Arabidopsis thaliana* and Nar1p in *Saccharomyces cerevisiae*, no functional homologs have been observed in prokaryotic systems (152). Phylogenetic analysis of NARF proteins and [FeFe]-hydrogenases indicates a strong evolutionary relationship between these two enzymes, although NARF lacks a catalytic H-cluster and has not been reported to demonstrate H_2-production or -uptake activity (152). Based on sequence similarity, NARF essentially mimics the catalytic domain of HydA and utilizes four cysteine residues to ligate a [4Fe4S] cluster that is analogous to the cubane of the H-cluster. A second [4Fe4S] cluster is ligated by a FS4A-like domain, and both of these clusters in NARF have been shown to be essential for protein function and cellular viability (154). Although several HydA-specific motifs are altered in NARF, the extent of amino acid substitution is not constant between species, providing further evidence that these proteins evolved from a common HydA ancestor. As a gene that is divergent from *hydA*, *NARF* is an excellent

outgroup during evolutionary analysis of hydrogenase genes and can be used as a root in phylogenetic trees.

The origin of NARF proteins has been hypothesized to be linked to the evolution of hydrogenosomes—organelles that couple H_2 production to ATP synthesis (36). Recent comparison of hydrogenosomal and mitochondrial DNAs suggests that these organelles are the product of a single endosymbiotic event, with rapid differentiation occurring before the roles of the respective organelles were fully established (38, 153). A unifying metabolic process between hydrogenosomes and mitochondria is the organellar synthesis of iron-sulfur clusters (38, 155, 156). An especially interesting feature observed in hydrogenosome-containing organisms is that, while *hydA* genes are present, no NARF proteins are encoded within either the nuclear or the hydrogenosomal genomes. These observations may indicate that the original endosymbiont—hypothesized to be an α-proteobacteria (37)—contained a *hydA* gene, which either changed in function during the organellar transition to a mitochondrion or retained H_2-evolving functionality within the hydrogenosome (91).

Thesis Goals

As the availability of fossil fuels diminishes and demand for energy continues to rise, an alternative to unsustainable 20^{th} century energy technologies is required. The biological production of H_2 holds great promise as a source of renewable and clean fuel. Industrial-scale levels of H_2 are needed to supplement both petroleum-based and alternative fuels in the global economy, and many important questions remain regarding

H_2-catalyzing enzymes and the organisms which utilize these proteins.

[FeFe]-hydrogenases have tremendous potential to contribute to the large-scale synthesis of H_2. A vital component of the enzymatic activity is intramolecular substrate transport, yet a detailed mechanism of this transport remains to be described. To elucidate and confirm pathways essential for proton (Chapter 2) and electron transport (Chapter 3) within the *C. pasteurianum* [FeFe]-hydrogenase, I have generated amino-acid substituted variant enzymes and provided strong evidence for the roles of individual residues in substrate transport activities.

Green algae are intriguing photosynthetic organisms which have the potential to be utilized for industrial-scale biofuel production, especially in the generation of biohydrogen. The multicellular green alga *Volvox carteri*, a close relative of *C. reinhardtii*, has been intensely studied at the level of cell differentiation and sexual/asexual reproduction, yet there remains a knowledge gap regarding anaerobic metabolism in *V. carteri*. To provide insight into this metabolism (Chapter 4), I have investigated H_2-evolution activity in the organism, characterized the enzymes responsible for this activity, and identified a unique gene cluster that may provide hints into the evolutionary origins of hydrogenase within modern-day green algae.

REFERENCES

REFERENCES

1. 2012, posting date. NOAA National Climatic Data Center, State of the Climate: Global Snow & Ice for June 2012. [Online.]

2. 2012, posting date. NOAA National Climatic Data Center, State of the Climate: Global Analysis for June 2012. [Online.]

3. 2012. Inventory of U.S. Greenhouse gas emissions and sinks: 1990 – 2010. U.S. Environmental Protection Agency.

4. Hansen J., Sato M. (2004). Greenhouse gas growth rates. *Proc Natl Acad Sci U S A* 101(46), 16109-16114.

5. Al-Majed A. A., Adebayo A. R., Hossain M. E. (2012). A sustainable approach to controlling oil spills. *J Environ Manage* 113C, 213-227.

6. Parry I. W. H., Strand J. 2010. International Fuel Tax Assessment: An Application to Chile. Resources for the Future.

7. Parry I. W. H. 2005. The Uneasy Case for Higher Gasoline Taxes. Miliken Intitute Review.

8. Cobb C. (1999). The Roads Aren't Free, vol. 42. M.E. Sharpe, Inc.

9. Dresselhaus M. S., Thomas I. L. (2001). Alternative energy technologies. *Nature* 414(6861), 332-337.

10. Gray K. A., Zhao L., Emptage M. (2006). Bioethanol. *Curr. Opin. Chem. Biol.* 10(2), 141-146.

11. Corapcioglu M. Y., Baehr A. L. (1987). A compositional multiphase model for groundwater contamination by petroleum products: 1. Theoretical considerations. *Water Resour. Res.* 23(1), 191-200.

12. Gagne F., Andre C., Douville M., Talbot A., Parrott J., McMaster M., Hewitt M. (2011). An examination of the toxic properties of water extracts in the vicinity of an oil sand extraction site. *J. Environ. Monit.* 13(11), 3075-3086.

13. Merem E., Robinson B., Wesley J. M., Yerramilli S., Twumasi Y. A. (2010). Using GIS in ecological management: green assessment of the impacts of petroleum activities in the state of Texas. *Int. J. Environ. Res. Public Health* 7(5), 2101-2130.

14. Gerbens-Leenes W., Hoekstra A. Y., van der Meer T. H. (2009). The water footprint of

bioenergy. *Proc. Natl. Acad. Sci. U.S.A.* 106(25), 10219-10223.

15. Wagner E. S., Froment G. F. (1992). Steam reforming analyzed. *Hydrocarb. Process.* 71(7), 69-77.

16. Zhang H., Lin G., Chen J. (2010). Evaluation and calculation on the efficiency of a water electrolysis system for hydrogen production. *Int. J. Hydrogen Energy* 35(20), 10851-10858.

17. Armaroli N., Balzani V. (2011). The hydrogen issue. *ChemSusChem.* 4(1), 21-36.

18. Hallenbeck P. C., Benemann J. R. (2002). Biological hydrogen production; fundamentals and limiting processes. *Int. J. Hydrogen Energy* 27(11–12), 1185-1193.

19. Ghirardi M. L., Dubini A., Yu J., Maness P. C. (2009). Photobiological hydrogen-producing systems. *Chem. Soc. Rev.* 38(1), 52-61.

20. Rupprecht J. (2009). From systems biology to fuel--*Chlamydomonas reinhardtii* as a model for a systems biology approach to improve biohydrogen production. *J. Biotechnol.* 142(1), 10-20.

21. Tamagnini P., Axelsson R., Lindberg P., Oxelfelt F., Wunschiers R., Lindblad P. (2002). Hydrogenases and hydrogen metabolism of cyanobacteria. *Microbiol. Mol. Biol. Rev.* 66(1), 1-20, table of contents.

22. Vignais P. M., Billoud B. (2007). Occurrence, classification, and biological function of hydrogenases: an overview. *Chem. Rev.* 107(10), 4206-4272.

23. Tian F., Toon O. B., Pavlov A. A., De Sterck H. (2005). A hydrogen-rich early Earth atmosphere. *Science* 308(5724), 1014-1017.

24. Nie W., Tang H., Fang Z., Chen J., Chen H., Xiu Q. (2012). Hydrogenase: the next antibiotic target? *Clin. Sci.* 122(12), 575-580.

25. Bothe H., Schmitz O., Yates M. G., Newton W. E. (2010). Nitrogen fixation and hydrogen metabolism in cyanobacteria. *Microbiol. Mol. Biol. Rev.* 74(4), 529-551.

26. Rey F. E., Heiniger E. K., Harwood C. S. (2007). Redirection of metabolism for biological hydrogen production. *Appl. Environ. Microbiol.* 73(5), 1665-1671.

27. Seefeldt L. C., Hoffman B. M., Dean D. R. (2009). Mechanism of Mo-dependent nitrogenase. *Annu. Rev. Biochem.* 78, 701-722.

28. Burgess B. K., Lowe D. J. (1996). Mechanism of molybdenum nitrogenase. *Chem. Rev.* 96(7), 2983-3012.

29. Hu Y., Ribbe M. W. (2011). Historic overview of nitrogenase research. *Methods Mol. Biol.* 766, 3-7.

30. Hwang J. C., Burris R. H. (1972). Nitrogenase-catalyzed reactions. *Biochim. Biophys. Acta* 283(2), 339-350.

31. Golden J. W., Yoon H. S. (2003). Heterocyst development in *Anabaena*. *Curr. Opin. Microbiol.* 6(6), 557-563.

32. Ghirardi M. L., Posewitz M. C., Maness P. C., Dubini A., Yu J., Seibert M. (2007). Hydrogenases and hydrogen photoproduction in oxygenic photosynthetic organisms. *Annu. Rev. Plant Biol.* 58, 71-91.

33. Cammack R., Frey M., Robson R. (ed.). 2001. Hydrogen as a Fuel. Taylor & Francis, London.

34. Hallenbeck P. C., Abo-Hashesh M., Ghosh D. (2012). Strategies for improving biological hydrogen production. *Bioresour. Technol.* 110, 1-9.

35. Vignais P. M., Billoud B., Meyer J. (2001). Classification and phylogeny of hydrogenases. *FEMS Microbiol. Rev.* 25(4), 455-501.

36. Müller M. (1993). The hydrogenosome. *J. Gen. Microbiol.* 139(12), 2879-2889.

37. Yang D., Oyaizu Y., Oyaizu H., Olsen G. J., Woese C. R. (1985). Mitochondrial origins. *Proc. Natl. Acad. Sci. U.S.A.* 82(13), 4443-4447.

38. Boxma B., de Graaf R. M., van der Staay G. W., van Alen T. A., Ricard G., Gabaldon T., van Hoek A. H., Moon-van der Staay S. Y., Koopman W. J., van Hellemond J. J., Tielens A. G., Friedrich T., Veenhuis M., Huynen M. A., Hackstein J. H. (2005). An anaerobic mitochondrion that produces hydrogen. *Nature* 434(7029), 74-79.

39. Muller M., Lindmark D. G. (1978). Respiration of hydrogenosomes of *Tritrichomonas foetus*. II. Effect of CoA on pyruvate oxidation. *J. Biol. Chem.* 253(4), 1215-1218.

40. Camsund D., Devine E., Holmqvist M., Yohanoun P., Lindblad P., Stensjo K. (2011). A HupS-GFP fusion protein demonstrates a heterocyst-specific localization of the uptake hydrogenase in *Nostoc punctiforme*. *FEMS Microbiol. Lett.* 316(2), 152-159.

41. Masukawa H., Mochimaru M., Sakurai H. (2002). Disruption of the uptake hydrogenase gene, but not of the bidirectional hydrogenase gene, leads to enhanced photobiological hydrogen production by the nitrogen-fixing cyanobacterium *Anabaena* sp. PCC 7120. *Appl. Microbiol. Biotechnol.* 58(5), 618-624.

42. Walker C. B., Redding-Johanson A. M., Baidoo E. E., Rajeev L., He Z., Hendrickson E. L., Joachimiak M. P., Stolyar S., Arkin A. P., Leigh J. A., Zhou J., Keasling J. D.,

Mukhopadhyay A., Stahl D. A. (2012). Functional responses of methanogenic archaea to syntrophic growth. *ISME J.* 6(11), 2045-2055.

43. Rotaru A. E., Shrestha P. M., Liu F., Ueki T., Nevin K., Summers Z. M., Lovley D. R. (2012). Interspecies electron transfer via hydrogen and formate rather than direct electrical connections in cocultures of *Pelobacter carbinolicus* and *Geobacter sulfurreducens*. *Appl. Environ. Microbiol.* 78(21), 7645-7651.

44. Ludwig M., Cracknell J. A., Vincent K. A., Armstrong F. A., Lenz O. (2009). Oxygen-tolerant H_2 oxidation by membrane-bound [NiFe] hydrogenases of Ralstonia species. Coping with low level H_2 in air. *J. Biol. Chem.* 284(1), 465-477.

45. Hedderich R. (2004). Energy-converting [NiFe] hydrogenases from archaea and extremophiles: ancestors of complex I. *J. Bioenerg. Biomembr.* 36(1), 65-75.

46. Thauer R. K. (2012). The Wolfe cycle comes full circle. *Proc. Natl. Acad. Sci. U.S.A.* 109(38), 15084-15085.

47. Lie T. J., Costa K. C., Lupa B., Korpole S., Whitman W. B., Leigh J. A. (2012). Essential anaplerotic role for the energy-converting hydrogenase Eha in hydrogenotrophic methanogenesis. *Proc. Natl. Acad. Sci. U.S.A.* 109(38), 15473-15478.

48. Noguchi K., Riggins D. P., Eldahan K. C., Kitko R. D., Slonczewski J. L. (2010). Hydrogenase-3 contributes to anaerobic acid resistance of *Escherichia coli*. *PLoS One* 5(4), e10132.

49. Fournier M., Dermoun Z., Durand M. C., Dolla A. (2004). A new function of the *Desulfovibrio vulgaris* Hildenborough [Fe] hydrogenase in the protection against oxidative stress. *J. Biol. Chem.* 279(3), 1787-1793.

50. Kohanski M. A., Dwyer D. J., Hayete B., Lawrence C. A., Collins J. J. (2007). A common mechanism of cellular death induced by bactericidal antibiotics. *Cell* 130(5), 797-810.

51. Ohsawa I., Ishikawa M., Takahashi K., Watanabe M., Nishimaki K., Yamagata K., Katsura K., Katayama Y., Asoh S., Ohta S. (2007). Hydrogen acts as a therapeutic antioxidant by selectively reducing cytotoxic oxygen radicals. *Nat. Med.* 13(6), 688-694.

52. Hall D. O. (1976). Photobiological energy conversion. *FEBS Lett.* 64(1), 6-16.

53. Fortier M. O., Sturm B. S. (2012). Geographic analysis of the feasibility of collocating algal biomass production with wastewater treatment plants. *Environ. Sci. Technol.* 46(20), 11426-11434.

54. Lakaniemi A. M., Tuovinen O. H., Puhakka J. A. (2012). Anaerobic conversion of microalgal biomass to sustainable energy carriers - A review. *Bioresour. Technol.*

55. Show K. Y., Lee D. J., Chang J. S. (2012). Algal biomass dehydration. *Bioresour. Technol.*

56. Maeda T., Sanchez-Torres V., Wood T. K. (2007). Enhanced hydrogen production from glucose by metabolically engineered *Escherichia coli*. *Appl. Microbiol. Biotechnol.* 77(4), 879-890.

57. McNeely K., Xu Y., Bennette N., Bryant D. A., Dismukes G. C. (2010). Redirecting reductant flux into hydrogen production via metabolic engineering of fermentative carbon metabolism in a cyanobacterium. *Appl. Environ. Microbiol.* 76(15), 5032-5038.

58. Maru B. T., Constanti M., Stchigel A. M., Medina F., Sueiras J. E. (2012). Biohydrogen production by dark fermentation of glycerol using *Enterobacter* and *Citrobacter* sp. *Biotechnol. Prog.*

59. Trchounian K., Soboh B., Sawers R. G., Trchounian A. (2012). Contribution of hydrogenase 2 to stationary phase H(2) production by *Escherichia coli* during fermentation of glycerol. *Cell Biochem. Biophys.*

60. Zhao L., Cao G. L., Wang A. J., Ren H. Y., Dong D., Liu Z. N., Guan X. Y., Xu C. J., Ren N. Q. (2012). Fungal pretreatment of cornstalk with *Phanerochaete chrysosporium* for enhancing enzymatic saccharification and hydrogen production. *Bioresour. Technol.* 114, 365-369.

61. Panagiotopoulos I. A., Bakker R. R., Budde M. A., de Vrije T., Claassen P. A., Koukios E. G. (2009). Fermentative hydrogen production from pretreated biomass: a comparative study. *Bioresour. Technol.* 100(24), 6331-6338.

62. Modenbach A. A., Nokes S. E. (2012). The use of high-solids loadings in biomass pretreatment--a review. *Biotechnol. Bioeng.* 109(6), 1430-1442.

63. Kruse O., Hankamer B. (2010). Microalgal hydrogen production. *Curr. Opin. Biotechnol.* 21(3), 238-243.

64. Stripp S. T., Goldet G., Brandmayr C., Sanganas O., Vincent K. A., Haumann M., Armstrong F. A., Happe T. (2009). How oxygen attacks [FeFe] hydrogenases from photosynthetic organisms. *Proc. Natl. Acad. Sci. U.S.A.* 106(41), 17331-17336.

65. Ghysels B., Franck F. (2010). Hydrogen photo-evolution upon S deprivation stepwise: an illustration of microalgal photosynthetic and metabolic flexibility and a step stone for future biotechnological methods of renewable H(2) production. *Photosynth. Res.* 106(1-2), 145-154.

66. Antal T. K., Krendeleva T. E., Rubin A. B. (2011). Acclimation of green algae to sulfur deficiency: underlying mechanisms and application for hydrogen production. *Appl. Microbiol. Biotechnol.* 89(1), 3-15.

67. Masukawa H., Inoue K., Sakurai H., Wolk C. P., Hausinger R. P. (2010). Site-directed mutagenesis of the *Anabaena* sp. strain PCC 7120 nitrogenase active site to increase photobiological hydrogen production. *Appl. Environ. Microbiol.* 76(20), 6741-6750.

68. Kim D. H., Kim M. S. (2011). Hydrogenases for biological hydrogen production. *Bioresour. Technol.* 102(18), 8423-8431.

69. Yahata N., Saitoh T., Takayama Y., Ozawa K., Ogata H., Higuchi Y., Akutsu H. (2006). Redox interaction of cytochrome c_3 with [NiFe] hydrogenase from *Desulfovibrio vulgaris* Miyazaki F. *Biochemistry* 45(6), 1653-1662.

70. ElAntak L., Morelli X., Bornet O., Hatchikian C., Czjzek M., Dolla A., Guerlesquin F. (2003). The cytochrome c_3-[Fe]-hydrogenase electron-transfer complex: structural model by NMR restrained docking. *FEBS Lett.* 548(1-3), 1-4.

71. Winkler M., Hemschemeier A., Jacobs J., Stripp S., Happe T. (2010). Multiple ferredoxin isoforms in *Chlamydomonas reinhardtii* - their role under stress conditions and biotechnological implications. *Eur. J. Cell Biol.* 89(12), 998-1004.

72. Schuchmann K., Müller V. (2012). A bacterial electron-bifurcating hydrogenase. *J. Biol. Chem.* 287(37), 31165-31171.

73. Lambertz C., Leidel N., Havelius K. G., Noth J., Chernev P., Winkler M., Happe T., Haumann M. (2011). O_2 reactions at the six-iron active site (H-cluster) in [FeFe]-hydrogenase. *J. Biol. Chem.* 286(47), 40614-40623.

74. Vincent K. A., Cracknell J. A., Lenz O., Zebger I., Friedrich B., Armstrong F. A. (2005). Electrocatalytic hydrogen oxidation by an enzyme at high carbon monoxide or oxygen levels. *Proc. Natl. Acad. Sci. U.S.A.* 102(47), 16951-16954.

75. Liebgott P. P., Leroux F., Burlat B., Dementin S., Baffert C., Lautier T., Fourmond V., Ceccaldi P., Cavazza C., Meynial-Salles I., Soucaille P., Fontecilla-Camps J. C., Guigliarelli B., Bertrand P., Rousset M., Leger C. (2010). Relating diffusion along the substrate tunnel and oxygen sensitivity in hydrogenase. *Nat. Chem. Biol.* 6(1), 63-70.

76. Peters J. W., Lanzilotta W. N., Lemon B. J., Seefeldt L. C. (1998). X-ray crystal structure of the Fe-only hydrogenase (CpI) from *Clostridium pasteurianum* to 1.8 angstrom resolution. *Science* 282(5395), 1853-1858.

77. Nicolet Y., Piras C., Legrand P., Hatchikian C. E., Fontecilla-Camps J. C. (1999). *Desulfovibrio desulfuricans* iron hydrogenase: the structure shows unusual coordination to an active site Fe binuclear center. *Structure* 7(1), 13-23.

78. Volbeda A., Charon M. H., Piras C., Hatchikian E. C., Frey M., Fontecilla-Camps J. C. (1995). Crystal structure of the nickel-iron hydrogenase from *Desulfovibrio gigas*. *Nature*

373(6515), 580-587.

79. Shima S., Pilak O., Vogt S., Schick M., Stagni M. S., Meyer-Klaucke W., Warkentin E., Thauer R. K., Ermler U. (2008). The crystal structure of [Fe]-hydrogenase reveals the geometry of the active site. *Science* 321(5888), 572-575.

80. Frey M. (2002). Hydrogenases: hydrogen-activating enzymes. *Chembiochem* 3(2-3), 153-160.

81. Meyer J. (2007). [FeFe] hydrogenases and their evolution: a genomic perspective. *Cell. Mol. Life Sci.* 64(9), 1063-1084.

82. Rippers Y., Utesch T., Hildebrandt P., Zebger I., Mroginski M. A. (2011). Insights into the structure of the active site of the O_2-tolerant membrane bound [NiFe] hydrogenase of *R. eutropha* H16 by molecular modelling. *Phys. Chem. Chem. Phys.* 13(36), 16146-16149.

83. Pandelia M. E., Ogata H., Lubitz W. (2010). Intermediates in the catalytic cycle of [NiFe] hydrogenase: functional spectroscopy of the active site. *Chemphyschem* 11(6), 1127-1140.

84. Ogata H., Kellers P., Lubitz W. (2010). The crystal structure of the [NiFe] hydrogenase from the photosynthetic bacterium *Allochromatium vinosum*: characterization of the oxidized enzyme (Ni-A state). *J. Mol. Biol.* 402(2), 428-444.

85. Casalot L., Rousset M. (2001). Maturation of the [NiFe] hydrogenases. *Trends Microbiol.* 9(5), 228-237.

86. Thauer R. K., Klein A. R., Hartmann G. C. (1996). Reactions with molecular hydrogen in microorganisms: evidence for a purely organic hydrogenation catalyst. *Chem. Rev.* 96(7), 3031-3042.

87. Corr M. J., Murphy J. A. (2011). Evolution in the understanding of [Fe]-hydrogenase. *Chem. Soc. Rev.* 40(5), 2279-2292.

88. McGlynn S. E., Boyd E. S., Shepard E. M., Lange R. K., Gerlach R., Broderick J. B., Peters J. W. (2010). Identification and characterization of a novel member of the radical AdoMet enzyme superfamily and implications for the biosynthesis of the Hmd hydrogenase active site cofactor. *J. Bacteriol.* 192(2), 595-598.

89. Mulder D. W., Shepard E. M., Meuser J. E., Joshi N., King P. W., Posewitz M. C., Broderick J. B., Peters J. W. (2011). Insights into [FeFe]-hydrogenase structure, mechanism, and maturation. *Structure* 19(8), 1038-1052.

90. Valente F. M., Oliveira A. S., Gnadt N., Pacheco I., Coelho A. V., Xavier A. V., Teixeira M., Soares C. M., Pereira I. A. (2005). Hydrogenases in *Desulfovibrio vulgaris* Hildenborough: structural and physiologic characterisation of the membrane-bound

[NiFeSe] hydrogenase. *J. Biol. Inorg. Chem.* 10(6), 667-682.

91. Vignais P. M. (2008). Hydrogenases and H^+-reduction in primary energy conservation. *Results Probl. Cell Differ.* 45, 223-252.

92. Adams M. W. W. (1990). The structure and mechanism of iron-hydrogenases. *Biochim. et Biophys. Acta* 1020(2), 115-145.

93. Mulder D. W., Ortillo D. O., Gardenghi D. J., Naumov A. V., Ruebush S. S., Szilagyi R. K., Huynh B., Broderick J. B., Peters J. W. (2009). Activation of $HydA^{\Delta DeltaEFG}$ requires a preformed [4Fe-4S] cluster. *Biochemistry* 48(26), 6240-6248.

94. Sybirna K., Antoine T., Lindberg P., Fourmond V., Rousset M., Mejean V., Bottin H. (2008). *Shewanella oneidensis*: a new and efficient system for expression and maturation of heterologous [Fe-Fe] hydrogenase from *Chlamydomonas reinhardtii*. *BMC Biotechnol.* 8, 73.

95. King P. W., Posewitz M. C., Ghirardi M. L., Seibert M. (2006). Functional studies of [FeFe] hydrogenase maturation in an *Escherichia coli* biosynthetic system. *J. Bacteriol.* 188(6), 2163-2172.

96. Girbal L., von Abendroth G., Winkler M., Benton P. M., Meynial-Salles I., Croux C., Peters J. W., Happe T., Soucaille P. (2005). Homologous and heterologous overexpression in *Clostridium acetobutylicum* and characterization of purified clostridial and algal Fe-only hydrogenases with high specific activities. *Appl. Environ. Microbiol.* 71(5), 2777-2781.

97. Greco C., Bruschi M., Fantucci P., Ryde U., De Gioia L. (2011). Probing the effects of one-electron reduction and protonation on the electronic properties of the Fe-S clusters in the active-ready form of [FeFe]-hydrogenases. A QM/MM investigation. *Chemphyschem* 12(17), 3376-3382.

98. Stiebritz M. T., Reiher M. (2009). Theoretical study of dioxygen induced inhibition of [FeFe]-hydrogenase. *Inorg. Chem.* 48(15), 7127-7140.

99. Silakov A., Reijerse E. J., Albracht S. P., Hatchikian E. C., Lubitz W. (2007). The electronic structure of the H-cluster in the [FeFe]-hydrogenase from *Desulfovibrio desulfuricans*: a Q-band ^{57}Fe-ENDOR and HYSCORE study. *J. Am. Chem. Soc.* 129(37), 11447-11458.

100. Silakov A., Wenk B., Reijerse E., Lubitz W. (2009). ^{14}N HYSCORE investigation of the H-cluster of [FeFe] hydrogenase: evidence for a nitrogen in the dithiol bridge. *Phys. Chem. Chem. Phys.* 11(31), 6592-6599.

101. Erdem O. F., Schwartz L., Stein M., Silakov A., Kaur-Ghumaan S., Huang P., Ott S., Reijerse E. J., Lubitz W. (2011). A model of the [FeFe] hydrogenase active site with a

biologically relevant azadithiolate bridge: a spectroscopic and theoretical investigation. *Angew. Chem. Int. Ed. Engl.* 50(6), 1439-1443.

102. Pandey A. S., Harris T. V., Giles L. J., Peters J. W., Szilagyi R. K. (2008). Dithiomethylether as a ligand in the hydrogenase h-cluster. *J. Am. Chem. Soc.* 130(13), 4533-4540.

103. Fontecilla-Camps J. C., Amara P., Cavazza C., Nicolet Y., Volbeda A. (2009). Structure-function relationships of anaerobic gas-processing metalloenzymes. *Nature* 460(7257), 814-822.

104. Hong G., Cornish A. J., Hegg E. L., Pachter R. (2011). On understanding proton transfer to the biocatalytic [Fe-Fe](H) sub-cluster in [Fe-Fe]H(2)ases: QM/MM MD simulations. *Biochim. Biophys. Acta* 1807(5), 510-517.

105. Greco C., Bruschi M., De Gioia L., Ryde U. (2007). A QM/MM investigation of the activation and catalytic mechanism of Fe-only hydrogenases. *Inorg. Chem.* 46(15), 5911-5921.

106. Shepard E. M., McGlynn S. E., Bueling A. L., Grady-Smith C. S., George S. J., Winslow M. A., Cramer S. P., Peters J. W., Broderick J. B. (2010). Synthesis of the 2Fe subcluster of the [FeFe]-hydrogenase H cluster on the HydF scaffold. *Proc. Natl. Acad. Sci. U.S.A.* 107(23), 10448-10453.

107. Cendron L., Berto P., D'Adamo S., Vallese F., Govoni C., Posewitz M. C., Giacometti G. M., Costantini P., Zanotti G. (2011). Crystal structure of HydF scaffold protein provides insights into [FeFe]-hydrogenase maturation. *J. Biol. Chem.* 286(51), 43944-43950.

108. Nicolet Y., Martin L., Tron C., Fontecilla-Camps J. C. (2010). A glycyl free radical as the precursor in the synthesis of carbon monoxide and cyanide by the [FeFe]-hydrogenase maturase HydG. *FEBS Lett.* 584(19), 4197-4202.

109. Shepard E. M., Duffus B. R., George S. J., McGlynn S. E., Challand M. R., Swanson K. D., Roach P. L., Cramer S. P., Peters J. W., Broderick J. B. (2010). [FeFe]-hydrogenase maturation: HydG-catalyzed synthesis of carbon monoxide. *J. Am. Chem. Soc.* 132(27), 9247-9249.

110. Kuchenreuther J. M., George S. J., Grady-Smith C. S., Cramer S. P., Swartz J. R. (2011). Cell-free H-cluster synthesis and [FeFe] hydrogenase activation: all five CO and CN(-) ligands derive from tyrosine. *PLoS One* 6(5), e20346.

111. Nicolet Y., Rubach J. K., Posewitz M. C., Amara P., Mathevon C., Atta M., Fontecave M., Fontecilla-Camps J. C. (2008). X-ray structure of the [FeFe]-hydrogenase maturase HydE from *Thermotoga maritima*. *J. Biol. Chem.* 283(27), 18861-18872.

112. Mulder D. W., Boyd E. S., Sarma R., Lange R. K., Endrizzi J. A., Broderick J. B., Peters

J. W. (2010). Stepwise [FeFe]-hydrogenase H-cluster assembly revealed in the structure of HydA(DeltaEFG). *Nature* 465(7295), 248-251.

113. McGlynn S. E., Ruebush S. S., Naumov A., Nagy L. E., Dubini A., King P. W., Broderick J. B., Posewitz M. C., Peters J. W. (2007). In vitro activation of [FeFe] hydrogenase: new insights into hydrogenase maturation. *J. Biol. Inorg. Chem.* 12(4), 443-447.

114. Nicolet Y., Fontecilla-Camps J. C. (2012). Structure-function relationships in [FeFe]-hydrogenase active site maturation. *J. Biol. Chem.* 287(17), 13532-13540.

115. Pierik A. J., Hagen W. R., Redeker J. S., Wolbert R. B., Boersma M., Verhagen M. F., Grande H. J., Veeger C., Mutsaers P. H., Sands R. H., et al. (1992). Redox properties of the iron-sulfur clusters in activated Fe-hydrogenase from *Desulfovibrio vulgaris* (Hildenborough). *Eur. J. Biochem.* 209(1), 63-72.

116. Vincent K. A., Parkin A., Lenz O., Albracht S. P., Fontecilla-Camps J. C., Cammack R., Friedrich B., Armstrong F. A. (2005). Electrochemical definitions of O_2 sensitivity and oxidative inactivation in hydrogenases. *J. Am. Chem. Soc.* 127(51), 18179-18189.

117. Hong G., Pachter R. (2012). Inhibition of biocatalysis in [Fe-Fe] hydrogenase by oxygen: molecular dynamics and density functional theory calculations. *ACS Chem. Biol.* 7(7), 1268-1275.

118. Lautier T., Ezanno P., Baffert C., Fourmond V., Cournac L., Fontecilla-Camps J. C., Soucaille P., Bertrand P., Meynial-Salles I., Leger C. (2011). The quest for a functional substrate access tunnel in FeFe hydrogenase. *Faraday Discuss.* 148, 385-407; discussion 421-341.

119. Cohen J., Kim K., King P., Seibert M., Schulten K. (2005). Finding gas diffusion pathways in proteins: application to O2 and H2 transport in CpI [FeFe]-hydrogenase and the role of packing defects. *Structure* 13(9), 1321-1329.

120. Duche O., Elsen S., Cournac L., Colbeau A. (2005). Enlarging the gas access channel to the active site renders the regulatory hydrogenase HupUV of Rhodobacter capsulatus O_2 sensitive without affecting its transductory activity. *FEBS J.* 272(15), 3899-3908.

121. Bennett B., Lemon B. J., Peters J. W. (2000). Reversible carbon monoxide binding and inhibition at the active site of the Fe-only hydrogenase. *Biochemistry* 39(25), 7455-7460.

122. Lemon B. J., Peters J. W. (1999). Binding of exogenously added carbon monoxide at the active site of the iron-only hydrogenase (CpI) from *Clostridium pasteurianum*. *Biochemistry* 38(40), 12969-12973.

123. Goldet G., Brandmayr C., Stripp S. T., Happe T., Cavazza C., Fontecilla-Camps J. C., Armstrong F. A. (2009). Electrochemical kinetic investigations of the reactions of [FeFe]-hydrogenases with carbon monoxide and oxygen: comparing the importance of gas

tunnels and active-site electronic/redox effects. *J. Am. Chem. Soc.* 131(41), 14979-14989.

124. Wait A. F., Brandmayr C., Stripp S. T., Cavazza C., Fontecilla-Camps J. C., Happe T., Armstrong F. A. (2011). Formaldehyde--a rapid and reversible inhibitor of hydrogen production by [FeFe]-hydrogenases. *J. Am. Chem. Soc.* 133(5), 1282-1285.

125. Foster C. E., Kramer T., Wait A. F., Parkin A., Jennings D. P., Happe T., McGrady J. E., Armstrong F. A. (2012). Inhibition of [FeFe]-hydrogenases by formaldehyde and wider mechanistic implications for biohydrogen activation. *J. Am. Chem. Soc.* 134(17), 7553-7557.

126. Fernandez V. M., Rua M. L., Reyes P., Cammack R., Hatchikian E. C. (1989). Inhibition of *Desulfovibrio gigas* hydrogenase with copper salts and other metal ions. *Eur. J. Biochem.* 185(2), 449-454.

127. Kamachi T., Uno S., Hiraishi T., Okura I. (1995). Effect of Hg(II) on hydrogenase activity from *Desulfovibrio vulgaris* (Miyazaki). *J. Mol. Catal. A Chem.* 96(3), 329-333.

128. Knorzer P., Silakov A., Foster C. E., Armstrong F. A., Lubitz W., Happe T. (2012). Importance of the protein framework for catalytic activity of [FeFe]-hydrogenases. *J. Biol. Chem.* 287(2), 1489-1499.

129. Stapleton J. A., Swartz J. R. (2010). Development of an in vitro compartmentalization screen for high-throughput directed evolution of [FeFe] hydrogenases. *PLoS One* 5(12), e15275.

130. Nagy L. E., Meuser J. E., Plummer S., Seibert M., Ghirardi M. L., King P. W., Ahmann D., Posewitz M. C. (2007). Application of gene-shuffling for the rapid generation of novel [FeFe]-hydrogenase libraries. *Biotechnol. Lett.* 29(3), 421-430.

131. Peters J. W. (1999). Structure and mechanism of iron-only hydrogenases. *Curr. Opin. Struct. Biol.* 9(6), 670-676.

132. Schultz B. E., Chan S. I. (2001). Structures and proton-pumping strategies of mitochondrial respiratory enzymes. *Annu. Rev. Biophys. Biomol. Struct.* 30, 23-65.

133. Cukierman S. (2006). Et tu, Grotthuss! and other unfinished stories. *Biochim. Biophys. Acta.* 1757(8), 876-885.

134. Marshall M. J., Plymale A. E., Kennedy D. W., Shi L., Wang Z., Reed S. B., Dohnalkova A. C., Simonson C. J., Liu C., Saffarini D. A., Romine M. F., Zachara J. M., Beliaev A. S., Fredrickson J. K. (2008). Hydrogenase- and outer membrane *c*-type cytochrome-facilitated reduction of technetium(VII) by *Shewanella oneidensis* MR-1. *Environ. Microbiol.* 10(1), 125-136.

135. ElAntak L., Morelli X., Bornet O., Hatchikian C., Czjzek M., Dolla A., Guerlesquin F.

(2003). The cytochrome c3-[Fe]-hydrogenase electron-transfer complex: structural model by NMR restrained docking. *FEBS Lett* 548(1-3), 1-4.

136. Odom J. M., Peck H. D., Jr. (1984). Hydrogenase, electron-transfer proteins, and energy coupling in the sulfate-reducing bacteria *Desulfovibrio*. *Annu. Rev. Microbiol.* 38, 551-592.

137. Long H., Chang C. H., King P. W., Ghirardi M. L., Kim K. (2008). Brownian dynamics and molecular dynamics study of the association between hydrogenase and ferredoxin from *Chlamydomonas reinhardtii*. *Biophys. J.* 95(8), 3753-3766.

138. Kummerle R., Kyritsis P., Gaillard J., Moulis J. M. (2000). Electron transfer properties of iron-sulfur proteins. *J. Inorg. Biochem.* 79(1-4), 83-91.

139. Dementin S., Belle V., Bertrand P., Guigliarelli B., Adryanczyk-Perrier G., De Lacey A. L., Fernandez V. M., Rousset M., Leger C. (2006). Changing the ligation of the distal [4Fe4S] cluster in NiFe hydrogenase impairs inter- and intramolecular electron transfers. *J. Am. Chem. Soc.* 128(15), 5209-5218.

140. Cohen J., Kim K., Posewitz M., Ghirardi M. L., Schulten K., Seibert M., King P. (2005). Molecular dynamics and experimental investigation of H_2 and O_2 diffusion in [Fe]-hydrogenase. *Biochem. Soc. Trans.* 33(Pt 1), 80-82.

141. Lautier T., Ezanno P., Baffert C., Fourmond V., Cournac L., Fontecilla-Camps J. C., Soucaille P., Bertrand P., Meynial-Salles I., Leger C. (2011). The quest for a functional substrate access tunnel in FeFe hydrogenase. *Faraday Discuss* 148, 385-407; discussion 421-341.

142. Horner D. S., Heil B., Happe T., Embley T. M. (2002). Iron hydrogenases--ancient enzymes in modern eukaryotes. *Trends Biochem. Sci.* 27(3), 148-153.

143. Posewitz M. C., King P. W., Smolinski S. L., Smith R. D., Ginley A. R., Ghirardi M. L., Seibert M. (2005). Identification of genes required for hydrogenase activity in *Chlamydomonas reinhardtii*. *Biochem. Soc. Trans.* 33(Pt 1), 102-104.

144. Posewitz M. C., King P. W., Smolinski S. L., Zhang L., Seibert M., Ghirardi M. L. (2004). Discovery of two novel radical S-adenosylmethionine proteins required for the assembly of an active [Fe] hydrogenase. *J. Biol. Chem.* 279(24), 25711-25720.

145. Kuchenreuther J. M., Grady-Smith C. S., Bingham A. S., George S. J., Cramer S. P., Swartz J. R. (2010). High-yield expression of heterologous [FeFe] hydrogenases in *Escherichia coli*. *PLoS One* 5(11), e15491.

146. Sybirna K., Antoine T., Lindberg P., Fourmond V., Rousset M., Mejean V., Bottin H. (2008). Shewanella oneidensis: a new and efficient system for expression and maturation of heterologous [Fe-Fe] hydrogenase from Chlamydomonas reinhardtii. *BMC Biotechnol*

8, 73.

147. Happe T., Kaminski A. (2002). Differential regulation of the Fe-hydrogenase during anaerobic adaptation in the green alga *Chlamydomonas reinhardtii*. *Eur. J. Biochem.* 269(3), 1022-1032.

148. Winkler M., Heil B., Happe T. (2002). Isolation and molecular characterization of the [Fe]-hydrogenase from the unicellular green alga *Chlorella fusca*. *Biochim. Biophys. Acta* 1576(3), 330-334.

149. Kamp C., Silakov A., Winkler M., Reijerse E. J., Lubitz W., Happe T. (2008). Isolation and first EPR characterization of the [FeFe]-hydrogenases from green algae. *Biochim. Biophys. Acta* 1777(5), 410-416.

150. Meuser J. E., Boyd E. S., Ananyev G., Karns D., Radakovits R., Narayana Murthy U. M., Ghirardi M. L., Dismukes G. C., Peters J. W., Posewitz M. C. (2011). Evolutionary significance of an algal gene encoding an [FeFe]-hydrogenase with F-domain homology and hydrogenase activity in *Chlorella variabilis* NC64A. *Planta* 234(4), 829-843.

151. Forestier M., King P., Zhang L., Posewitz M., Schwarzer S., Happe T., Ghirardi M. L., Seibert M. (2003). Expression of two [Fe]-hydrogenases in *Chlamydomonas reinhardtii* under anaerobic conditions. *Eur. J. Biochem.* 270(13), 2750-2758.

152. Hackstein J. H. (2005). Eukaryotic Fe-hydrogenases -- old eukaryotic heritage or adaptive acquisitions? *Biochem. Soc. Trans.* 33(Pt 1), 47-50.

153. Shiflett A. M., Johnson P. J. (2010). Mitochondrion-related organelles in eukaryotic protists. *Annu. Rev. Microbiol.* 64, 409-429.

154. Urzica E., Pierik A. J., Muhlenhoff U., Lill R. (2009). Crucial role of conserved cysteine residues in the assembly of two iron-sulfur clusters on the CIA protein Nar1. *Biochemistry* 48(22), 4946-4958.

155. Lill R., Kispal G. (2000). Maturation of cellular Fe-S proteins: an essential function of mitochondria. *Trends. Biochem. Sci.* 25(8), 352-356.

156. Tachezy J., Sánchez L. B., Müller M. (2001). Mitochondrial type iron-sulfur cluster assembly in the amitochondriate eukaryotes *Trichomonas vaginalis* and *Giardia intestinalis*, as indicated by the phylogeny of IscS. *Mol. Biol. Evol.* 18(10), 1919-1928.

CHAPTER 2

Investigating the mechanism of Proton Transfer in [FeFe]-hydrogenase from *Clostridium pasteurianum*[1]

[1] This chapter is adapted from Cornish A. J., Gärtner K., Yang H., Peters J. W., Hegg E. L. (2011). Mechanism of proton transfer in [FeFe]-hydrogenase from *Clostridium pasteurianum*. *J. Biol. Chem.* 286(44), 38341-38347.

INTRODUCTION

Hydrogenases are found in a diverse array of microorganisms where they mainly function either to a) reduce protons utilizing electrons accumulated during fermentation or b) couple the oxidation of H_2 to energy-yielding reactions (1). Hydrogenases are separated into three subclasses based on the composition of their active sites: [FeFe]-, [NiFe]-, and [Fe]-hydrogenase (2). [FeFe]-hydrogenases demonstrate the highest *in vitro* catalytic turnover among hydrogen-producing enzymes, and there is great interest in elucidating the enzymatic mechanism of these hydrogenases (3, 4). Current research has primarily focused on examining the catalytic activity (5, 6), active site assembly (7, 8, 9, 10), and irreversible oxygen inactivation of these enzymes (11, 12, 13), but relatively few data are available concerning intramolecular transport of substrates between the active site and the enzyme surface (14, 15, 16). Proton transfer is an essential component of reversible hydrogen production by [FeFe]-hydrogenases, and biochemical investigation is required for a complete understanding of the enzymatic mechanism.

Two structures of [FeFe]-hydrogenases have been solved by crystallography (*Clostridium pasteurianum* (17, 18) (Figure 2.1A) and *Desulfovibrio desulfuricans* (19)), and there is considerable structural homology near the active site. This active site (H-cluster) is best described as a [4Fe4S] cubane cluster attached via a cysteinyl sulfur linkage to a diiron moiety. Each iron is coordinated by a terminal cyanide and a carbon monoxide ligand, and an additional CO bridges the two irons (17, 20). A five-atom dithiolate ligand bridges the diiron moiety (Figure 2.1B). The exact identity of this ligand

has not been determined through direct chemical or biochemical analysis, but this ligand has been proposed to be dithiomethylamine (DTMA) because of the close proximity of the amine group to the presumed H_2 oxidation site, and the ability of amines to cycle between protonation states at physiological pH (21). The assignment of an amine group at this position is consistent with the results of a recent electron spin echo envelope modulation (ESEEM) and hyperfine sub-level correlation (HYSCORE) spectroscopic study (22). Direct experimental results addressing whether an amine` group within the dithiolate ligand could cycle between protonation states in the enzyme, however, is still lacking.

Figure 2.1. **[FeFe]-hydrogenase structure and putative proton transfer pathway.** *A*, Crystal structure of the [FeFe]-hydrogenase from *C. pasteurianum* (3C8Y www.pdb.org) resolved to 1.39 Å. The protein is a monomer separated into a catalytic domain containing the [6Fe6S] H-cluster and three N-terminal domains containing three [4Fe4S] clusters and a [2Fe2S] cluster. *B*, Chemical structure of the H-cluster emphasizing the diiron active site. X is generally postulated to be nitrogen, although oxygen and carbon remain possibilities. *C*, Putative proton transfer relay inferred by multiple sequence alignment analysis and examination of the crystal structure of the [FeFe]-hydrogenase from *C. pasteurianum*. H-cluster→C299→H_2O612→E279→S319→E282.

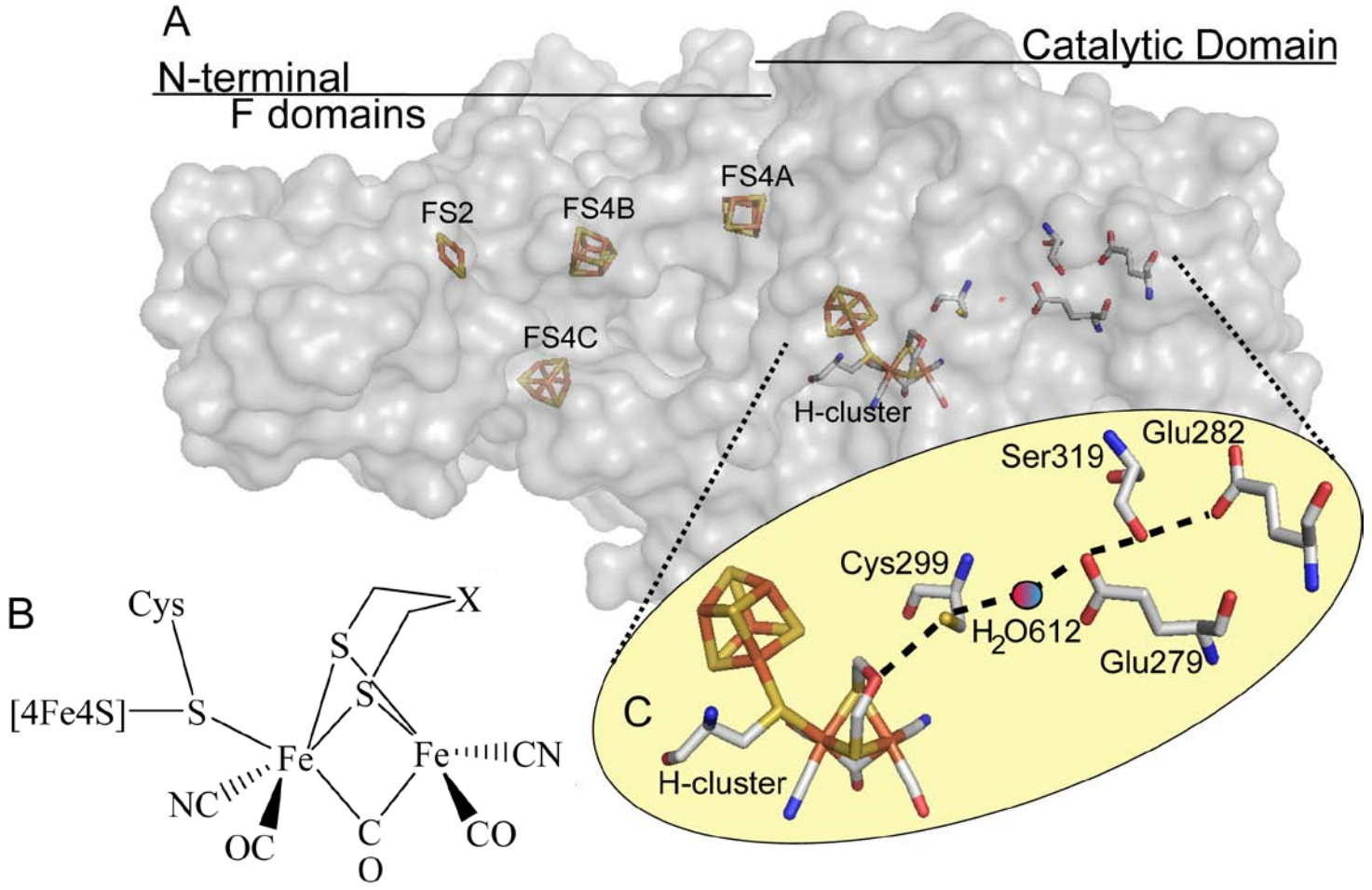

Intramolecular transfer of substrates is necessary for efficient catalysis at the active site, which is sequestered ~20 Å within the interior of the enzyme. Accessory iron-sulfur clusters provide pathways to facilitate the transport of electrons between the protein surface and the H-cluster (23, 24). Rationalizing pathways for bidirectional proton transfer, however, is less intuitive. In previous work, it has been observed that proton exchange within proteins can be facilitated via negatively charged side-chains and water molecules (25, 26, 27). Understanding this key mechanism in [FeFe]-hydrogenases is critical for targeted protein engineering, as perturbing proton transfer can cause unintended deleterious effects on the catalytic rate (28). To date, detailed experiments investigating proton transport within [FeFe]-hydrogenases have not been reported.

In this chapter, we provide biochemical evidence that four residues (Cys299, Glu279, Ser319, and Glu282) in the [FeFe]-hydrogenase from *C. pasteurianum* are important for hydrogenase activity and are likely to be involved in proton transfer between the active site and the enzyme surface. The strict conservation of these residues among this class of hydrogenases suggests a ubiquitous proton transport pathway. In addition, we have observed that Zn^{2+}-based inhibition of [FeFe]-hydrogenase specifically targets this proton pathway.

METHODS

Multiple Sequence Alignment—Using the *C. pasteurianum* [FeFe]-hydrogenase as the base sequence, we performed Position-Specific Iterated Basic Local Alignment Search Tool (BLAST) (29) to identify an additional 62 unique amino acid sequences. These 63 [FeFe]-hydrogenase sequences (acquired from National Center for Biotechnology Information [NCBI]) were examined for side-chain conservation using ClustalX (30).

Plasmid Construction—The coding sequence of the [FeFe]-hydrogenase from *C. pasteurianum* was amplified by Polymerase Chain Reaction (PCR) and ligated into the NcoI/SacI sites of pAC-BAD (a modified pBAD/D-TOPO vector from Invitrogen lacking the N-terminal thioredoxin tag) containing a kanamycin resistance cassette and an L-arabinose inducible promoter. Constructs were transformed into DH5α *Escherichia coli* competent cells and selected for resistance to 50 μg/mL kanamycin.

Site-directed Mutagenesis—Specific amino acid codons in the [FeFe]-hydrogenase gene from *C. pasteurianum* were mutated by site-directed mutagenesis PCR (*pfu* turbo, Stratagene) using appropriately designed primers (Table 2.1) (31). Segregation of mutated DNA from wild-type DNA was achieved by DpnI digestion of methylated DNA. After isolation of mutated DNA from *E. coli*, the sequences were confirmed and the constructs transformed into *S. oneidensis* MR-1 *ΔhydA/ΔhyaB* electrocompetent cells as described by Ozawa (32) and selected for resistance to 50 μg/mL kanamycin.

Table 2.1. **Primer pairs used for site-directed mutagenesis PCR of the *C. pasteurianum HydA* gene in the pAC-BAD vector**

Identity	Primer Pair
C299A Sense	5'-TGTTTACATCTGCCTGCCCAGGTTG-3'
C299A Antisense	5'-CAACCTGGGCAGGCAGATGTAAACA-3'
C299S Sense	5'-TGTTTACATCTTCTTGCCCAGGTTG-3'
C299S Antisense	5'-CAACCTGGGCAAGAAGATGTAAACA-3'
E279D Sense	5'-CAATTATGGAAGATGCTACAGAAT-3'
E279D Antisense	5'-ATTCTGTAGCATCTTCCATAATTG-3'
E279L Sense	5'-CAATTATGGAACTGGCTACAGAAT-3'
E279L Antisense	5'-ATTCTGTAGCCAGTTCCATAATTG-3'
S319A Sense	5'-AAATAATCTTGCATCAGCTAAAT-3'
S319A Antisense	5'-ATTTAGCTGATGCAAGATTATTT-3'
E282D Sense	5'-AGAGGCTACAGATTAGTTCAAA-3'
E282D Antisense	5'-TTTGAACTAAATCTGTAGCCTCT-3'
E282L Sense	5'-AGAGGCTACACTATTAGTTCAAA-3'
E282L Antisense	5'-TTTGAACTAATAGTGTAGCCTCT-3'

Cell Growth and Induction—A 0.5 mL inoculum of overnight transformant *S. oneidensis* MR-1 *ΔhydA/ΔhyaB* culture was transferred to 50 mL of 50 μg/mL kanamycin-supplemented lysogeny broth (LB) in a 250-mL Erlenmeyer flask and was shaken at 200 rpm at 30 °C until reaching an OD_{600} of 0.4 (Eppendorf BioPhotometer). The entire culture was transferred into 500 mL of 50 μg/mL kanamycin-supplemented LB in a 2-L Erlenmeyer flask and shaken at 30 °C until reaching an OD_{600} of 0.4. The culture was then transferred to a 2-L round-bottom flask, supplemented with ammonium iron citrate to a final concentration of 100 μM, and sparged with Ar to remove ambient O_2. After 30 min, 0.5 mL of 1.3 M L-arabinose (final concentration 1.3 mM) was added and the culture was sparged for an additional 30 min. The flask was then sealed with a rubber septum and shaken at 200 rpm at 30 °C for an additional 16 h.

Protein Purification—All steps for hydrogenase purification were performed anaerobically. Cells were collected by spinning the culture in airtight 250-mL Nalgene tubes at 2,800× *g* for 20 min. Inside an anaerobic Coy Chamber, the cell pellet was resuspended in 7.0 mL of Ni-NTA wash buffer (100 mM Tris-HCl [pH 8.0], 200 mM NaCl, 5.0 % glycerol) supplemented with 10 mM sodium dithionite. The resuspended cell pellet was transferred to 1.7 mL Eppendorf tubes in 1.0 mL aliquots and sonicated 8 times for 4 s each at a power setting of 4 (Fischer Scientific Sonic Dismembrator Model 100). The sonicated cell suspension was cleared of cell debris by centrifugation at 20,000× g in airtight 40-mL tubes. A column containing 1.0 mL Ni-nitriloacetic acid (NTA) agarose resin (Qiagen) was first equilibrated with 20 mL of wash buffer supplemented with 10 mM sodium dithionite to remove residual O_2, and then the

supernatant was passed over the column. The column was washed with 15 mL of wash buffer supplemented with 20 mM imidazole. The protein was eluted from the column in 1.0 mL fractions by increasing the concentration of imidazole to 100 mM.

Hydrogenase Activity Assays—Hydrogen evolution and uptake assays were modified from King et al. (33). Briefly, H_2 evolution was measured by incubating 0.1 mL of protein sample in 1.9 mL of H_2 evolution assay buffer (50 mM HEPES [pH 7.0], 500 mM NaCl, 100 mM sodium dithionite, 10 mM methyl viologen (MV)) in a 13 mL serum vial at 25 °C with continuous shaking. A 100 µL syringe was used to inject 50 µL of headspace gas into a TRACE GC Ultra Gas Chromatograph (Thermo Scientific) and H_2 accumulation was measured over time by plotting the peak area against a standard curve. To measure H_2 consumption, 0.1 mL of protein sample was incubated in 1.9 mL of H_2 uptake assay buffer (50 mM Tris-HCl [pH 8.0], 10 mM benzyl viologen (BV), 0.2% triton x-100) in a 13 mL serum vial at 25 °C with 2.5% H_2 in the headspace and shaken continuously. Uptake of H_2 was measured over time by injecting 50 µL of the headspace into the gas chromatograph and plotting the peak area against a standard curve.

Azide Rescue Assay—To determine the effect of sodium azide on hydrogenase activity, H_2 evolution activity of native and variant enzymes was measured (see Hydrogenase Activity Assays) in the presence of different amounts of sodium azide (0, 50, 100, 250 mM).

Zn^{2+} Inhibition Assay—Zn^{2+} inhibition assays were performed measuring H_2 evolution activity (see Hydrogenase Activity Assays) in a 2.0 mL total volume. Because $ZnCl_2$ only dissolves in the H_2 evolution assay buffer below pH 6.3, 0.02 mL of the buffer (pH 6.3), with or without dissolved $ZnCl_2$, was added to each assay. The effect of Zn^{2+} on the native enzyme was assayed by measuring H_2 evolution activity over several $ZnCl_2$ concentrations (0, 0.05, 0.125, 0.25. 0.50 mM) as the concentration of methyl viologen was varied (3.0, 5.0, 8.0, 10.0 mM) and the data were graphed on both Dixon and Cornish-Bowden plots. The effect of $ZnCl_2$ on the activity of amino acid-substituted [FeFe]-hydrogenases was assayed at either 0 or 0.50 mM $ZnCl_2$.

Activation Energy Assays—H_2 evolution and uptake assays were performed as previously noted over a range of temperatures (0˚C, 8 ˚C, 25 ˚C, 30 ˚C, 35 ˚C, and 40 ˚C). The natural log of k_{obs} was plotted against the reciprocal of the temperature. The resulting slope was multiplied by the negative value of the gas constant R (8.314 J K^{-1} mol^{-1}) to calculate the activation energy (E_a).

RESULTS

Proton Pathway Identification—Based on their crystallographic analysis, a putative proton transfer relay composed of Cys299, a modeled water, Glu279, Ser319, and Glu282 that connect the enzyme surface to the H-cluster of the *C. pasteurianum* [FeFe]-hydrogenase was initially proposed by Peters et al. (17). Reasoning that residues involved in proton transport should be highly conserved, we performed multiple sequence alignment on 63 unique [FeFe]-hydrogenases (Figure 2.2). Our results revealed that these four residues are strictly conserved among both algal and bacterial [FeFe]-hydrogenase genes. In comparison, these residues are *not* conserved among Nar1 proteins, a class of protein that share a number of sequence motifs with [FeFe]-hydrogenases (8, 34). Together, these data strongly implicate the importance of these four residues to hydrogenase function.

Figure 2.2. **Multiple sequence alignment.** Partial multiple sequence alignment (ClustalX) of [FeFe]-hydrogenases from *C. pasteurianum*, *D. desulfuricans, Chlamydomonas reinhardtii, Thermotoga maritima*, *Trichomonas vaginalis, Shewanella oneidensis,* and *Neocallimastix frontalis*. Amino acids predicted to participate in proton transfer are denoted by asterisks. Strictly conserved residues are in a black box while highly conserved residues are in bold. Residues with low conservation but chemically similar side-chains are boxed. Every tenth amino acid of the *C. pasteurianum* sequence is denoted by a black dot.

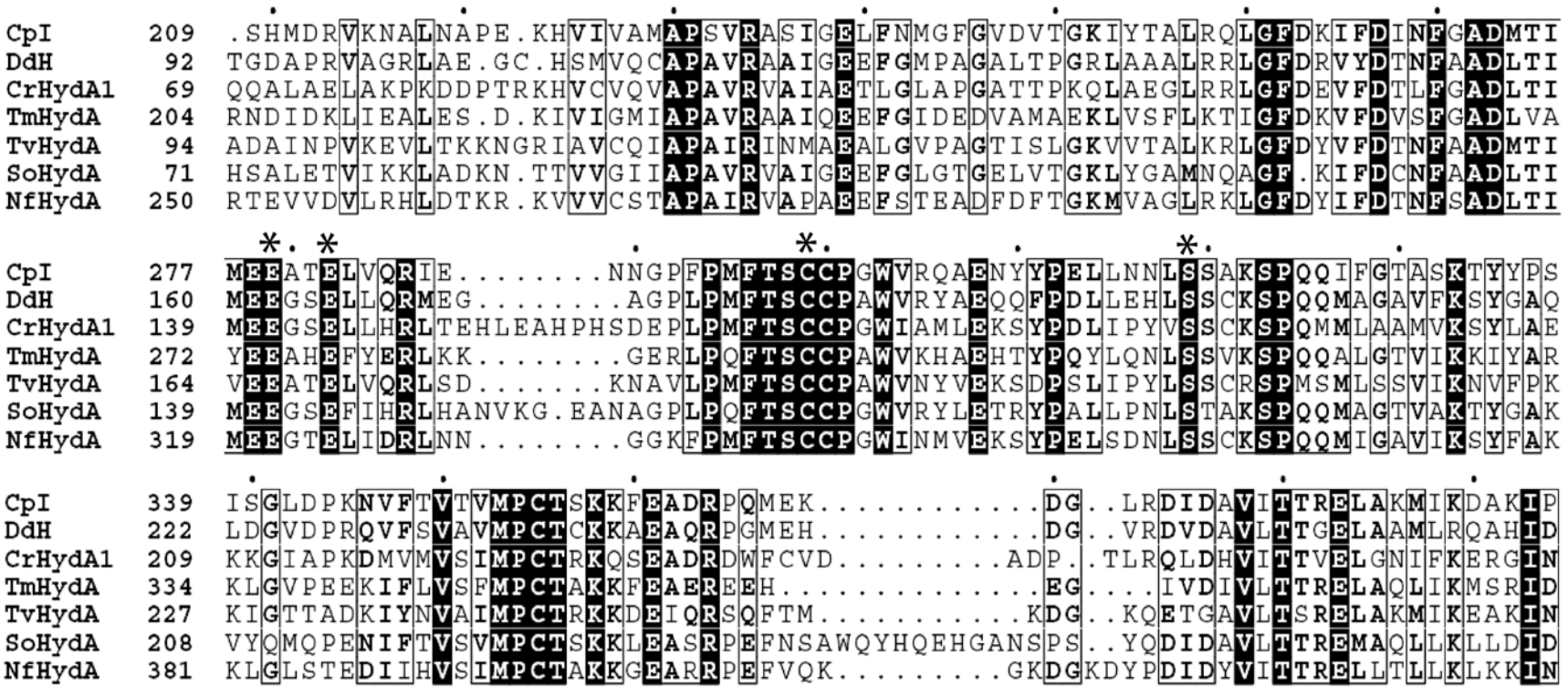

Amino Acid-Substituted Enzyme Studies—The coding sequence of the putative proton transport residues was mutated by site-directed mutagenesis PCR in the [FeFe]-hydrogenase gene from *C. pasteurianum*. N-terminal His-tagged wild-type and mutated genes were overexpressed anaerobically in a *ΔhydA/ΔhyaB strain* of *S. oneidensis* MR-1 and the resulting enzymes purified by Ni-NTA affinity chromatography. The k_{cat} of native *C. pasteurianum* hydrogenase H_2 evolution activity was calculated to be ~1,000 s^{-1}. When compared to native enzyme, all amino acid-substituted [variant] enzymes demonstrated sharp decreases in hydrogenase activity (Figure 2.3). Interestingly, in all variant enzymes, the hydrogen evolution activity is depressed to a greater extent than the hydrogen uptake activity.

In close proximity to the H-cluster, Cys299 is an ideal candidate for donating protons to the dithiolate ligand at the active site. Substitution of this residue by alanine or serine strongly decreased k_{obs}^{rel} [specific activity of variant enzyme relative to native enzyme] for both evolution and uptake activities. Substitution by serine retained slightly more hydrogenase activity, which may be due to the fact that the serine side-chain preserves a hydrogen-bonding hydroxyl group, while the alanine side-chain is aliphatic and unable to participate in proton transfer.

The residues adjacent to Cys299 in the putative pathway, Glu279 and Ser319, are also important for enzyme activity. When these residues were substituted, H_2 uptake activity of the resulting enzymes was reduced to ~85% of k_{obs}^{rel} while evolution activity was decreased by >99%.

Figure 2.3. **Relative reduction in hydrogenase activity of proton pathway variants.** k_{obs}^{rel} (specific activity of variant enzyme relative to the specific activity of native enzyme) values for H_2 evolution and uptake activities (black and gray bars, respectively). To determine the effect of substitution, the specific activity of native enzyme was normalized to 1.0. Variant enzyme k_{obs}^{rel} values were calculated from individual experiments and averaged. Error bars denote one unit of standard deviation. N=3-8.

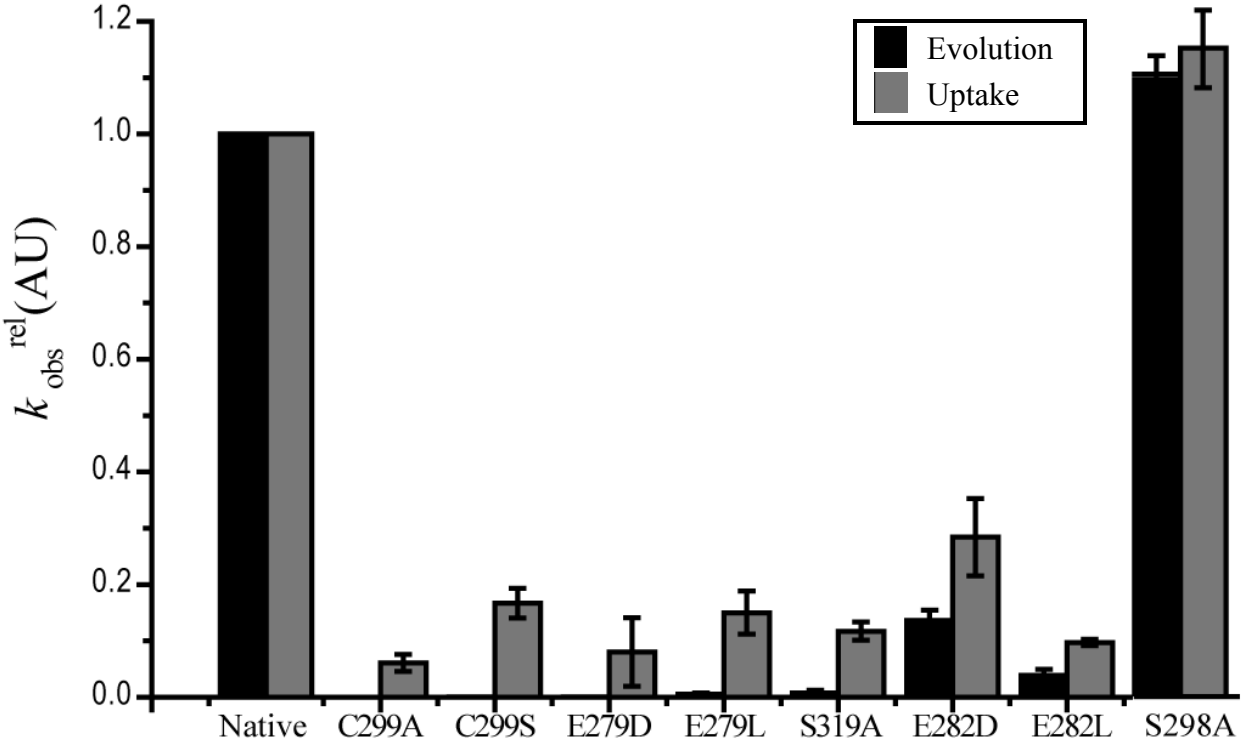

At the enzyme surface, the Glu282 residue is solvent-exposed and ideally positioned to exchange protons between Ser319 and bulk solvent. The residual activity of Glu282 variant enzymes was dependent on the specific substitution. A greater reduction in activity was observed in the E282L variant compared to the E282D variant, especially with regard to H_2 uptake. These results are consistent with the structural differences of the side chains. Whereas aspartic acid and glutamic acid differ only in side-chain length, leucine lacks a protonatable side chain.

To probe the apparent discrepancy noted between the percent reduction in H_2 uptake vs. evolution activities in the amino acid-substituted hydrogenases, we calculated the E_a for each direction for the native enzyme. Our results revealed activation energies of 24 ± 3 kJ/mol (n = 5) and 45 ± 2 kJ/mol (n = 3) for H_2 evolution and uptake, respectively. The difference in the activation energies could partially explain the apparent discrepancy in the uptake vs. evolution assays to amino acid substitutions.

A second putative proton transfer pathway can be imagined from the *C. pasteurianum* hydrogenase crystal structure, starting at Cys299, passing through several modeled water molecules and Ser298, and ending at the non-conserved Lys571 residue at the enzyme surface (Figure 2.4). However, when we substituted Ser298 to alanine, the resulting enzyme had activity similar to the native enzyme (Figure 2.3), indicating that this residue is not critical for activity.

Figure 2.4. **Two potential proton transfer relays identified via analysis of the *C. pasteurianum* [FeFe]-hydrogenase crystal structure.** *A.* Residues composing pathway examined in this paper (DTMA → Cys299 → H_2O612 → Glu279 → Ser319 → Glu282). *B.* Residues composing alternate pathway (Cys299 → H_2O612 → H_2O605 → Ser298 → H_2O594 → H_2O675 → H_2O668 → Lys571). However, Lys298 is not strictly conserved, and our data reveal that Ser298 is not required for activity (Figure 2.3).

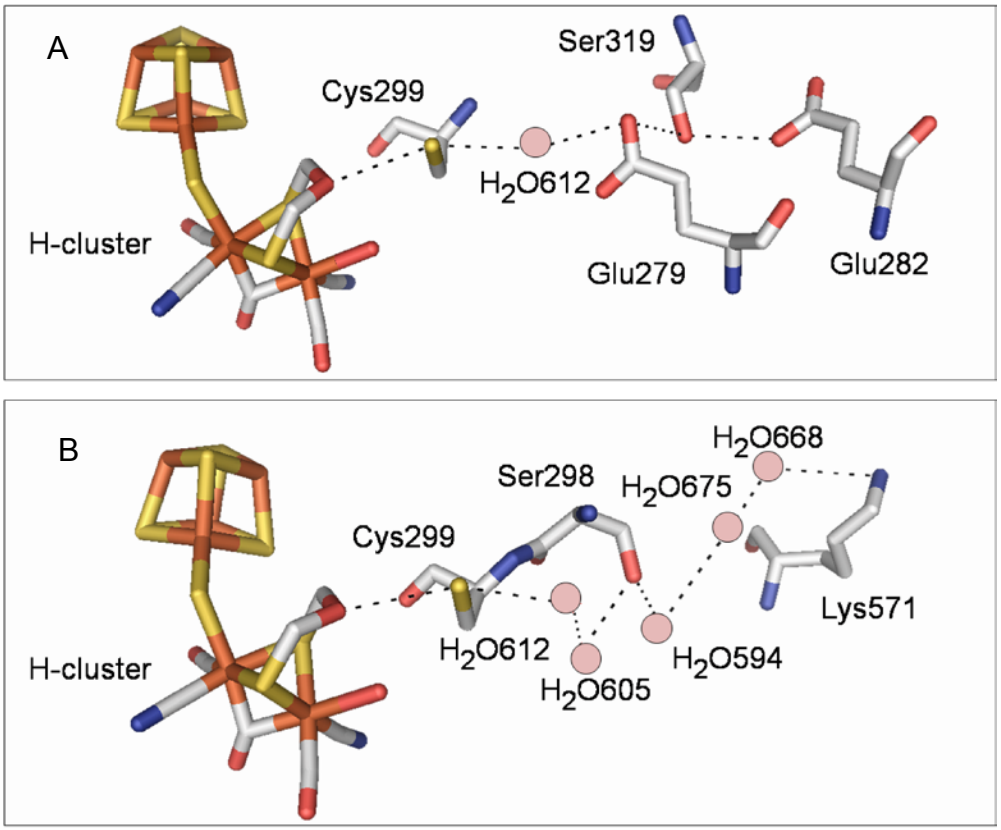

Chemical Rescue of Variant Enzyme Activity by Sodium Azide—To examine further the role of the residues identified as being potentially involved in proton transfer, hydrogen evolution activity was stimulated by the addition of a chemical recovery agent. Sodium azide has been previously demonstrated to enhance specifically *in vitro* proton transfer activity of variant enzymes deficient in proton transport (35, 36, 37). Importantly, the H_2 evolution activity of the native enzyme was unaffected by the addition of sodium azide; the chemical neither significantly promotes nor represses the hydrogenase activity. The activities of C299 and E279 variants were not stimulated by addition of sodium azide, possibly as a result of azide's inability to penetrate into the interior of the protein. In contrast, the H_2 evolution activities of the S319A, E282D, and E282L variants were all stimulated as the concentration of sodium azide was increased, providing additional evidence that the S319 and E282 residues participate in proton transfer (Table 2.2).

Table 2.2. **Measured properties of native and variant enzymes.** k_{obs}^{rel} values of evolution activities calculated as described in Figure 2.3. Zn^{2+}-binding constants, K_i, were determined for native and variant enzymes at 0.50 mM $ZnCl_2$. Fold-stimulation values are the ratio of enzyme activity with and without addition of 250 mM sodium azide. N=3-8.

	k_{obs}^{rel} (evolution)	K_i (μM)	Fold-stimulation
Wild-type	1.0000	171.9	0.89
C299S	0.0004	477.3	0.28 *
E279D	0.0004	236.9	0.73 *
E279L	0.0055	283.5	0.30 *
S319A	0.0076	107.3	1.30 *
E282D	0.1361	383.8	2.37
E282L	0.0389	3546.1	3.75 *

* p-value <0.1

Zn^{2+}-based Inhibition—Previous studies have revealed that certain divalent metal cations inhibit [FeFe]-hydrogenase, but the specific mechanism for this inhibition was not elucidated (38, 39). Importantly, divalent cations such as Zn^{2+} have been previously shown to inhibit intramolecular proton transfer in a variety of biomolecular reactions (27, 40). To determine the inhibitory effect of Zn^{2+} on *C. pasteurianum* [FeFe]-hydrogenase activity, we measured the H_2 evolution activity over a range of $ZnCl_2$ and MV concentrations. H_2 evolution activity decreased as the Zn^{2+} concentration increased. Kinetic analyses from Dixon and Cornish-Bowden plots indicated non-competitive mixed inhibition (Figure 2.5), with nearly equal values of K_i and K_i', 0.171 and 0.170 mM, respectively. These results indicate that Zn^{2+} likely binds with similar affinity to the enzyme and substrate-bound enzyme and is not competing for binding with MV. Addition of 0.50 mM $CaCl_2$ or NaCl has only a negligible effect on hydrogenase activity (data not shown), indicating that the inhibition is not due to chloride ions or a change in ionic strength. When the Zn^{2+} chelator ethylenediaminetetraacetic acid (EDTA), was titrated into a reaction containing Zn^{2+}, the enzyme activity was restored in proportion to amount of chelator added. Together, these results clarify that Zn^{2+} does not occlude MV-binding to the *C. pasteurianum* [FeFe]-hydrogenase, and that Zn^{2+} may depress enzyme activity by inhibiting proton transport.

Figure 2.5. **Inhibition plots of the effect of $ZnCl_2$ on the [FeFe]-hydrogenase from *C. pasteurianum* as a function of the concentration of methyl viologen.** *A.* Dixon plot: Concentration of $ZnCl_2$ versus the reciprocal of velocity. *B.* Cornish-Bowden plot: Concentration of $ZnCl_2$ versus the concentration of substrate over velocity. The lines from each data set intersect, indicating mixed inhibition. The K_i and K_i' calculated from each plot is 0.171 μM and 0.170 μM, respectively, indicative of noncompetitive mixed inhibition.

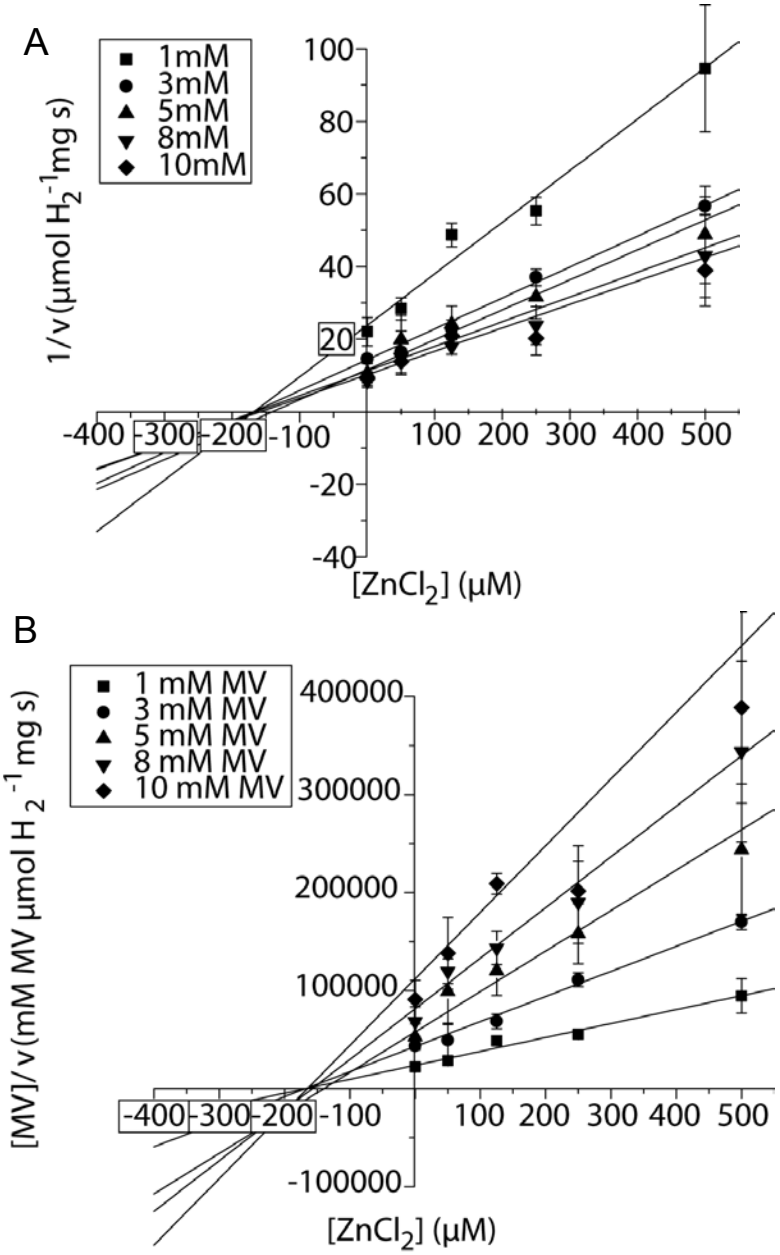

Recognizing that Zn^{2+} has high affinity for negatively-charged residues, we hypothesized that Zn^{2+} might inhibit [FeFe]-hydrogenase activity through coordination to the surface-exposed Glu282 residue, thereby blocking proton transfer. To examine more fully the effect of $ZnCl_2$, native and variant enzymes were assayed for H_2 evolution activity in both the presence and absence of 0.50 mM $ZnCl_2$. Addition of 0.50 mM $ZnCl_2$ to the assay mixture results in a 70-80% reduction in relative H_2 evolution activity for native and most variant enzymes, while the activity of the E282D variant is depressed by only ~40% (Figure 2.6). The binding constants (K_i) of Zn^{2+} to the native and most variant enzymes range between 0.1 mM and 0.4 mM (Table 2.2), with the exception of E282L. This variant enzyme maintains the same level of activity independent of Zn^{2+} concentration, with a binding constant an order of magnitude greater than that observed in the native enzyme. These data indicate that the E282L substitution renders the enzyme insensitive to Zn^{2+}, providing experimental evidence that Zn^{2+} inhibits [FeFe]-hydrogenases by binding to Glu282.

Figure 2.6. **Inhibitory effects of $ZnCl_2$ on activity of native and variant enzymes.** Relative H_2 evolution activity after addition of 0.05, 0.10, 0.25, or 0.50 mM $ZnCl_2$. Residual activity is relative to enzyme activity with 0 mM $ZnCl_2$ (1.0). Error bars denote one unit of standard deviation. N=3-8.

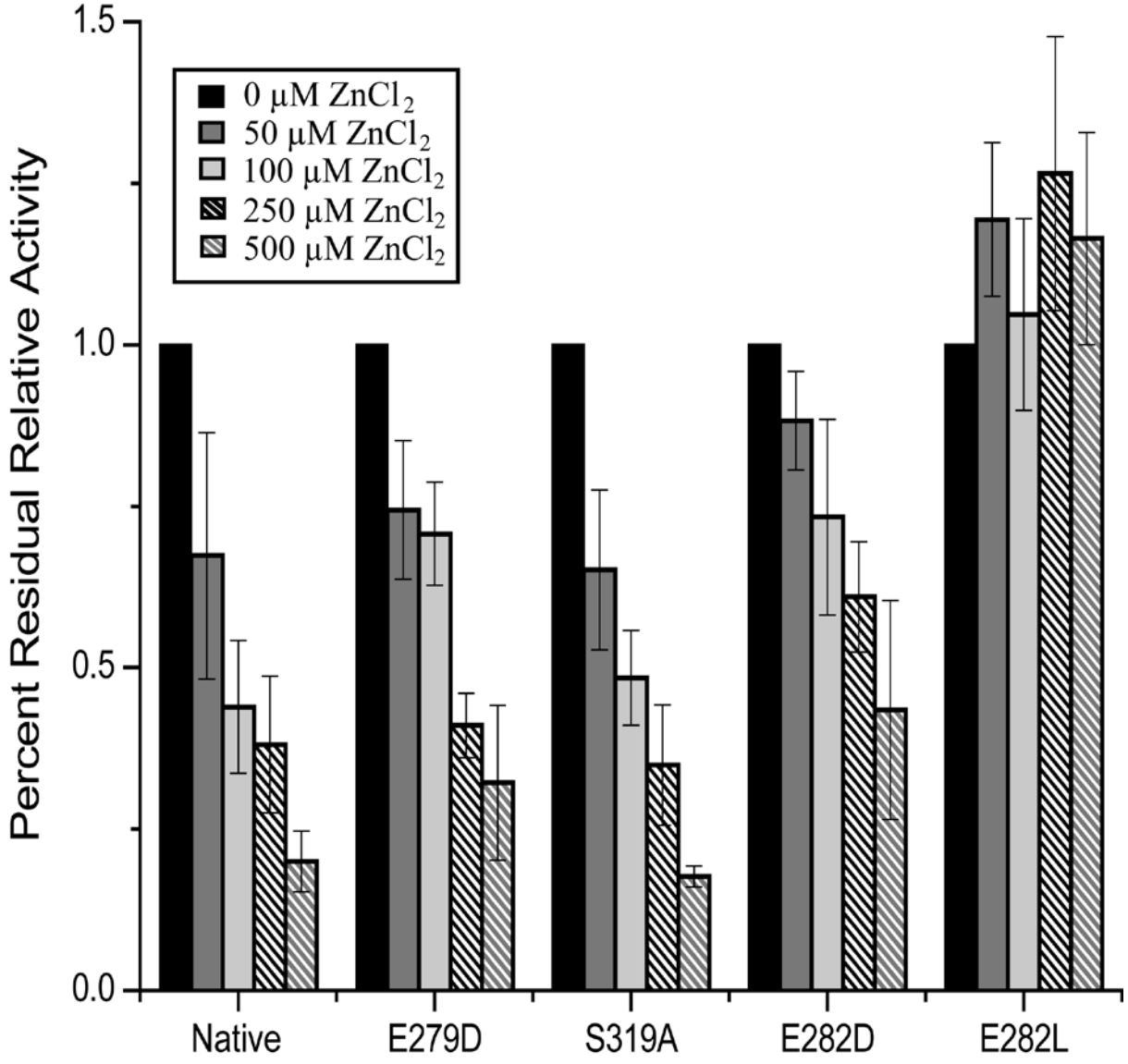

DISCUSSION

The activity of [FeFe]-hydrogenase is dependent on the transfer of protons between the enzyme surface and the H-cluster. Active intramolecular proton transport is an essential function for a variety of enzymes, and this process occurs via a proton-hopping method (Grothuss mechanism) between water molecules and the side chains of amino acid residues (26, 41, 42). Although hypothesized, this essential transfer activity has not been characterized experimentally for [FeFe]-hydrogenases.

The *C. pasteurianum* [FeFe]-hydrogenase is a soluble 63 kilodalton (kDa) periplasmic protein. Four iron-sulfur clusters, termed F clusters, are sequestered in the three N-terminal domains, while the H-cluster is buried within the catalytic domain (Figure 2.1A). From analysis of the crystal structure, the cysteine residue at position 299 has been proposed to act as a proton donor/acceptor for the H-cluster (17, 43).

When the structure of the *C. pasteurianum* hydrogenase was first determined, a putative proton transfer pathway was envisioned involving residues within hydrogen bonding-distance that link the H-cluster to the enzyme surface (17). This pathway consists of Cys299, a water molecule, Glu279, Ser319, and Glu282 (24) (Figure 2.1C). Importantly, we determined that these residues are strictly conserved, supporting the viability of this pathway (Figure 2.2).

Recent theoretical work has examined this proton pathway via quantum mechanical and molecular mechanics calculations (QM/MM) (44). As part of this study, direct proton transport between the active site dithiolate ligand and a nearby cysteine residue (analogous to Cys299) in the *D. desulfuricans* [FeFe]-hydrogenase was

calculated to be energetically favorable. Parallel simulations on the *C. pasteurianum* hydrogenase demonstrate low energy barriers for proton transfer from Glu282 to Glu279 and from Glu279 to Cys299 (44). This work therefore provides computational evidence for a putative proton transfer relay in *C. pasteurianum* [FeFe]-hydrogenase, and it establishes a basis for direct biochemical experimentation.

To investigate experimentally the role of Cys299, Glu279, Ser319, and Glu282 in the *C. pasteurianum* hydrogenase, we generated amino acid substitutions of these residues to limit hydrogen-bonding and, thus, proton transfer. Substitution of these residues causes a dramatic reduction in both H_2 uptake and evolution, indicating their importance for hydrogenase activity. Based on the crystal structure, these residues are unlikely to participate in electron transfer or significantly alter the redox potential of any of the N-terminal [FeS] clusters (Figure 2.1A) (45). Substitution of a residue responsible for coordinating either the FS2 or the FS4C [FeS] cluster (C34S and C98S, respectively) has only a moderate effect on hydrogenase activity when MV is the electron donor (data not shown). Additionally, the similarity between K_i values of the native and proton pathway variant enzymes indicates that the reduction in k_{obs}^{rel} is not due to structural changes. Finally, to examine the proton transfer activity of these residues, sodium azide was used as a chemical rescue agent. Addition of sodium azide stimulates the H_2 evolution activity of the E282 and S319 variants, whereas the native enzyme is not enhanced by azide (Table 2.2). Based on this stimulation of variant enzyme activity by azide, the noted Zn^{2+} insensitivity of the E282L variant, and computational calculations (44), the most parsimonious explanation for the observed reduction in activity of the variants is that proton transfer has been impaired.

Within hydrogen-bonding distance of the H-cluster's dithiolate ligand, Cys299 is an ideal candidate as the direct proton donor to the active site. Substitution of this residue demonstrates a dramatic reduction in hydrogenase activity and matches QM/MM predictions previously described (44). The C299S variant retains low level activity and can be further inhibited by the addition of Zn^{2+}, with a K_i similar in value to the native enzyme. Together with its close proximity to the dithiolate ligand, these results indicate that Cys299 could participate in proton transfer to the H-cluster.

In recent work examining H_2 diffusion channels, Lautier et al. measured the effect of changing the residue analogous to C299A in the [FeFe]-hydrogenase from *Clostridium acetobutylicum* (C298A) (16). The reported H_2 oxidation k_{cat} value of the C298A variant was 6-fold less than native enzyme, indicating that, under their assay conditions, a significant decrease in activity could be noted, albeit to a lesser extent than noted in our experiments (~20-fold decrease for H_2 uptake). This difference in the magnitude of reduced activity for the C299/C298 variant enzyme might be explained by the very different reaction conditions used by Lautier et al. (16). Nevertheless, both studies clearly indicate the importance of this residue for hydrogenase activity.

The solvent-exposed Glu282 residue is expected to act as a proton acceptor at the protein surface. Substitution of this residue by either leucine or aspartate causes a decrease in k_{obs}^{rel}. Interestingly, whereas the E282D variant is susceptible to Zn^{2+}-based inhibition, the E282L variant is unaffected even at 0.50 mM $ZnCl_2$. These results are consistent with previous work which established that divalent metal cations can specifically inhibit proton transfer via interactions with negatively-charged residue side-chains (27, 40). Together, our work suggests a mechanism for preferential binding of

Zn^{2+} to the surface-exposed Glu282 residue, presumably occluding proton binding and transfer.

An apparent discrepancy was noted between the k_{obs}^{rel}(uptake) and k_{obs}^{rel}(evolution) of the variant enzymes, with H_2 evolution activity more strongly impaired by substitution relative to uptake activity (Figure 2.3). To investigate this apparent discrepancy, we measured the activities of native and variant enzymes (C299S, E279D, and E282D) with a variety of buffers, salt concentrations, and varying pH. No set of tested conditions resulted in k_{obs}^{rel}(uptake) being equal to k_{obs}^{rel}(evolution). Next, we determined the E_a of the native enzyme for both evolution and uptake (24 ± 3 kJ/mol and 45 ± 2 kJ/mol, respectively). The fact that the two values are different is not surprising because the forward and reverse directions of a reaction will always have different E_as unless the free energies of the products and reactants are identical. In this particular case, however, this difference is also impacted by the fact that the H_2 uptake and evolution reactions are performed under distinct assay conditions (pH and redox partner).

The noted discrepancy (k_{obs}^{rel} of evolution versus uptake) is likely a result of this disparity between the calculated E_a values. The effect of mutating a residue important for hydrogenase activity is expected to increase the energy of the transition state by the same magnitude for both directions of the reaction. Because H_2 uptake has a higher activation energy under our reaction conditions, however, the percent change in the E_a between native and variant enzyme will be less for H_2 uptake. Thus, one would predict that mutations would have a smaller observed effect on the rate constant for H_2 uptake, which is exactly what we observe experimentally. Ultimately, because of the different

reaction conditions, these systems are not directly comparable, and the apparent discrepancies therefore do not imply different proton pathways for H_2 evolution and H_2 uptake.

Hong et al. identified a second potential proton transfer pathway, composed of Cys299, Ser298, five modeled water molecules, and Lys571 (44) (Figure 2.4). The surface-exposed lysine, however, is not well-conserved among [FeFe]-hydrogenase genes. In addition, our results indicate that the activity of the S298A variant enzyme is not impaired under our reaction conditions relative to the native enzyme. Thus, this potential pathway does not appear to be essential for proton transfer activity, although its potential role as a substitute pathway under certain conditions cannot be dismissed.

The five crystallographically modeled water molecules described above are in close proximity to the putative proton transfer pathway examined in this study. Thus, it could be argued that the residues we have examined play only an indirect role in proton transfer via interactions with this water channel. While theoretically possible, this scenario seems unlikely given the insensitivity of hydrogenase activity to amino acid substitutions of Ser298 and the importance of Glu282 to proton transport as determined by Zn^{2+} inhibition. Importantly, there does not appear to be any other chain of crystallographically-observed water molecules in the vicinity of our putative proton channel.

In conclusion, we demonstrated the importance of Cys299, Glu279, Ser319, and Glu282 in the [FeFe]-hydrogenase from *C. pasteurianum* for activity. Together with a crystallographically characterized water molecule, these residues form a potential hydrogen bonding chain from the active site to the enzyme surface. Amino acid

substitution of any of these residues causes a severe reduction in hydrogenase activity. In many cases, this activity could be partially restored by incubation with sodium azide, providing additional evidence that these residues (Ser319 and Glu282) are important for proton transfer. Substitution of the solvent-exposed Glu282 by leucine renders the enzyme insensitive to $ZnCl_2$, indicating that Zn^{2+} inhibits enzyme activity by binding to this residue and occluding the proton transfer pathway. Because Cys299, Glu279, Ser319, and Glu282 are strictly conserved, these residues may constitute a key proton transport relay in all [FeFe]-hydrogenases.

REFERENCES

REFERENCES

1. Ghirardi M. L., Posewitz M. C., Maness P. C., Dubini A., Yu J., Seibert M. (2007). Hydrogenases and hydrogen photoproduction in oxygenic photosynthetic organisms. *Annu. Rev. Plant Biol.* 58, 71-91.

2. Vignais P. M., Billoud B., Meyer J. (2001). Classification and phylogeny of hydrogenases. *FEMS Microbiol. Rev.* 25(4), 455-501.

3. Frey M. (2002). Hydrogenases: hydrogen-activating enzymes. *Chembiochem* 3(2-3), 153-160.

4. Adams M. W. (1990). The structure and mechanism of iron-hydrogenases. *Biochim. Biophys. Acta* 1020(2), 115-145.

5. Wright J. A., Pickett C. J. (2009). Protonation of a subsite analogue of [FeFe]-hydrogenase: mechanism of a deceptively simple reaction revealed by time-resolved IR spectroscopy. *Chem. Commun. (Camb)* (38), 5719-5721.

6. Vannucci A. K., Wang S., Nichol G. S., Lichtenberger D. L., Evans D. H., Glass R. S. (2010). Electronic and geometric effects of phosphatriazaadamantane ligands on the catalytic activity of an [FeFe] hydrogenase inspired complex. *Dalton Trans.* 39(12), 3050-3056.

7. Shepard E. M., Duffus B. R., George S. J., McGlynn S. E., Challand M. R., Swanson K. D., Roach P. L., Cramer S. P., Peters J. W., Broderick J. B. (2010). [FeFe]-hydrogenase maturation: HydG-catalyzed synthesis of carbon monoxide. *J. Am. Chem. Soc.* 132(27), 9247-9249.

8. Mulder D. W., Boyd E. S., Sarma R., Lange R. K., Endrizzi J. A., Broderick J. B., Peters J. W. (2010). Stepwise [FeFe]-hydrogenase H-cluster assembly revealed in the structure of $HydA^{\Delta EFG}$. *Nature* 465(7295), 248-251.

9. Czech I., Stripp S., Sanganas O., Leidel N., Happe T., Haumann M. (2011). The [FeFe]-hydrogenase maturation protein HydF contains a H-cluster like [4Fe4S]-2Fe site. *FEBS Lett.* 585(1), 225-230.

10. Shepard E. M., McGlynn S. E., Bueling A. L., Grady-Smith C. S., George S. J., Winslow M. A., Cramer S. P., Peters J. W., Broderick J. B. (2010). Synthesis of the 2Fe subcluster of the [FeFe]-hydrogenase H cluster on the HydF scaffold. *Proc. Natl. Acad. Sci. U.S.A.* 107(23), 10448-10453.

11. Goldet G., Brandmayr C., Stripp S. T., Happe T., Cavazza C., Fontecilla-Camps J. C., Armstrong F. A. (2009). Electrochemical kinetic investigations of the reactions of [FeFe]-hydrogenases with carbon monoxide and oxygen: comparing the importance of gas tunnels and active-site electronic/redox effects. *J. Am. Chem. Soc.* 131(41), 14979-14989.

12. Liebgott P. P., Leroux F., Burlat B., Dementin S., Baffert C., Lautier T., Fourmond V., Ceccaldi P., Cavazza C., Meynial-Salles I., Soucaille P., Fontecilla-Camps J. C., Guigliarelli B., Bertrand P., Rousset M., Leger C. (2010). Relating diffusion along the substrate tunnel and oxygen sensitivity in hydrogenase. *Nat. Chem. Biol.* 6(1), 63-70.

13. Stripp S. T., Goldet G., Brandmayr C., Sanganas O., Vincent K. A., Haumann M., Armstrong F. A., Happe T. (2009). How oxygen attacks [FeFe] hydrogenases from photosynthetic organisms. *Proc. Natl. Acad. Sci. U.S.A.* 106(41), 17331-17336.

14. Fontecilla-Camps J. C., Amara P., Cavazza C., Nicolet Y., Volbeda A. (2009). Structure-function relationships of anaerobic gas-processing metalloenzymes. *Nature* 460(7257), 814-822.

15. English C. M., Eckert C., Brown K., Seibert M., King P. W. (2009). Recombinant and in vitro expression systems for hydrogenases: new frontiers in basic and applied studies for biological and synthetic H_2 production. *Dalton Trans.* (45), 9970-9978.

16. Lautier T., Ezanno P., Baffert C., Fourmond V., Cournac L., Fontecilla-Camps J. C., Soucaille P., Bertrand P., Meynial-Salles I., Leger C. (2011). The quest for a functional substrate access tunnel in FeFe hydrogenase. *Faraday Discuss.* 148, 385-407; discussion 421-341.

17. Peters J. W., Lanzilotta W. N., Lemon B. J., Seefeldt L. C. (1998). X-ray crystal structure of the Fe-only hydrogenase (CpI) from *Clostridium pasteurianum* to 1.8 angstrom resolution. *Science* 282(5395), 1853-1858.

18. Pandey A. S., Harris T. V., Giles L. J., Peters J. W., Szilagyi R. K. (2008). Dithiomethylether as a ligand in the hydrogenase h-cluster. *J. Am. Chem. Soc.* 130(13), 4533-4540.

19. Nicolet Y., Piras C., Legrand P., Hatchikian C. E., Fontecilla-Camps J. C. (1999). *Desulfovibrio desulfuricans* iron hydrogenase: the structure shows unusual coordination to an active site Fe binuclear center. *Structure* 7(1), 13-23.

20. Bethel R. D., Singleton M. L., Darensbourg M. Y. (2010). The modular assembly of clusters is the natural synthetic strategy for the active site of [FeFe] hydrogenase. *Angew. Chem. Int. Ed. Engl.* 49(46), 8567-8569.

21. Nicolet Y., de Lacey A. L., Vernede X., Fernandez V. M., Hatchikian E. C., Fontecilla-Camps J. C. (2001). Crystallographic and FTIR spectroscopic evidence of changes in Fe coordination upon reduction of the active site of the Fe-only hydrogenase from *Desulfovibrio desulfuricans*. *J. Am. Chem. Soc.* 123(8), 1596-1601.

22. Silakov A., Wenk B., Reijerse E., Lubitz W. (2009). ^{14}N HYSCORE investigation of the H-cluster of [FeFe] hydrogenase: evidence for a nitrogen in the dithiol bridge. *Phys Chem Chem Phys* 11(31), 6592-6599.

23. Florin L., Tsokoglou A., Happe T. (2001). A novel type of iron hydrogenase in the green alga *Scenedesmus obliquus* is linked to the photosynthetic electron transport chain. *J. Biol. Chem.* 276(9), 6125-6132.

24. Peters J. W. (1999). Structure and mechanism of iron-only hydrogenases. *Curr. Opin. Struct. Biol.* 9(6), 670-676.

25. Schultz B. E., Chan S. I. (2001). Structures and proton-pumping strategies of mitochondrial respiratory enzymes. *Annu. Rev. Biophys. Biomol. Struct.* 30, 23-65.

26. Cukierman S. (2006). Et tu, Grotthuss! and other unfinished stories. *Biochim. Biophys. Acta* 1757(8), 876-885.

27. Whitehead S. J., Iwaki M., Cotton N. P., Rich P. R., Jackson J. B. (2009). Inhibition of proton-transfer steps in transhydrogenase by transition metal ions. *Biochim. Biophys. Acta* 1787(10), 1276-1288.

28. Dementin S., Burlat B., De Lacey A. L., Pardo A., Adryanczyk-Perrier G., Guigliarelli B., Fernandez V. M., Rousset M. (2004). A glutamate is the essential proton transfer gate during the catalytic cycle of the [NiFe] hydrogenase. *J. Biol. Chem.* 279(11), 10508-10513.

29. Altschul S. F., Madden T. L., Schaffer A. A., Zhang J., Zhang Z., Miller W., Lipman D. J. (1997). Gapped BLAST and PSI-BLAST: a new generation of protein database search programs. *Nucleic Acids Res.* 25(17), 3389-3402.

30. Larkin M. A., Blackshields G., Brown N. P., Chenna R., McGettigan P. A., McWilliam H., Valentin F., Wallace I. M., Wilm A., Lopez R., Thompson J. D., Gibson T. J., Higgins D. G. (2007). Clustal W and Clustal X version 2.0. *Bioinformatics* 23(21), 2947-2948.

31. Zheng L., Baumann U., Reymond J. L. (2004). An efficient one-step site-directed and site-saturation mutagenesis protocol. *Nucleic Acids Res* 32(14), e115.

32. Ozawa K., Yasukawa F., Fujiwara Y., Akutsu H. (2001). A simple, rapid, and highly efficient gene expression system for multiheme cytochromes *c*. *Biosci. Biotechnol. Biochem.* 65(1), 185-189.

33. King P. W., Posewitz M. C., Ghirardi M. L., Seibert M. (2006). Functional studies of [FeFe] hydrogenase maturation in an *Escherichia coli* biosynthetic system. *J. Bacteriol.* 188(6), 2163-2172.

34. Fujii M., Adachi N., Shikatani K., Ayusawa D. (2009). [FeFe]-hydrogenase-like gene is involved in the regulation of sensitivity to oxygen in yeast and nematode. *Genes Cells* 14(4), 457-468.

35. Takahashi E., Wraight C. A. (2006). Small weak acids reactivate proton transfer in reaction centers from Rhodobacter sphaeroides mutated at AspL210 and AspM17. *J. Biol. Chem.* 281(7), 4413-4422.

36. Takahashi E., Wraight C. A. (1991). Small weak acids stimulate proton transfer events in site-directed mutants of the two ionizable residues, GluL212 and AspL213, in the QB-binding site of *Rhodobacter sphaeroides* reaction center. *FEBS Lett.* 283(1), 140-144.

37. Chang Y. H., Chuang L. Y., Hwang C. C. (2007). Mechanism of proton transfer in the 3alpha-hydroxysteroid dehydrogenase/carbonyl reductase from *Comamonas testosteroni*. *J. Biol. Chem.* 282(47), 34306-34314.

38. Fernandez V. M., Rua M. L., Reyes P., Cammack R., Hatchikian E. C. (1989). Inhibition of *Desulfovibrio gigas* hydrogenase with copper salts and other metal ions. *Eur. J. Biochem.* 185(2), 449-454.

39. Kamachi T., Uno S., Hiraishi T., Okura I. (1995). Effect of Hg(II) on hydrogenase activity from *Desulfovibrio vulgaris* (Miyazaki). *Journal of Molecular Catalysis A: Chemical* 96(3), 329-333.

40. Faxen K., Salomonsson L., Adelroth P., Brzezinski P. (2006). Inhibition of proton pumping by zinc ions during specific reaction steps in cytochrome *c* oxidase. *Biochim. Biophys. Acta* 1757(5-6), 388-394.

41. Nagle J. F., Morowitz H. J. (1978). Molecular mechanisms for proton transport in membranes. *Proc. Natl. Acad. Sci. U.S.A.* 75(1), 298-302.

42. Xu J., Voth G. A. (2005). Computer simulation of explicit proton translocation in cytochrome *c* oxidase: the D-pathway. *Proc. Natl. Acad. Sci. U.S.A.* 102(19), 6795-6800.

43. Nicolet Y., Lemon B. J., Fontecilla-Camps J. C., Peters J. W. (2000). A novel FeS cluster in Fe-only hydrogenases. *Trends Biochem. Sci.* 25(3), 138-143.

44. Hong G., Cornish A. J., Hegg E. L., Pachter R. (2011). On understanding proton transfer to the biocatalytic [Fe-Fe]$_H$ sub-cluster in [Fe-Fe]H$_2$ases: QM/MM MD simulations. *Biochim. Biophys. Acta* 1807(5), 510-517.

45. Moulis J. M., Davasse V. (1995). Probing the role of electrostatic forces in the interaction of *Clostridium pasteurianum* ferredoxin with its redox partners. *Biochemistry* 34(51), 16781-16788.

CHAPTER 3

An Electron Transfer Relay in the *Clostridium pasteurianum* [FeFe]-hydrogenase

INTRODUCTION

[FeFe]-hydrogenases catalyze the reversible reduction of protons to hydrogen gas (H_2) utilizing a unique catalytic [6Fe6S]-cluster (1, 2). Electrons for this reduction are donated by intracellular carriers (e.g., ferredoxin) and are typically derived from fermentation or photosynthesis (3, 4). Intermolecular electron transfer between various carriers and [FeFe]-hydrogenases has been investigated (5, 6, 7, 8), but there remains a paucity of information regarding intramolecular electron transfer. In [NiFe]-hydrogenases, a series of iron-sulfur clusters has been reported to act cooperatively as a relay to shuttle electrons between the active site and enzyme surface for H_2 production/oxidation (9). Likewise, electron transfer in [FeFe]-hydrogenases also presumably occurs through coordinated relays of iron-sulfur clusters, and understanding this pathway is integral to enhancing [FeFe]-hydrogenase activity.

[FeFe]-hydrogenases can be classified based on the number of iron-sulfur cluster-binding domains (F-domains) present in the N-terminal region of the protein. Clusters ligated by these F-domains in the hydrogenase resemble ferredoxin clusters and are either [2Fe2S] or [4Fe4S]-clusters (10, 11). Individual F-domains are characterized by their binding to either [4Fe4S] or [2Fe2S] clusters, as well as the coordination environment. The number of these domains can vary between different [FeFe]-hydrogenases (12), except for green algal hydrogenases, which lack F-domains and instead permit direct transfer between an electron carrier and the active site (1, 6). The [FeFe]-hydrogenase from *Clostridium pasteurianum* has four F-domains, three of which utilize a typical four-cysteine motif to ligate one [2Fe2S]-cluster and two [4Fe4S]-

clusters (FS2, FS4A, and FS4B, respectively). A fourth F-domain coordinates an additional [4Fe4S]-cluster, which is ligated by three cysteines and a histidine (FS4C). This overall domain structure is conserved among approximately 75% of known and putative [FeFe]-hydrogenases (Figure 3.1A).

By examining the *C. pasteurianum* hydrogenase three-dimensional structure (3C8Y, www.pdb.org), a putative electron transfer relay can be inferred between the active site and medial FS4B From this cluster, the relay branches into two distal F-domains (FS4C and FS2), preventing a definitive role for these two clusters in electron transfer activity to be assigned (Figure 3.1B) (13). An identical electron transfer relay in *Clostridium acetobutylicum* HydA has been shown to be functional during light-induced H_2 production experiments directly connecting the hydrogenase to photosystem I (14). In addition, Brownian dynamics studies have indicated that ferredoxin could potentially bind to positively-charged residues on the enzyme surface and pass electrons to the FS4C (15). Without direct experimental evidence, however, the role of the FS4C and FS2 clusters in electron transfer can only be surmised, and the prevalence of this domain structure among [FeFe]-hydrogenases provides a rationale for investigating the importance of these clusters.

Figure 3.1 **Iron-sulfur clusters and cluster domains in [FeFe]-hydrogenases.** A) Graphic illustration of iron-sulfur cluster-binding domains and the amino acid motifs associated with each domain. B) Putative electron transfer *of Clostridium pasteurianum* [FeFe]-hydrogenase (3C8Y (16)) composed of four iron-sulfur clusters between the catalytic active site and the enzyme surface. Based on sequence homology, ~75% of sequence [FeFe]-hydrogenases are predicted to have similar cluster organization.

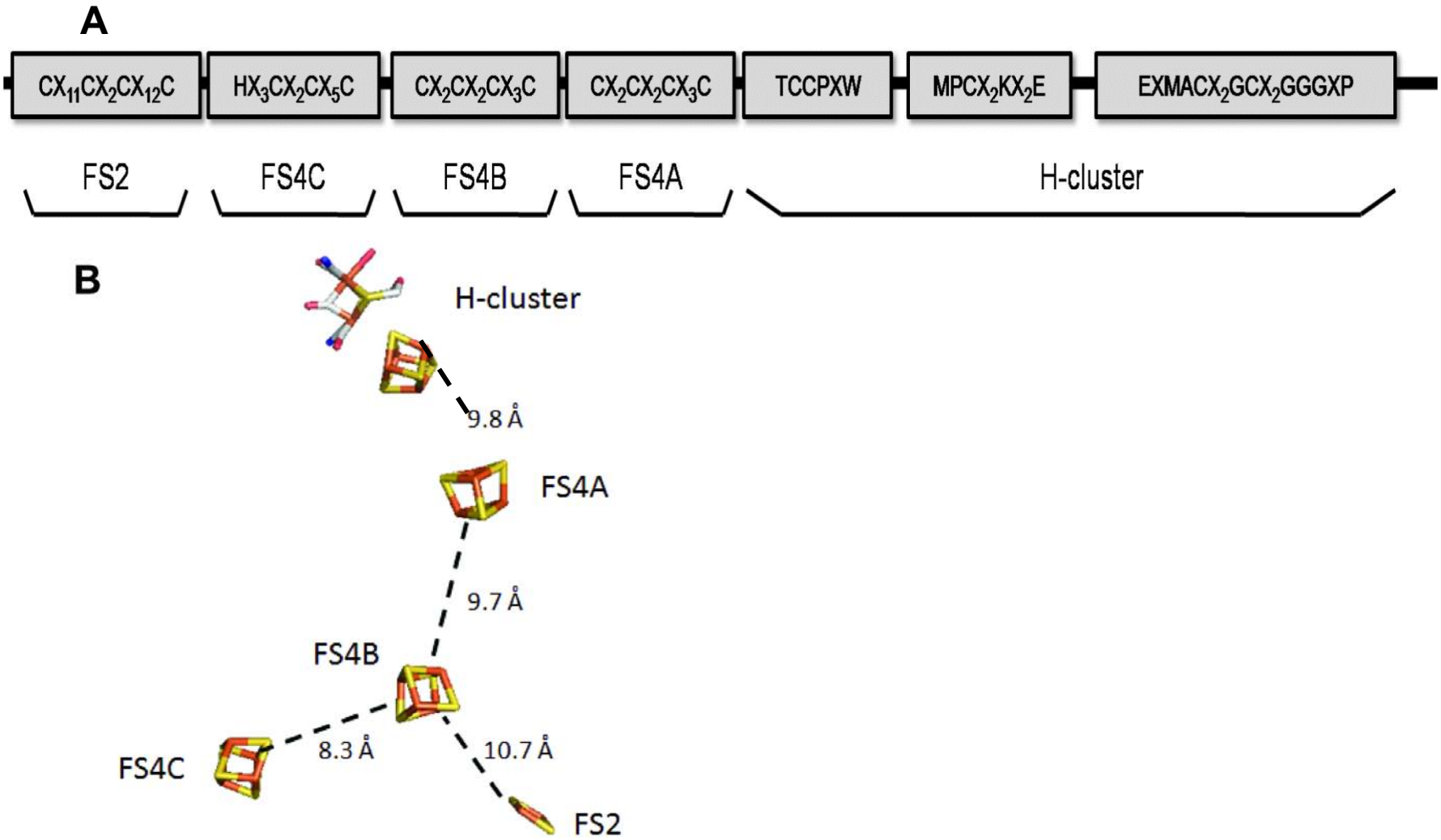

To test the role of this relay in hydrogenase activity, we exchanged two cysteine residues with serines (C98S and C34S) in the *C. pasteurianum* [FeFe]-hydrogenase to alter the reduction potential of the two distal iron-sulfur clusters (FS4C and FS2, respectively). Single substitutions of these residues caused a decrease in both *in vitro* and *in vivo* activities when compared to the native enzyme, and this effect was compounded in the doubly-substituted variants. Protein-folding analyses demonstrated that the variant and native enzymes share similar folding characteristics, suggesting that these amino-acid substitutions alter [FeFe]-hydrogenase activity by disrupting the FS4C and FS2 clusters.

METHODS

Overexpression, Plasmid Construction, and Site-directed Mutagenesis—The *C. pasteurianum hydA* gene was PCR amplified and inserted into the pAC-BAD vector as previously described by Cornish et al. (17). Selected amino acid codons in the *hydA* gene were mutated by site-directed mutagenesis PCR using the primers (*Pfu* turbo, Stratagene) listed in Table 3.1 (18). Mutated PCR product was isolated by DpnI digestion (New England Bioloabs) of the methylated template DNA at 37˚C for 2 h , followed by transformation into DH5α *E. coli* cells and selection on LB plates supplemented with 50 μg/mL kanamycin sulfate. DNA was isolated from appropriate transformant colonies, and the desired mutations were confirmed by DNA sequencing. The constructs were transformed into electrocompetent *Shewanella oneidensis* MR-1 *ΔhydAΔhyaB* cells and selected for resistance to 50 μg/mL kanamycin (19).

Table 3.1. **Primer pairs used for site-directed mutagenesis PCR of the *C. pasteurianum* HydA gene in the pAC-BAD vector**

Identity	Sequence
C34S Sense	5'-ATATCTGCACTGTCTTTTTTAAATAAT-3'
C34S Antisense	5'-ATTATTTAAAAAAGACAGTGCAGATAT-3'
C98S Sense	5'-CATGAATTCAAATCTGGTCCTTGCAAT-3'
C98S Antisense	5'-ATTGCAAGGACCAGATTTGAATTCATG-3'

Cell Growth, Induction, and Purification—S. oneidensis MR-1 *ΔhydAΔhyaB* cells harboring the wild-type and mutated pAC-BAD:*hydA* constructs were cultured and gene expression was induced as described by Cornish et. al (17), except that all cultures were grown in a final volume of 1 L of antibiotic- and L-arabinose-supplemented LB media. All purification steps were performed anaerobically, using either a glove box (Coy Laboratory Products) or airtight Nalgene tubes. 16 h after addition of L-arabinose, the cells were pelleted by centrifugation at 2,800× *g* and the supernatant was discarded. The pellet was resuspended in 7 mL of nickel-nitrilotriacetic acid (Ni-NTA) wash buffer (100 mM Tris-HCl [pH 8.0], 200 mM NaCl, and 5.0% glycerol) that was supplemented with 10 mM $Na_2S_2O_4$. The resuspension was aliquoted into seven 1.7 mL disposable tubes (Eppendorf) and was lysed by sonicating each sample 8 times at 4 s intervals and a power setting of 4 using the Fisher Scientific Model 100 Sonic Dismembrator at 4 sec intervals. Lysed cells were centrifuged at 20,000× *g* to clear the lysate. Columns for protein purification were filled with 1 ml Ni-NTA agarose (Qiagen) and washed with 15 mL of 10 mM $Na_2S_2O_4$-supplemented Ni-NTA buffer to remove residual O_2. The supernatant was applied to the column and allowed to completely flow through. The column was sequentially washed with 10 mL of $Na_2S_2O_4$-supplemented Ni-NTA buffer, 10 mL of unsupplemented Ni-NTA buffer, and 5 mL of 20 mM imidazole-supplemented Ni-NTA buffer. Bound protein was eluted from the column in 1 mL-fractions by applying 100 mM imidazole-supplemented Ni-NTA buffer. Qualitative hydrogenase uptake activity was measured by incubating 20 µL of elution fraction with 20 µL of 10 mM benzyl viologen dichloride (BV) for 5 min and noting the appearance of a purple color. Consistently, the second elution fraction from each purification showed the greatest

change in color. The protein concentration of the elution fractions was determined using the Pierce BCA Assay Kit and comparison to a bovine serum albumin (BSA) standard curve.

Circular Dichroism—Protein samples were desalted and concentrated prior to measuring the circular dichroism (CD) spectra. To desalt/concentrate the sample, a 0.5 mL aliquot of an elution fraction containing the 100 mM imidazole and purified enzyme was applied to an Amplicon Ultra-0.5 centrifugal filter device (Millipore). The sample was by centrifuged at 14,000× *g* for 10 min and the flow through was discarded. The remaining elution fraction (~0.4 mL) was applied to the filter and the procedure repeated. The samples were then resuspended in 0.4 ml of Ni-NTA buffer and centrifuged again for 10 min at 14,000× *g* for 10 min to desalt the solution. This step was repeated once more.

The concentrated sample was transferred to a quartz cuvette with a 1.0 mm pathlength, and CD spectra were recorded using a Chirascan CD spectrometer (Applied Photophysics). The scan speed was 6 nm/min, and the spectra were recorded using a 1 nm bandwidth over the range of 180 - 260 nm. Analysis was carried out utilizing the DichroWeb Interface (http://dichroweb.cryst.bbk.ac.ukl), using the CDSSTR program (20) and comparison to the Set 7 reference.

Hydrogen Uptake Activity Assays—Hydrogen uptake activity was measured by preparing 1.9 mL of H_2 uptake buffer [100 mM potassium phosphate buffer (pH 6.8), 2 mM dithiothreitol, 10 mM methyl viologen dichloride (MV) or BV] in a Pyrex Schlenk

cuvette. After sealing the cuvette with a rubber septum, the headspace gas was exchanged with 100% H_2 gas at 1 atm. The cuvette was returned to the glove box and 0.1 mL of the protein sample was added to the reaction. The Abs_{604} of the samples was measured every 20 sec using a UV-Visible Spectrophotometer (Hewlett-Packard) using the "kinetics" mode on the Agilent UV-Vis ChemStation software. The reaction time was 3 min and the cuvette was briefly shaken between measurements.

Hydrogen Evolution Activity Assays—H_2 evolution activity with an abiotic electron donor was measured by first preparing 1.9 mL of H_2 evolution buffer (100 mM potassium phosphate buffer [pH 6.8], 100 mM $Na_2S_2O_4$, 10 mM MV) in 10 mL serum vials (Wheaton). The vials were sealed with rubber septa (Bellco) and the headspace gas exchanged with Ar at 1 atm. After returning the vials to the glove box, 0.1 mL of protein sample was added to each and the vials were shaken at ~100 rpm at 25°C. A 100 µL syringe (Hamilton) was used to inject 20 µL of headspace gas into a TRACE GC Ultra gas chromatograph (Thermo Scientific) and the resulting peak area was converted to µmol H_2 by comparison to a standard curve. The rate of H_2 evolution was measured as the change in µmol of H_2 in the headspace over time per mg of protein. For determination of K_m and V_{max}, the concentration of MV was varied from 0.5 to 10 mM.

H_2 evolution activity with a biotic electron donor was measured as described for activity with an abiotic donor, except that the 10 mM MV was replaced by 20 µM *C. pasteurianum* ferredoxin. In addition, the vials were incubated at 30°C. For determination of K_m and V_{max} the concentration of ferredoxin was varied from 5 to 20 µM.

RESULTS

Enzyme Purification and Circular Dichroism Spectroscopy—Specific cysteine residues ligating the FS4C and FS2 clusters (Cys98 and Cys34, respectively) were substituted with serine residues, generating both singly- and doubly-substituted forms of the enzyme. N-terminally His-tagged forms of both the native and amino acid-substituted proteins [variants] were purified from *S. oneidensis* MR-1 *ΔhydAΔhyaB* cells using Ni-NTA affinity chromatography.

Altering the native ligand coordination of an iron-sulfur cluster has the potential to disrupt binding and cause loss of the cluster, thereby destabilizing protein folding. To investigate folding properties of the native and variant enzymes, protein samples were washed (to remove imidazole) and concentrated, and the overall folding of each enzyme samples was analyzed by CD spectroscopy. Analyses of the spectra indicate that the length and number of α-helices and β-strands are consistent between the enzymes, suggesting that the variants have similar folding characteristics to the native enzyme (Table 3.2, Figure 3.2). In addition, these spectra are in agreement with secondary structure predictions of the *C. pasteurianum* hydrogenase, as well as solved crystal structures of the enzyme. The overall structures of the variants are similar to the native enzyme and changes in folding are unlikely to disrupt hydrogenase activity.

Table. 3.2. **Secondary structure analysis of native and variant enzymes.** "Observed" denotes expected results based on the solved crystal structure of the *C. pasteurianum* [FeFe]-hydrogenase.

	Observed	**Variant**	**C34S**	**C98S**	**C34S/C98S**
α-helices per 100 residues	3.6	3.5	4.2	3.5	3.5
Average length of α-helices	13.3	16.3	14.0	16.1	14.7
β-strands per 100 residues	3.6	4.0	3.8	3.5	4.3
Average length of β-strands	4.6	4.6	4.3	4.7	4.3

Figure 3.2. **CD spectra of native and variant enzymes.** Circular dichroism spectra of native and variant enzymes recorded in millidegrees, ranging from 200-260 nm. Spectra <200 nm are unordered and were not used for analysis. Spectra have not been normalized to protein concentration.

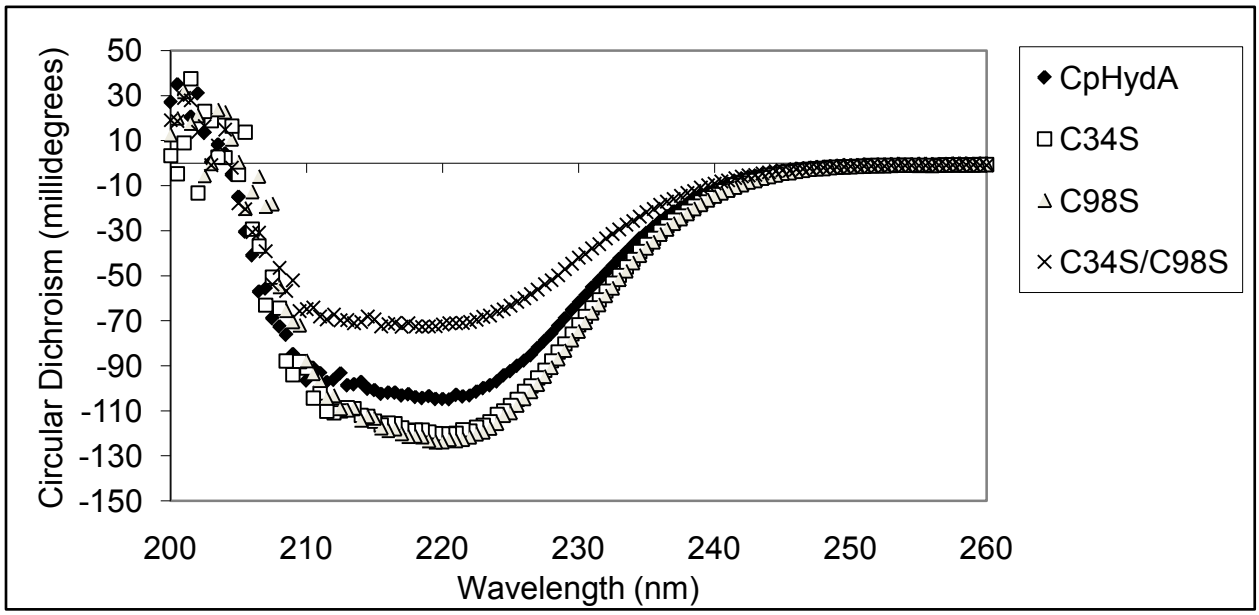

H_2 Uptake Assays—Purified native and variant proteins were tested for H_2 uptake activity in the presence of an abiotic electron acceptor (BV) under 1 atm H_2. A sharp decrease in the k_{obs}^{rel} [specific activity of variant enzyme relative to that of the native enzyme] for both the C34S and C98S variants was noted (Table 3.3, Figure 3.3). The doubly-substituted variant (C34S/C98S) demonstrated uptake activity that was barely above detection limit of the assay (0.00075 AU/s) and was only 0.3% as active as the native enzyme. These results indicate that proper ligation of both clusters is required for maximal H_2 uptake activity.

To learn more about the interaction between BV and the enzymes during H_2 uptake, K_m and V_{max} values of the native and variant proteins for H_2 uptake were calculated as a function of BV concentration (Table 3.4). The V_{max} values calculated for the singly- and doubly-substituted variants were 5- and >100-fold less, respectively, than the native enzyme V_{max}, closely resembling the k_{obs}^{rel} data. Conversely, there was little difference between the calculated BV K_m values, suggesting that, although hydrogenase activity is impaired in the variants, the relationship between enzyme and substrate may remain unaltered.

Table 3.3. **Native and variant enzyme k_{obs}^{rel} values.** Comparison of k_{obs}^{rel} H_2 uptake activities using benzyl viologen (BV) and evolution activities using methyl viologen (MV) and ferredoxin. Values are calculated as described in Figure 3.3.

	Uptake BV	Evolution MV	Evolution ferredoxin
Native	1.00	1.00	1.00
C34S	0.267	0.119	0.109
C98S	0.244	0.116	0.139
C34S/C98S	0.003	0.052	0.078

Figure 3.3. **Relative reduction in hydrogenase activity of singly- and doubly-substituted variants.** k_{obs}^{rel} (rate of variant enzyme relative to the rate of native enzyme) values for H_2 uptake using benzyl viologen (BV) and evolution activities using methyl viologen (MV) or ferredoxin. To determine the effect of substitution, the specific activity of native enzyme was normalized to 1.0. Variant enzyme k_{obs}^{rel} values were calculated from individual experiments and averaged.

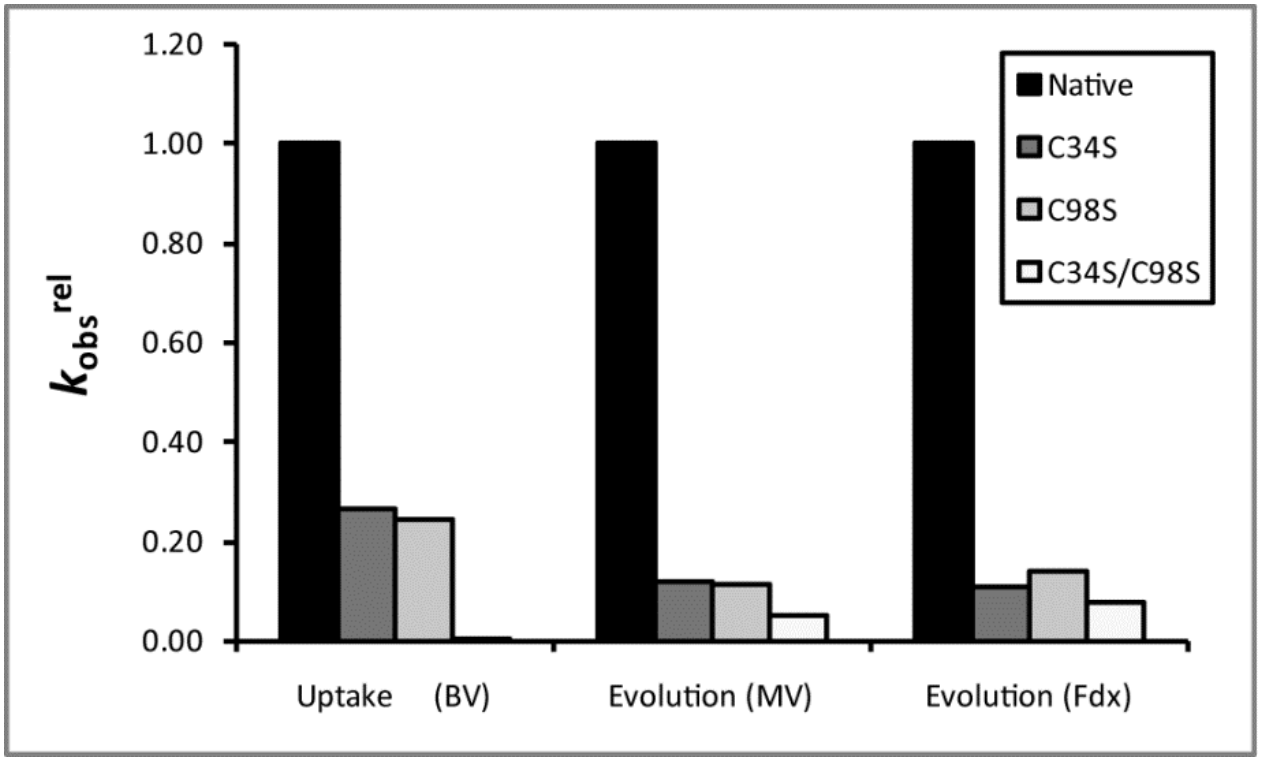

Table 3.4. **Kinetic values of native and variant enzymes.** K_m and V_{max} values calculated for H_2 uptake using benzyl viologen (BV) and H_2 evolution using methyl viologen (MV) and ferredoxin.

K_m (μM)	Uptake BV	Evolution MV	Evolution ferredoxin
Native	2990	1160	1.70
C34S	2370	1550	1.67
C98S	2240	1170	1.91
C34S/C98S	1380	3780	2.02

V_{max} (μmol H_2/mg/s)	Uptake BV	Evolution MV	Evolution ferredoxin*
Native	11.4	1.11	37.3
C34S	2.23	0.08	4.28
C98S	2.66	0.16	6.30
C34S/C98S	0.03	0.003	0.23

*units are in nmol H_2/mg/s

H_2 Evolution Assays—To examine the effect of the serine substitutions on H_2 evolution, the native and variant enzymes were tested for H_2 evolution activity using an abiotic electron donor system (10 mM MV and 100 mM $Na_2S_2O_4$). All three variant enzymes were deficient in evolution activity relative to the native enzyme, retaining only 5-12% of k_{obs}^{rel} (Table 3.3, Figure 3.3), similar to the H_2 uptake data.

To calculate K_m and V_{max} values for H_2 evolution, the primary electron donor ($Na_2S_2O_4$) concentration was kept constant as the concentration of the direct electron donor (MV) was varied between 1 and 10 mM. As observed with the k_{obs}^{rel} data, the singly-substituted enzyme V_{max} values were greatly reduced in comparison to the native enzyme, while the calculated V_{max} for C34S/C98S variant was <1% (Table 3.4), again closely matching the H_2 uptake results, indicating that the FS2 and FS4C clusters must be fully ligated for optimal activity with abiotic donors.

The variant enzymes are decreased in activity relative to the native enzyme when supplied with an artificial electron carrier, but this provides no direct information on putative interactions with biotic electron donors. To explore these interactions, native and variant enzymes were tested for H_2 evolution activity using 20 μM *C. pasteurianum* ferredoxin (and 100 mM $Na_2S_2O_4$ as a reductant) as a biotic electron donor system. The k_{obs}^{rel} values for all of the variants were less than the native enzyme, generating values which closely matched the pattern of the abiotic donor H_2 evolution activities (Table 3.3, Figure 3.3), and suggesting that disrupting the clusters has a similar impact on accepting electrons from both abiotic and biotic donors. When kinetic parameters were calculated using ferredoxin, all enzymes were found to have similar K_m values,

whereas the variant V_{max} values were at least 5-fold reduced in comparison to the native enzyme (Table 3.4), again resembling the MV data.

DISCUSSION

The *C. pasteurianum* [FeFe]-hydrogenase ligates four iron-sulfur clusters that are hypothesized to compose an electron transfer relay between the active site and enzyme surface. The iron-sulfur cluster-binding domains (FS4A, FS4B, FS4C, and FS2) which coordinate the clusters in this relay are conserved among 75% of sequenced [FeFe]-hydrogenases. This relay branches near the enzyme surface to the FS4C and FS2 clusters, but the role of this branch point has yet to be directly investigated.

During H_2 oxidation, electrons are passed from the H-cluster to FS4A and then FS4B, which is the branchpoint for the relay. From FS4B, electrons can be transferred to an electron acceptor at the enzyme surface via either the FS4C or FS2 clusters (Fig 3.1). Peters et al. hypothesized either that these clusters could modulate the redox potential for optimal electron transfer, that specific clusters were associated with only H_2 evolution or H_2 uptake activities, or that different physiological electron carriers might interact separately with these clusters (13) and we set out to test these hypotheses.

To investigate the roles of the FS4C and FS2 clusters in both electron transfer and hydrogenase activity, residues ligating these clusters (Cys98 and Cys34, respectively) were substituted with serine residues to alter the reduction potential of the clusters (21). Serine can act as a ligand to iron-sulfur clusters, and this type of substitution has been used previously to alter the reduction potential of a cluster while still maintaining a stable coordination environment (9). To test if the single or double substitutions in the *C. pasteurianum* hydrogenase disrupted protein folding, the secondary structure of the native and variant enzymes was investigated using CD spectroscopy and subsequently

compared to predicted structural models. As seen in Figure 3.2, the spectra are similar in shape, although differ in amplitude, which may be due to differences in protein concentration between the samples. Importantly, spectral analysis indicates that all of the enzymes share similar secondary structures to one another. In addition, the values of the native and variant proteins closely matched predicted structural models, further suggesting that protein folding is not disrupted in the variant enzymes.

When serine was substituted for cysteine, the activity of the singly-and doubly-substituted variants were reduced in comparison to the native enzyme for *both* H_2 evolution and H_2 uptake activities (k_{obs}^{rel} and V_{max}). Additionally, extremely similar reductions in H_2 evolution k_{obs}^{rel} and V_{max} values were calculated when the enzymes were supplied with either biotic or abiotic donors. Together, these results provide evidence that both H_2 evolution and uptake are impaired by these mutations, that incorrect ligation of *either* of the distal clusters can cause this impairment, and that the decrease in H_2 evolution activity of the variants is independent of the electron donor identity.

Comparison of the H_2 uptake and H_2 evolution data reveals that, for the C34S and C98S variants in relation to native enzyme, there was a greater reduction in H_2 evolution activity than there was in H_2 uptake activity. This effect was observed previously by Cornish et al. while investigating hydrogenase proton transfer (17). A possible explanation for this disparity may lie in the difference between the driving forces and that each reaction was far outside of equilibrium (excess substrate conditions). In addition, the reduction potentials for MV and BV differ (-450 mV and -350

mV, respectively), which could also cause a disparity between the measured H_2 uptake and H_2 evolution k_{obs}^{rel} values (22).

A strange pattern was observed in examining the K_m values calculated using abiotic donors. These data would suggest that disruption of one or both distal clusters leads to an *increase* in reactivity with BV during H_2 uptake and a *decrease* in reactivity with MV during H_2 evolution, and this does not seem to match the values calculated with ferredoxin. These experiments need to be repeated using a broader range of substrate concentrations to determine the cause of these conflicting data.

In conclusion, we have explored the importance of two distal iron-sulfur clusters that constitute a branching point in the *C. pasteurianum* [FeFe]-hydrogenase. Substitution of residues affecting either cluster causes a reduction in both H_2 evolution and H_2 uptake activity relative to native enzyme, and activity of the doubly-substituted enzyme is reduced by >90%. CD spectral analysis provide strong evidence that impairment of activity does not correlate to protein misfolding. Together, these results demonstrate that this relatively common electron transfer relay is dependent on both of the distal clusters for hydrogenase activity, as these clusters are essential in either directly accepting electrons or modulating the reduction potential of the cluster involved in electron transfer. Importantly, further characterization of this relay may provide important insight into the mechanisms of [FeFe]-hydrogenase activity.

REFERENCES

REFERENCES

1. Vignais P. M., Billoud B. (2007). Occurrence, classification, and biological function of hydrogenases: an overview. *Chem. Rev.* 107(10), 4206-4272.

2. Adams M. W. W. (1990). The structure and mechanism of iron-hydrogenases. *Biochim. Biophys. Acta* 1020(2), 115-145.

3. Ghirardi M. L., Dubini A., Yu J., Maness P. C. (2009). Photobiological hydrogen-producing systems. *Chem. Soc. Rev.* 38(1), 52-61.

4. Kim D. H., Kim M. S. (2011). Hydrogenases for biological hydrogen production. *Bioresour. Technol.* 102(18), 8423-8431.

5. Schuchmann K., Müller V. (2012). A bacterial electron-bifurcating hydrogenase. *J. Biol. Chem.* 287(37), 31165-31171.

6. Winkler M., Hemschemeier A., Jacobs J., Stripp S., Happe T. (2010). Multiple ferredoxin isoforms in *Chlamydomonas reinhardtii* - their role under stress conditions and biotechnological implications. *Eur. J. Cell. Biol.* 89(12), 998-1004.

7. Jacobs J., Pudollek S., Hemschemeier A., Happe T. (2009). A novel, anaerobically induced ferredoxin in *Chlamydomonas reinhardtii*. *FEBS Lett.* 583(2), 325-329.

8. ElAntak L., Morelli X., Bornet O., Hatchikian C., Czjzek M., Dolla A., Guerlesquin F. (2003). The cytochrome c_3-[Fe]-hydrogenase electron-transfer complex: structural model by NMR restrained docking. *FEBS Lett* 548(1-3), 1-4.

9. Dementin S., Belle V., Bertrand P., Guigliarelli B., Adryanczyk-Perrier G., De Lacey A. L., Fernandez V. M., Rousset M., Leger C. (2006). Changing the ligation of the distal [4Fe4S] cluster in NiFe hydrogenase impairs inter- and intramolecular electron transfers. *J. Am. Chem. Soc.* 128(15), 5209-5218.

10. Vignais P. M., Billoud B., Meyer J. (2001). Classification and phylogeny of hydrogenases. *FEMS Microbiol. Rev.* 25(4), 455-501.

11. Mulder D. W., Shepard E. M., Meuser J. E., Joshi N., King P. W., Posewitz M. C., Broderick J. B., Peters J. W. (2011). Insights into [FeFe]-hydrogenase structure, mechanism, and maturation. *Structure* 19(8), 1038-1052.

12. Meyer J. (2007). [FeFe] hydrogenases and their evolution: a genomic perspective. *Cell. Mol. Life Sci.* 64(9), 1063-1084.

13. Peters J. W. (1999). Structure and mechanism of iron-only hydrogenases. *Curr. Opin. Struct. Biol.* 9(6), 670-676.

14. Lubner C. E., Knorzer P., Silva P. J., Vincent K. A., Happe T., Bryant D. A., Golbeck J. H. (2010). Wiring an [FeFe]-hydrogenase with photosystem I for light-induced hydrogen production. *Biochemistry* 49(48), 10264-10266.

15. Long H., Chang C. H., King P. W., Ghirardi M. L., Kim K. (2008). Brownian dynamics and molecular dynamics study of the association between hydrogenase and ferredoxin from *Chlamydomonas reinhardtii*. *Biophys. J.* 95(8), 3753-3766.

16. Pandey A. S., Harris T. V., Giles L. J., Peters J. W., Szilagyi R. K. (2008). Dithiomethylether as a ligand in the hydrogenase h-cluster. *J. Am. Chem. Soc.* 130(13), 4533-4540.

17. Cornish A. J., Gärtner K., Yang H., Peters J. W., Hegg E. L. (2011). Mechanism of proton transfer in [FeFe]-hydrogenase from *Clostridium pasteurianum*. *J. Biol. Chem.* 286(44), 38341-38347.

18. Zheng L., Baumann U., Reymond J. L. (2004). An efficient one-step site-directed and site-saturation mutagenesis protocol. *Nucleic Acids Res.* 32(14), e115.

19. Ozawa K., Yasukawa F., Fujiwara Y., Akutsu H. (2001). A simple, rapid, and highly efficient gene expression system for multiheme cytochromes *c*. *Biosci. Biotechnol. Biochem.* 65(1), 185-189.

20. Sreerama N., Woody R. W. (2000). Estimation of protein secondary structure from circular dichroism spectra: comparison of CONTIN, SELCON, and CDSSTR methods with an expanded reference set. *Anal. Biochem.* 287(2), 252-260.

21. Babini E., Bertini I., Borsari M., Capozzi F., Dikiy A., Eltis L. D., Luchinat C. (1996). A serine → cysteine ligand mutation in the high potential iron−sulfur protein from *Chromatium vinosum* provides insight into the electronic structure of the [4Fe-4S] cluster. *J. Am. Chem. Soc.* 118(1), 75-80.

22. Wardman P. (1991). The reduction potential of benzyl viologen: an important reference compound for oxidant/radical redox couples. *Free Radic. Res. Commun.* 14(1), 57-67.

Chapter 4

Characterization of hydrogen metabolism in the multicellular green alga *Volvox carteri*[1]

[1] This chapter is adapted from Cornish A. J., Gärtner K., Green, R., Mason, S., Hegg E. L. (2012). Characterization of hydrogen metabolism in the multicellular green alga *Volvox carteri*. *Appl. Environ. Microbiol.* Submitted
Saundra Mason and Robin contributed significantly to H_2 evolution assays, RNA isolation, and plasmid construction.

INTRODUCTION

Hydrogen gas is a potent energy carrier and has the potential to supplement existing transportation fuels (1, 2). A clean-burning gas, H_2 can be synthesized from renewable sources (3) and releases only water vapor during energy conversion via combustion. Certain autotrophic microorganisms, such as green algae, are able to channel photosynthetically-derived reducing equivalents to H_2 production (4, 5, 6, 7). Many green algae can be cultured at an industrial scale utilizing non-arable land, thereby avoiding competition with agricultural feedstocks (8). Extensive studies of H_2 metabolism in several algal species have established a basis for investigation of algal biohydrogen production, and these studies can be used to inform future efforts to generate renewable alternative fuels (9, 10).

Green algae evolve H_2 using [FeFe]-hydrogenases (EC#1.12.7.2), metalloproteins which catalyze both the reduction of protons and the oxidation of H_2 (11, 12). Electrons for H_2 production can either be channeled from photosynthetic water-splitting or be obtained by the fermentation of carbon sources (11, 13). In a variety of green algae, hydrogenases are encoded by two gene paralogs (*HYDA1* and *HYDA2*) that have high sequence similarity, although the respective physiological functions of each enzyme are still unclear (14, 15). Maturation proteins are required to assemble the catalytic active site, and the corresponding genes (*HydE, HydF*, and *HydG* in bacteria - *HYDEF* and *HYDG* in green algae) are ubiquitous in the genomes of organisms which utilize [FeFe]-hydrogenase (16). Although these genes in green algae were likely acquired by lateral gene transfer (17), hydrogenase gene clustering has not

been noted in sequenced green algal genomes. Despite this lack of clustering, hydrogenase and maturation factor gene expression is tightly co-regulated. In addition, the enzyme is irreversibly-inactivated by the presence of O_2, and the *HYD* genes are expressed only under anaerobiosis (12, 18).

The O_2-sensitivity of [FeFe]-hydrogenase renders H_2 synthesis dependent on micro-aerobic conditions and thus limits production during light-driven oxygenic photosynthesis (5, 19, 20). In *Chlamydomonas reinhardtii*, a model unicellular green alga, this inhibition may be overcome by sulfur deprivation, which limits O_2 production by photosystem II (PSII) while still allowing electrons gained from photosystem I (PSI) to be coupled to H_2 production (21). In addition, anaerobic conditions are quickly established in the dark as respiration depletes O_2, thereby allowing carbon stores generated during photosynthesis to be utilized for H_2 production (5, 6). Both of these methods allow for channeling of electrons to H_2 synthesis.

Volvox carteri is a multicellular green alga separated from *C. reinhardtii* by approximately 220 million years of evolution (22). *V. carteri* is composed of two cell types, gonidia and somatic, which are embedded within an extracellular matrix (23, 24). Recently, the *V. carteri* genome was sequenced and, as expected, it shares a great deal of genome sequence similarity and metabolic processes (22, 25) with *C. reinhardtii*. Two putative [FeFe]-hydrogenase genes were annotated in the genome of *V. carteri* (22). However, the ability of this organism to evolve H_2 was not established.

In this manuscript we demonstrate that the green alga *V. carteri* is able to utilize an abiotic electron donor system to drive H_2 production. To our knowledge, this is the first report of H_2 metabolism in a multicellular eukaryote with differentiated cells. Genes

responsible for hydrogenase assembly and maturation are up-regulated under anaerobic conditions, and both *HYDA* genes encode functional [FeFe]-hydrogenases. In relation to other green algae, these genes in *V. carteri* are uniquely arranged in an operon-like structure within the genome, providing evolutionary evidence for the potential origins of horizontal gene transfer. Together, these data support a role for H_2 in the metabolism of *V. carteri* and provide a basis for further investigation of the ancestral acquisition of [FeFe]-hydrogenase genes in green algae.

METHODS

Growth Conditions—Unless otherwise noted, *V. carteri* f. *nagariensis* EVE (22) cells were grown with continuous light (90 μE m^{-2} s^{-1}) and shaking (100 rpm) in standard *Volvox* medium (SVM) at 22 ˚C as previously described (26).

Anaerobic Acclimation—To acclimate *V. carteri* cells to anaerobiosis, a culture of light-adapted cells was centrifuged at 1,000× *g* for 5 min. The resulting cell pellet was washed three times in an anaerobic chamber (Coy Laboratory Products) with degassed SVM supplemented with 0.16 mM $MgCl_2$ rather than 0.16 mM $MgSO_4$ [SVM (-SO_4)] to exclude sulfate from the medium. Sulfate-depleted medium was utilized to decrease photosystem II activity and thus limit oxygenic photosynthesis. The cells were resuspended in degassed SVM (-SO_4) to a final concentration of 75 μg chlorophyll/mL, and 2 mL of this mixture were sealed in a 10 mL air-tight serum vial (Wheaton). The resuspension was shaken for 4 h. To prevent any remaining photosynthetic activity from photosystem II, the vials were wrapped with aluminum foil.

Hydrogen Production Measurements—H_2 evolution using an artificial electron donor was measured by incubating 0.1 mL of either aerobically- or anaerobically-acclimated cells (75 μg chlorophyll/mL) with 1.9 mL of H_2 evolution assay solution [SVM (-SO_4), 100 mM sodium dithionite, 10 mM methyl viologen dichloride (MV)] in a sealed 10 mL serum vial at 22 ˚C in the dark with continuous shaking. At various time points, 20 μL of headspace gas were injected into a TRACE GC Ultra Gas Chromatograph (Thermo

Scientific) using a 100 µL syringe. The peak at 1.4 min corresponded to H_2, and the absolute value of H_2 gas was determined by comparison to a standard curve. The resulting values were plotted versus time to monitor the accumulation of H_2 in the headspace, and the rates were determined per µg of chlorophyll.

H_2 evolution measurements using exogenous carbon sources were performed as described above, except that the cell resuspension was incubated in 1.9 mL of SVM (-SO_4) supplemented with either 0.174 mM sodium acetate, D-glucose, or glycerol.

RNA Isolation—To isolate total RNA from *V. carteri*, cell cultures were centrifuged at 10,000× *g* for 10 min. The resulting pellets were resuspended in 0.5 mL of TRIzol (Invitrogen) and frozen in liquid nitrogen. The frozen TRIzol/cell mass mixture was crushed using a mortar and pestle, thawed, and resuspended with an additional 0.5 mL of TRIzol. To this suspension, 0.2 mL of chloroform was added, and the mixture was vortexed at top speed at room temperature for 15 min. To pellet cell debris, the suspension was centrifuged at 10,000× *g* for 15 min at 10 ˚C. The aqueous phase was transferred to a 1.7 mL tube (Denville) containing 0.25 mL of 0.8 M sodium citrate and 1.0 M sodium chloride, and the suspension was gently mixed by inversion. Following the addition of 0.25 mL of isopropanol, the mixture was centrifuged at 10,000× *g* for 25 min at 10 ˚C. The supernatant was discarded and the RNA pellet washed twice with ice-cold 75% ethanol. The pellet was allowed to dry and then resuspended in 20 µL diethylpyrocarbonate-treated water.

RT-PCR—Reverse transcription of mRNA was performed using M-MLV Reverse Transcriptase (Invitrogen), and the cDNA was amplified via PCR using GoTaq Green Master Mix (Promega) and the primer sets listed in Table 4.1. Genomic and cDNA sequences of *HYDA1*, *HYDA2*, *HYDEF*, and *HYDG* can be accessed from the DDBJ/EMBL/GenBank database with the accession numbers XM_002948441, XM_002948437, XM_002948568, and XM_002948439, respectively.

Cloning of HYDA1 and HYDA2—The *HYDA1* and *HYDA2* genes were PCR amplified with *PfuTurbo* DNA polymerase (Stratagene) from reverse-transcribed cDNA using the primers listed in Table 4.1. The amplified products were ligated into the SacI/HindIII site of pAC-BAD, a pBAD/D-TOPO (Invitrogen) expression vector (contains a kanamycin-resistant cassette and an L-arabinose inducible promoter) that was modified to remove the N-terminal thioredoxin-tag (27). The constructs were transformed into *S. oneidensis* MR-1 Δ*hydA/*Δ*hyaB* (28) electrocompetent cells as described by Ozawa (29) and selected for antibiotic resistance on 50 μg/mL kanamycin LB plates.

Overexpression, Protein Purification, and Hydrogen Evolution Assay—Cells harboring the pAC-BAD_*HYDA1* and pAC-BAD_*HYDA2* vectors were induced for gene overexpression and protein synthesis as previously described (27). Enzymes were purified in an anaerobic chamber and assayed for H_2 evolution activity as described by Cornish et al. (27).

Table 4.1. **List of primers used for cloning and cDNA amplification.** Restriction digest sites are *italicized.* 6xHis-tag sequences are underlined. Genomic sequences amplified by the cloning primers are in **bold**.

Cloning	Sequence
HYDA1 Sense	GCGCGC *CCATGG* CG CAT CAC CAT CAC CAT CAC GGTGGCGGA **ATGGACGAGCTAGACAAGCC**
HYDA1 Antisense	GCGCGC *AAGCTT* **TCTACTCGGCCTCGACACCA**
HYDA2 Sense	GCGCGC *CCATGG* GA CAT CAC CAT CAC CAT CAC GGAGGCGGT **AAGTGCACTTCGGCTGTCC**
HYDA2 Antisense	GCGCGC *AAGCTT* **ACTCGGTATCGACGCCC**

RT-PCR	Sequence
HYDA1 Sense	GTCGTCGTGCAAGAGCCCCC
HYDA1 Antisense	ATAGCCTTGGCAGCCGCACG
HYDA2 Sense	ATCATGCCGTGCGTCCGCAA
HYDA2 Antisense	GAAGACGACACCGGCACCCG
ACTA Sense	GTGGGCGACGAGGCACAGTC
ACTA Antisense	CCGGCAAGGTCCAGACGCAG

Phylogenetic Analysis—Using BLAST, 86 unique [FeFe]-hydrogenase amino acid sequences were collected from the National Center for Biotechnical Information and aligned by MUSCLE (30) using a gap extension of 13 and opening penalty of 0.05. Pairwise distances were calculated from the alignment and sequences with a distance <0.1 were eliminated. The remaining 52 sequences were aligned as stated previously, and the alignment was trimmed to isolate only the representative H-cluster-binding domain from HYDA. Evolutionary history was inferred using the Neighbor-Joining method (31) and evolutionary distances computed using the p-distance method (32). 2000 bootstrap replicates were performed. All analyses were conducted in MEGA5 (33).

RESULTS

Hydrogen Evolution Studies—V. carteri is closely related to *C. reinhardtii*, a green alga with well-described hydrogen metabolism (19, 20). Recent sequencing and annotation of the *V. carteri* genome (22) uncovered two genes with sequence similarity to algal [FeFe]-hydrogenase genes (*HYDA1, HYDA2*) (Figure 4.1) as well as two genes predicted to be necessary for [FeFe]-hydrogenase maturation (*HYDEF, HYDG*).

V. carteri was tested for *in vivo* H_2 production in SVM ($-SO_4$) after a 4 h anaerobic acclimation period. Aliquots of anaerobically-acclimated cells were transferred to anaerobic assay vials containing an abiotic electron donor system (MV and $Na_2S_2O_4$), and the headspace was tested for accumulation of H_2. H_2 production could be measured within the first 45 min of incubation with MV/$Na_2S_2O_4$, eventually achieving a rate of 380 nmol H_2/mg chlorophyll/s after 3 h (Figure 2). When oxygen-exposed cells (i.e. aerobic cells) were assayed under similar conditions, no H_2 accumulation was observed over the course of the assay (Figure 4.2). This indicates that *V. carteri* requires anaerobic acclimation for H_2 evolution. Cells that were not supplemented with MV/$Na_2S_2O_4$ did not accumulate a significant amount of H_2 in the headspace even 48 h after initiating the assay.

Figure 4.1. **Partial multiple sequence alignment of *V. carteri* and *C. reinhardtii* HYDA amino acid sequences.** Black boxes denote strictly conserved residues, while regions with high conservation are boxed and are in boldface. The HYDA1 proteins from *V. carteri* and *C. reinhardtii* share 74.1% sequence identity, while the HYDA2 proteins share 75.1% sequence identity. Accession numbers for *C. reinhardtii* HYDA1 and HYDA2 are XP_001693376 and XP_001694503, respectively.

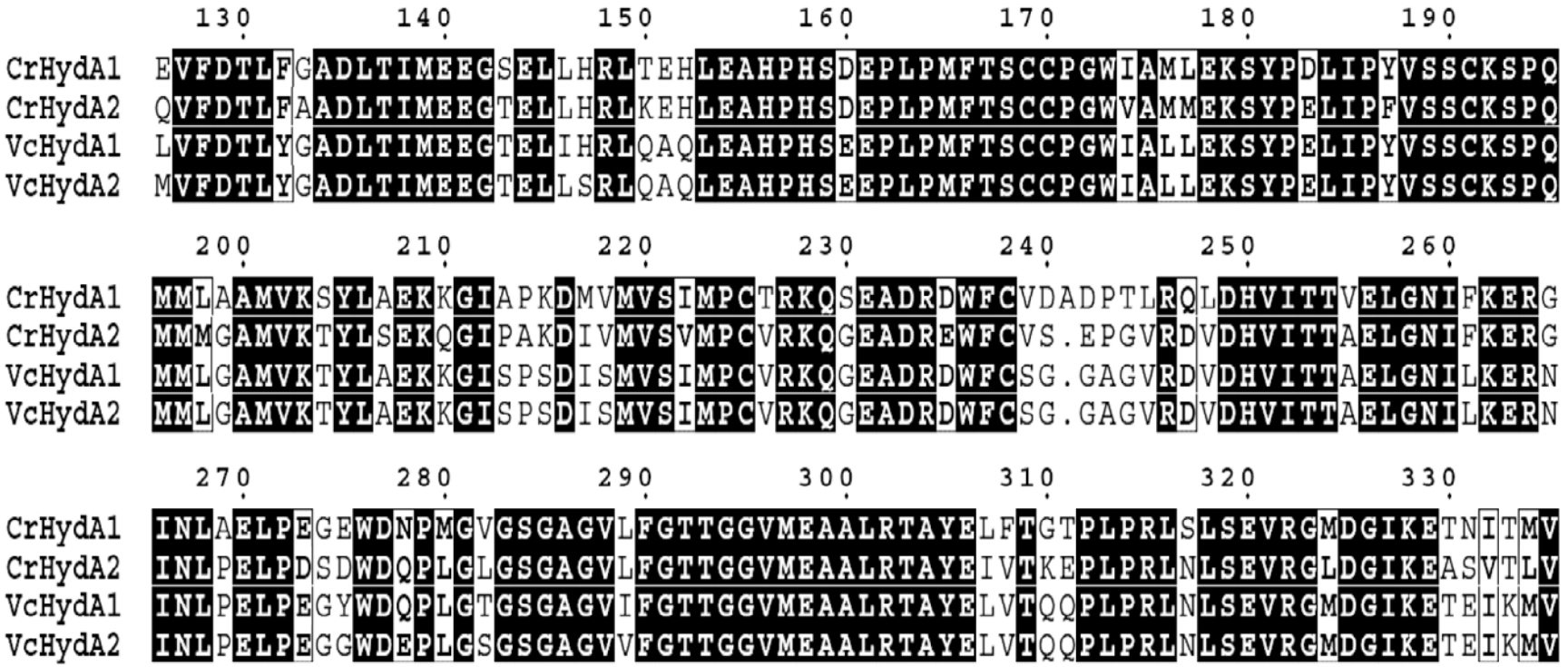

Figure 4.2. **H_2 evolution rate of aerobically- or anaerobically-acclimated *V. carteri* cells.** Following a 4 h acclimation period, cells were incubated in SVM (-SO_4) with and without an abiotic electron donor system. H_2 production rates were measured over a 3 h period and normalized on a per mg chlorophyll basis. Error bars denote standard deviation (n ≥ 3).

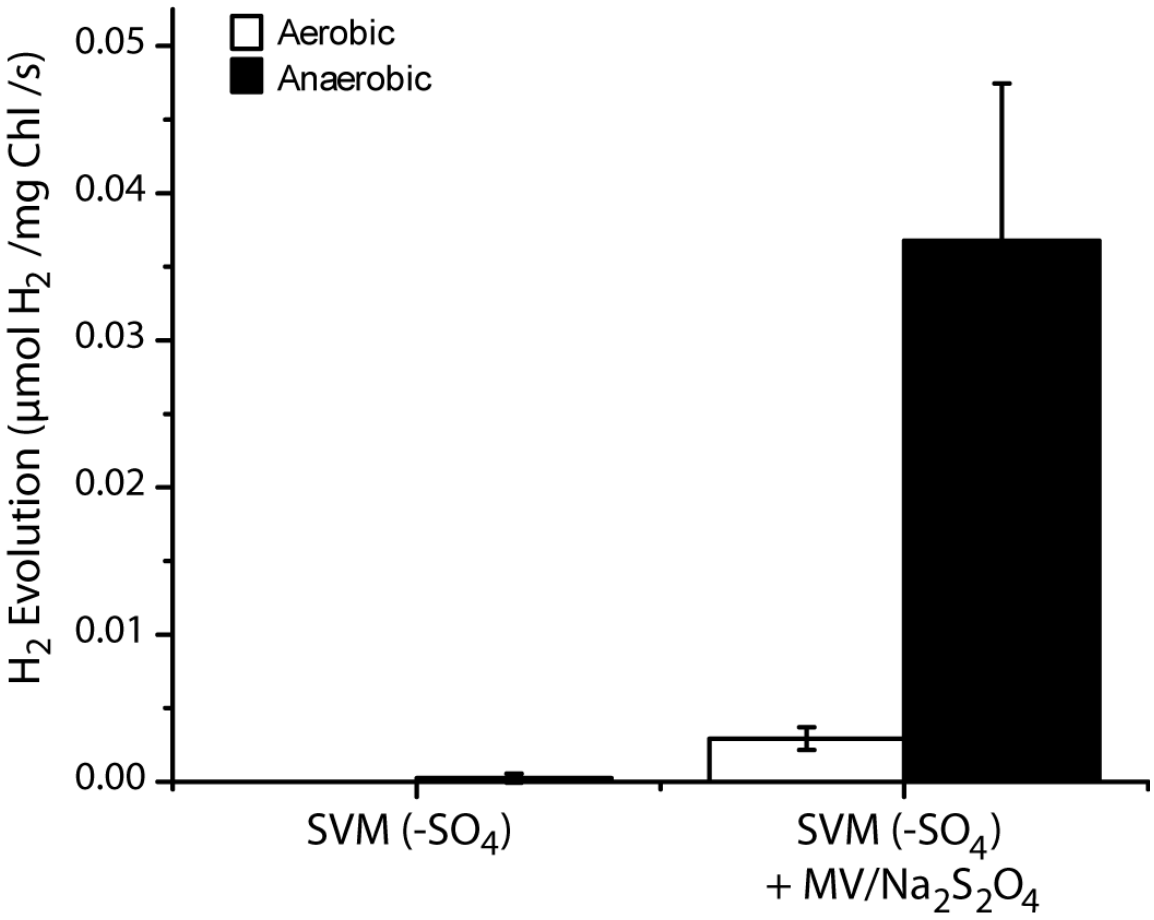

Fermentative H_2 Production—Having established H_2 metabolism in *V. carteri* using an artificial electron system, we sought to drive H_2 production utilizing electrons generated during fermentation. A recent report suggests that *V. carteri* may be able to import glycerol (34), which could then be fed into fermentation. To test for fermentative H_2 evolution in *V. carteri*, anaerobically-induced cultures were supplemented with either 0.174 mM sodium acetate, D-glucose, or glycerol and compared to the H_2 evolution from cells in unsupplemented medium. No quantifiable increase in H_2 could be noted even 48 h after supplementation, indicating that addition of these exogenous carbon sources does not drive H_2 production under these conditions.

Transcript Analysis—Based on H_2 accumulation under anaerobiosis, we predicted that the putative *HYDA* genes played a role in H_2 production. To test for *HYDA* expression during anaerobiosis, RNA was collected from both aerobically- and anaerobically acclimated cells. The RNA was reverse-transcribed and PCR amplified with primers specific to the putative [FeFe]-hydrogenase genes, *HYDA1* and *HYDA2*. Strong amplification of mRNA for both genes was observed in anaerobic samples, while very little transcript could be observed in the aerobic samples when compared to a housekeeping gene, *ACTA* (accession number XP_002955536) (Figure 4.3). These results indicate that the anaerobic expression of *HYDA1* and *HYDA2* correlate with the H_2 production observed in *V. carteri*.

Figure 4.3. **Gene transcript accumulation observed by RT-PCR.** *HYDA1* and *HYDA2* transcripts were strongly amplified using RNA isolated from anaerobically-acclimated *V. carteri* cells. The *ACTA* gene was constitutively expressed under both aerobic and anaerobic conditions and was used as a control.

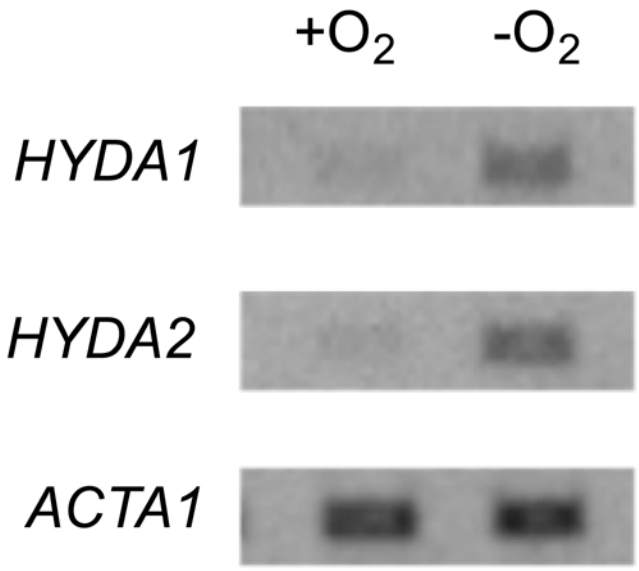

Hydrogenase Cloning and Characterization—The two putative *HYDA* genes have high sequence similarity to known green algal hydrogenase genes (Figure 4.1) and likely code for active H_2-producing enzymes. To test for this, the two genes were amplified from cDNA, cloned into pAC-BAD, and transformed into *S. oneidensis* Δ*hydA*Δ*hyaB* cells. Gene expression was induced by the addition of L-arabinose, and the N-terminally His-tagged proteins were purified by nickel-affinity chromatography. The HYDA1 and HYDA2 proteins were active when supplied with MV/$Na_2S_2O_4$, and both had similar K_m values when measured for MV (2.76 mM and 2.82 mM, respectively). The specific activity of HYDA1 was ~1,000-fold greater than HYDA2 (4,000 nmol H_2/mg/s and 2.2 nmol H_2/mg/s, respectively). This differs from previously reported values for recombinant *C. reinhardtii* HYDA1 and HYDA2 specific activities, which were nmol H_2/mg/s and nmol H_2/mg/s, respectively (35).

Phylogenetic Analysis—The two hydrogenase genes and the two assembly factor genes in the *V. carteri* genome (*HYDA1*, *HYDA2*, *HYDEF*, *HYDG*) were found to be in relatively close proximity to one another. The distance between the furthest genes (HYDA1 and HYDA2) is ~57 kb, and the main cluster of genes is within a ~23 kb span (Figure 4.4). This level of [FeFe]-hydrogenase gene clustering has not been previously observed in the sequenced genomes of green algae (*C. reinhardtii* and *Chlorella variabilis)*. Green algae are theorized to have obtained their hydrogenase genes via horizontal gene transfer, likely from an operon or operon-like gene structure.

Figure 4.4. **[FeFe]-hydrogenase operon-like gene cluster in *V. carteri*.** Four genes with sequence similarity to *HYDA1*, *HYDA2*, *HYDEF*, and *HYDG* are arranged within 60 kb of one another. Three additional putative genes are within this region; ACKA (XP_002948613), a phosphate acetyltransferase (XP_002948484), and a predicted gene, Q85 (XP_002948486). The predicted gene products are not hypothesized to catalyze H_2 production or assist in the assembly of the [FeFe]-hydrogenase active site, and these genes are not found within investigated bacterial [FeFe]-hydrogenase gene clusters.

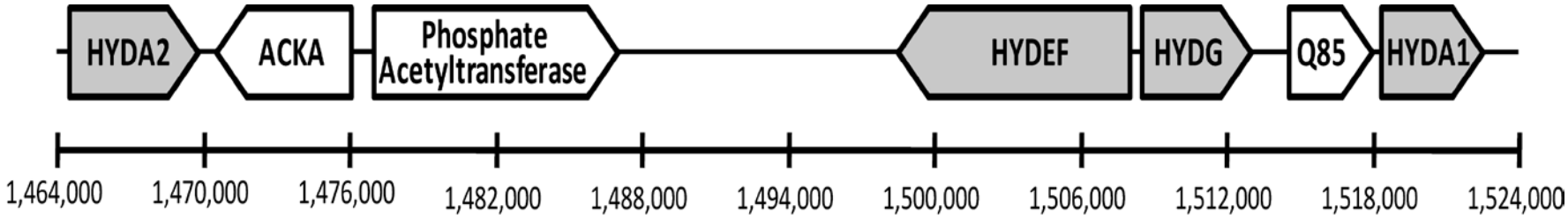

To investigate potential origins of this operon-like cluster in *V*. *carteri*, a phylogenetic analysis was performed utilizing [FeFe]-hydrogenase protein sequences. As previously observed, green algal hydrogenase sequences group closely together, with the sequences from *C. variabilis* showing greater divergence (Figure 4.5) (17). A grouping of thermophilic anaerobic bacterial sequences suggests a relationship to the green algal clade, indicating that these genes may have arisen from a common ancestor. Within the clade, the bacterial genomes each contain an operon-like cluster composed of hydrogenase and hydrogenase maturation genes. In particular, the genomes of *Fervidobacterium nodosum*, *Fervidobacterium pennivorans*, and *Thermotoga thermarum* contain operon-like clusters composed of five hydrogenase genes that cover a <22 kb span (Figure 4.6). These findings provide hints for a common ancestor among these bacteria and the possible origin of hydrogenase genes in green algae.

Figure 4.5. **Phylogenetic analysis of representative HYDA homologs.** Evolutionary history of [FeFe]-hydrogenase amino acid sequences was inferred by the Neighbor-Joining method and the bootstrap consensus tree was inferred from 2,000 replicates. Partitions reproduced in less than 50% bootstrap replicates are collapsed and bootstrap values are represented at individual nodes. The tree is drawn to scale, with evolutionary distances calculated by the p-distance method and the units are described as the number of amino acid differences per site.

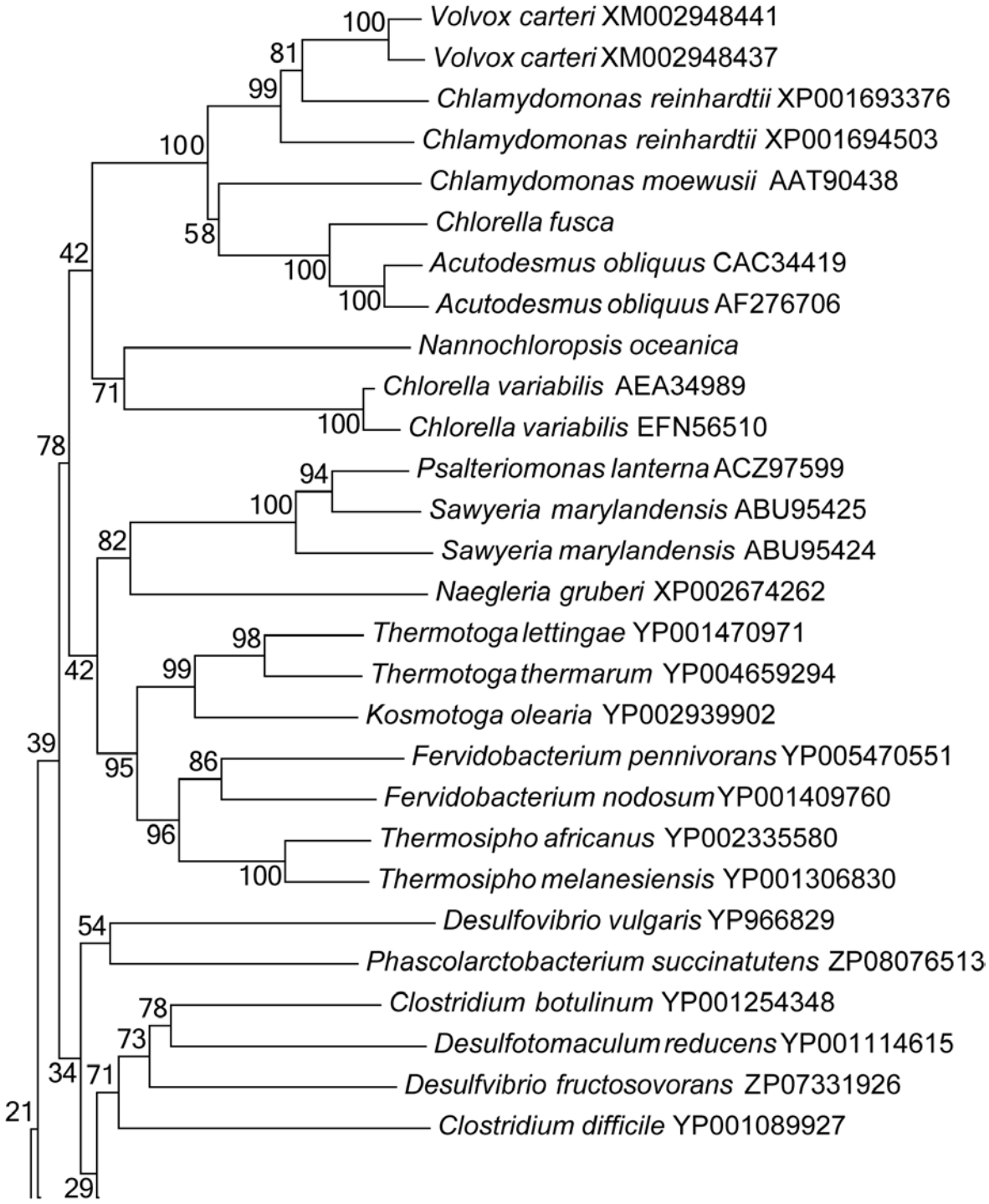

Figure 4.5 (cont'd)

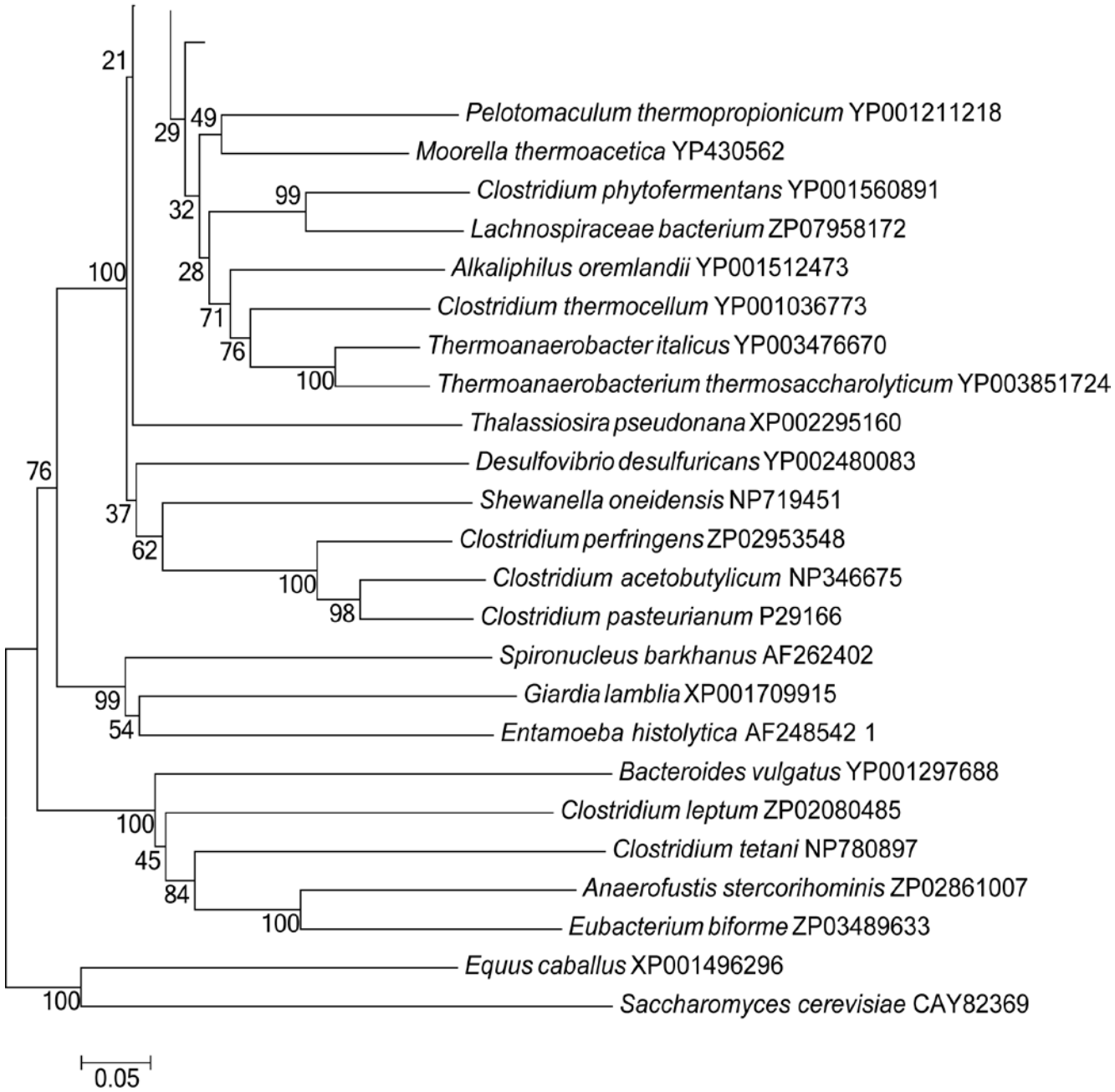

Figure 4.6. **[FeFe]-hydrogenase gene clusters observed in *V. carteri*, *F. nodosum*, *F. pennivorans*, and *T. thermarum*.** Clusters are all on the same scale and the putative *HYD* genes are denoted by color (*HYDA* sequences, orange and pink; *HYDE*, green; *HYDF,* blue; *HYDG,* purple; *HYDEF* fusion gene, green-to-blue). The coding sequence of the *F. nodosum* and *T. thermarum* clusters has been reversed (reading 3' to 5') to more closely match the orientation of the *V. carteri* cluster.

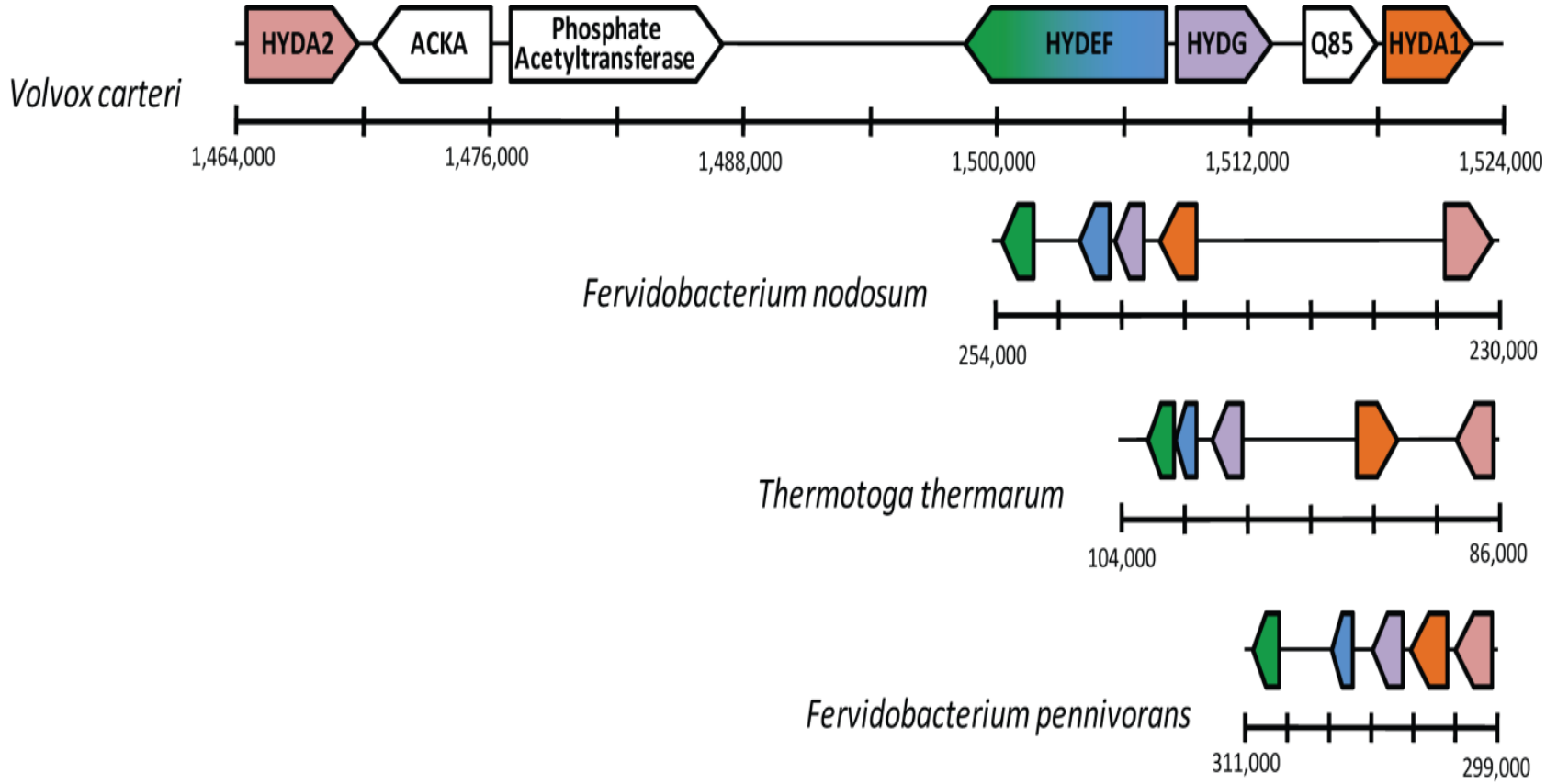

DISCUSSION

A variety of green algae have been characterized for their ability to couple energy derived from photosynthesis to the production of H_2, especially the model organism *C. reinhardtii* (4, 5, 6). *V. carteri* is separated from *C. reinhardtii* by ~220 million years of evolution, yet the two organisms share many traits at the physiological and genetic levels (22). This forms a logical basis for investigating the unique multicellular alga *V. carteri* for H_2 metabolism.

To test the H_2 metabolism of *V. carteri*, anaerobic algal cell cultures were provided with an electron donor system and H_2 accumulation was measured. Under the conditions tested, *V. carteri* cultures evolved appreciable amounts of H_2 when supplied with an exogenous electron source (MV/$Na_2S_2O_4$). The addition of fermentable carbon sources (acetate, glycerol, and D-glucose) did not drive H_2 production in anaerobically-acclimated cells. Based on previous reports, *V. carteri* cannot take up acetate under dark anaerobiosis (36) and lacks glucose importers (37), and therefore the inability of acetate and glucose to drive H_2 production is to be expected. Intriguingly, although Anderberg et al. hypothesized that *V. carteri* could take up glycerol via putative aquaporins (34), no H_2 production was noted upon glycerol supplementation. This result could be explained by the inability of glycerol to enter the cells under our assay conditions or because electrons derived from glycerol-breakdown are not channeled into H_2 metabolism.

Transcript for the hydrogenase homologs *HYDA1* and *HYDA2* accumulated under anaerobic conditions, and the heterologously-expressed gene products

demonstrated quantifiable *in vitro* H_2 evolution activity when supplied with an artificial electron donor. In addition, HYDA1 and HYDA2 have similar K_m values of ~2.8 mM for MV. Interestingly, the specific activities measured for each enzyme were dissimilar, with HYDA1 being approximately 1000-fold more active than HYDA2. This may be due to incomplete maturation of HYDA2 in the *S. oneidensis* MR-1 expression system.

In addition to similar kinetic values, HYDA1 and HYDA2 also share common structural features with other characterized green algal [FeFe]-hydrogenases. For example, both proteins contain two short sequences not observed in non-algal hydrogenases and also lack the canonical iron-sulfur cluster-containing F-domains (18). When analyzed with several localization prediction servers (ChloroP 1.1 (38), PCLR (39), WoLF PSORT (40), and CELLO (41)), a chloroplast-targeting peptide was identified at the N-terminus of HYDA2, which is a typical feature of green algal hydrogenases. Due the ubiquitous nature of this peptide among algal hydrogenases, it was intriguing to find that these programs do not predict that HYDA1 is chloroplast-localized. If the localization prediction is accurate, targeting to different subcellular compartments could imply the utilization of different physiological donors.

While examining the hydrogenase genes within the *V. carteri* genome, it was noted that the *HYDA1* and *HYDA2* genes are within proximity to genes encoding the maturation proteins *HYDEF* and *HYDG*. This clustering is unique to *V. carteri* among currently sequenced green algal genomes, but an [FeFe]-hydrogenase gene cluster was also recently reported in the genomes of the photosynthetic heterokonts *Nannochloropsis oceanica* CCMP1779 (42) and *Nannochloropsis gaditana* CCMP526 (43). Currently, hydrogenase genes within eukaryotic genomes have been assumed to

be acquired from bacteria via horizontal gene transfer, although the exact origin of the *HYD* genes is not known (44, 45).

We investigated possible evolutionary relationships between *HYDA* genes via phylogenetic analysis, particularly concentrating on known green algal protein sequences, and including representative bacterial and protist homologs. Our phylogram matches well with analyses conducted by Meuser et al. (17), showing a distinct grouping of green algal genes (Figure 4.5). In addition, a clade of thermophilic bacterial anaerobes demonstrates a relationship to this group of green algal genes, and three genomes of bacteria within this clade contain operon-like clusters (>22 kb span) with genes encoding two hydrogenases and all three maturation proteins. However, distinct differences exist between the *V. carteri* and bacterial gene clusters, such as the orientation of the genes and the fusion of the *HYDE* and *HYDF* genes in *V. carteri*. It is therefore intriguing that the relative positions of the genes are identical between *V. carteri* and bacterial clusters, although the bacterial genes, lacking introns, are shorter in length (Figure 4.6). Together, this information suggests that *HYD* genes in modern green algae may have been attained via lateral gene transfer from an ancestor of the thermophilic bacteria clade. In addition, sequences from several protists, including *N. oceanica* CCMP1779, also have a close relationship to these algal sequences, indicating that these organisms may have acquired *HYDA* genes from a similar bacterial ancestor.

In conclusion, we have provided the first direct evidence for H_2 metabolism in a multicellular eukaryote with differentiated cells. The green alga *V. carteri* is able to drive H_2 production in the dark utilizing at least one of two [FeFe]-hydrogenases, both of

which were show to be active *in vitro* and have similar K_m values for MV. A unique gene cluster encodes the hydrogenases and maturation machinery in the *V. carteri* genome, and this cluster provides new hints to the origin of these genes in green algae.

REFERENCES

REFERENCES

1. Züttel A., Remhof A., Borgschulte A., Friedrichs O. (2010). Hydrogen: the future energy carrier. *Philos. Transact. A Math. Phys. Eng. Sci.* 368(1923), 3329-3342.

2. Jacobson M. Z., Colella W. G., Golden D. M. (2005). Cleaning the air and improving health with hydrogen fuel-cell vehicles. *Science* 308(5730), 1901-1905.

3. Tran P., Artero V., Fontecave M. (2010). Water electrolysis and photoelectrolysis on electrodes engineered using biological and bio-inspired molecular systems. *Energy Environ. Sci.* 3(6), 727-747.

4. McKinlay J. B., Harwood C. S. (2010). Photobiological production of hydrogen gas as a biofuel. *Curr. Opin. Biotechnol.* 21(3), 244-251.

5. Ghirardi M. L., Dubini A., Yu J., Maness P. C. (2009). Photobiological hydrogen-producing systems. *Chem. Soc. Rev.* 38(1), 52-61.

6. Hemschemeier A., Melis A., Happe T. (2009). Analytical approaches to photobiological hydrogen production in unicellular green algae. *Photosynth. Res.* 102(2-3), 523-540.

7. McNeely K., Xu Y., Bennette N., Bryant D. A., Dismukes G. C. (2010). Redirecting reductant flux into hydrogen production via metabolic engineering of fermentative carbon metabolism in a cyanobacterium. *Appl. Environ. Microbiol.* 76(15), 5032-5038.

8. Singh A., Nigam P. S., Murphy J. D. (2011). Renewable fuels from algae: an answer to debatable land based fuels. *Bioresour. Technol.* 102(1), 10-16.

9. Rupprecht J. (2009). From systems biology to fuel--*Chlamydomonas reinhardtii* as a model for a systems biology approach to improve biohydrogen production. *J. Biotechnol.* 142(1), 10-20.

10. Beer L. L., Boyd E. S., Peters J. W., Posewitz M. C. (2009). Engineering algae for biohydrogen and biofuel production. *Curr. Opin. Biotechnol.* 20(3), 264-271.

11. Ghirardi M. L., Posewitz M. C., Maness P.-C., Dubini A., Yu J., Seibert M. (2007). Hydrogenases and hydrogen photoproduction in oxygenic photosynthetic organisms. *Annu. Rev. Plant Biol.* 58(1), 71-91.

12. Vignais P. M., Billoud B., Meyer J. (2001). Classification and phylogeny of hydrogenases. *FEMS Microbiol. Rev.* 25(4), 455-501.

13. Winkler M., Hemschemeier A., Jacobs J., Stripp S., Happe T. (2010). Multiple ferredoxin isoforms in *Chlamydomonas reinhardtii* - their role under stress conditions and biotechnological implications. *Eur. J. Cell Biol.* 89(12), 998-1004.

14. Godman J. E., Molnár A., Baulcombe D. C., Balk J. (2010). RNA silencing of hydrogenase(-like) genes and investigation of their physiological roles in the green alga *Chlamydomonas reinhardtii*. *Biochem. J.* 431(3), 345-351.

15. Posewitz M. C., King P. W., Smolinski S. L., Smith R. D., Ginley A. R., Ghirardi M. L., Seibert M. (2005). Identification of genes required for hydrogenase activity in *Chlamydomonas reinhardtii*. *Biochem. Soc. Trans.* 33(Pt 1), 102-104.

16. Mulder D. W., Shepard E. M., Meuser J. E., Joshi N., King P. W., Posewitz M. C., Broderick J. B., Peters J. W. (2011). Insights into [FeFe]-hydrogenase structure, mechanism, and maturation. *Structure* 19(8), 1038-1052.

17. Meuser J. E., Boyd E. S., Ananyev G., Karns D., Radakovits R., Narayana Murthy U. M., Ghirardi M. L., Dismukes G. C., Peters J. W., Posewitz M. C. (2011). Evolutionary significance of an algal gene encoding an [FeFe]-hydrogenase with F-domain homology and hydrogenase activity in *Chlorella variabilis* NC64A. *Planta* 234(4), 829-843.

18. Forestier M., King P., Zhang L., Posewitz M., Schwarzer S., Happe T., Ghirardi M. L., Seibert M. (2003). Expression of two [Fe]-hydrogenases in *Chlamydomonas reinhardtii* under anaerobic conditions. *Eur. J. Biochem.* 270(13), 2750-2758.

19. Grossman A. R., Catalanotti C., Yang W., Dubini A., Magneschi L., Subramanian V., Posewitz M. C., Seibert M. (2011). Multiple facets of anoxic metabolism and hydrogen production in the unicellular green alga *Chlamydomonas reinhardtii*. *New Phytol.* 190(2), 279-288.

20. Hemschemeier A., Happe T. (2011). Alternative photosynthetic electron transport pathways during anaerobiosis in the green alga *Chlamydomonas reinhardtii*. *Biochim. Biophys. Acta* 1807(8), 919-926.

21. Antal T. K., Krendeleva T. E., Rubin A. B. (2011). Acclimation of green algae to sulfur deficiency: underlying mechanisms and application for hydrogen production. *Appl. Microbiol. Biotechnol.* 89(1), 3-15.

22. Prochnik S. E., Umen J., Nedelcu A. M., Hallmann A., Miller S. M., Nishii I., Ferris P., Kuo A., Mitros T., Fritz-Laylin L. K., Hellsten U., Chapman J., Simakov O., Rensing S. A., Terry A., Pangilinan J., Kapitonov V., Jurka J., Salamov A., Shapiro H., Schmutz J., Grimwood J., Lindquist E., Lucas S., Grigoriev I. V., Schmitt R., Kirk D., Rokhsar D. S. (2010). Genomic analysis of organismal

complexity in the multicellular green alga *Volvox carteri*. *Science* 329(5988), 223-226.

23. Schmitt R. (2003). Differentiation of germinal and somatic cells in *Volvox carteri*. *Curr. Opin. Microbiol.* 6(6), 608-613.

24. Tam L. W., Kirk D. L. (1991). Identification of cell-type-specific genes of *Volvox carteri* and characterization of their expression during the asexual life cycle. *Dev. Biol.* 145(1), 51-66.

25. Kirk D. L. (1999). Evolution of multicellularity in the volvocine algae. *Curr. Opin. Plant. Biol.* 2(6), 496-501.

26. Kirk D. L., Kaufman M. R., Keeling R. M., Stamer K. A. (1991). Genetic and cytological control of the asymmetric divisions that pattern the *Volvox* embryo. *Dev. Suppl.* 1, 67-82.

27. Cornish A. J., Gärtner K., Yang H., Peters J. W., Hegg E. L. (2011). Mechanism of proton transfer in [FeFe]-hydrogenase from *Clostridium pasteurianum*. *J. Biol. Chem.* 286(44), 38341-38347.

28. Marshall M. J., Plymale A. E., Kennedy D. W., Shi L., Wang Z., Reed S. B., Dohnalkova A. C., Simonson C. J., Liu C., Saffarini D. A., Romine M. F., Zachara J. M., Beliaev A. S., Fredrickson J. K. (2008). Hydrogenase- and outer membrane c-type cytochrome-facilitated reduction of technetium(VII) by *Shewanella oneidensis* MR-1. *Environ. Microbiol.* 10(1), 125-136.

29. Ozawa K., Yasukawa F., Fujiwara Y., Akutsu H. (2001). A simple, rapid, and highly efficient gene expression system for multiheme cytochromes *c*. *Biosci. Biotechnol. Biochem.* 65(1), 185-189.

30. Edgar R. C. (2004). MUSCLE: multiple sequence alignment with high accuracy and high throughput. *Nucleic Acids Res.* 32(5), 1792-1797.

31. Saitou N., Nei M. (1987). The neighbor-joining method: a new method for reconstructing phylogenetic trees. *Mol. Biol. Evol.* 4(4), 406-425.

32. Nei M., Kumar S. (2000). Molecular Evolution and Phylogenetics. Oxford University Press, New York.

33. Tamura K., Peterson D., Peterson N., Stecher G., Nei M., Kumar S. (2011). MEGA5: molecular evolutionary genetics analysis using maximum likelihood, evolutionary distance, and maximum parsimony methods. *Mol. Biol. Evol.* 28(10), 2731-2739.

34. Anderberg H. I., Danielson J. A., Johanson U. (2011). Algal MIPs, high diversity and conserved motifs. *BMC Evol. Biol.* 11, 110.

35. King P. W., Posewitz M. C., Ghirardi M. L., Seibert M. (2006). Functional studies of [FeFe] hydrogenase maturation in an *Escherichia coli* biosynthetic system. *J. Bacteriol.* 188(6), 2163-2172.

36. Gibbs M., Gfeller R. P., Chen C. (1986). Fermentative metabolism of Chlamydomonas reinhardii: III. Photoassimilation of acetate. *Plant Physiol.* 82(1), 160-166.

37. Hallmann A., Sumper M. (1996). The *Chlorella* hexose/H^+ symporter is a useful selectable marker and biochemical reagent when expressed in *Volvox*. *Proc. Natl. Acad. Sci. U.S.A.* 93(2), 669-673.

38. Emanuelsson O., Nielsen H., von Heijne G. (1999). ChloroP, a neural network-based method for predicting chloroplast transit peptides and their cleavage sites. *Protein Sci.* 8(5), 978-984.

39. Schein A. I., Kissinger J. C., Ungar L. H. (2001). Chloroplast transit peptide prediction: a peek inside the black box. *Nucleic Acids Res.* 29(16), E82.

40. Horton P., Park K. J., Obayashi T., Fujita N., Harada H., Adams-Collier C. J., Nakai K. (2007). WoLF PSORT: protein localization predictor. *Nucleic Acids Res.* 35(Web Server issue), W585-587.

41. Yu C. S., Lin C. J., Hwang J. K. (2004). Predicting subcellular localization of proteins for Gram-negative bacteria by support vector machines based on n-peptide compositions. *Protein Sci.* 13(5), 1402-1406.

42. Vieler A., Wu G., Tsai C.-H., Bullard B., Cornish A. J., Harvey C., Reca I.-B., Thornburg C., Achawanantakun R., Buehl C. J., Campbell M. S., Cavalier D., Childs K. L., Clark T. J., Deshpande R., Erickson E., Ferguson A. A., Handee W., Kong Q., Li X., Liu B., Lundback S., Peng C., Roston R. L., Sanjaya, Simpson J. P., TerBush A., Warakanont J., Zäuner S., Farre E. M., Hegg E. L., Jiang N., Kuo M.-H., Lu Y., Niyogi K. K., Ohlrogge J., Osteryoung K. W., Shachar-Hill Y., Sears B. B., Sun Y., Takahashi H., Yandell M., Shiu S.-H., Benning C. (2012). Genome, Functional Gene Annotation, and Nuclear Transformation of the Heterokont Oleaginous Alga *Nannochloropsis oceanica* CCMP1779. *PLoS Genet.* Accepted.

43. Jinkerson R. E., Radakovits R., Posewitz M. C. (2012). Genomic insights from the oleaginous model alga *Nannochloropsis gaditana*. *Bioengineered* 4(1).

44. Horner D. S., Heil B., Happe T., Embley T. M. (2002). Iron hydrogenases – ancient enzymes in modern eukaryotes. *Trends in Biochem. Sci.* 27(3), 148-153.

45. Nixon J. E., Field J., McArthur A. G., Sogin M. L., Yarlett N., Loftus B. J., Samuelson J. (2003). Iron-dependent hydrogenases of *Entamoeba histolytica* and *Giardia lamblia*: activity of the recombinant entamoebic enzyme and evidence for lateral gene transfer. *Biol. Bull.* 204(1), 1-9.

SUPPLEMENTAL CHAPTER 1

Discovery and Identification of Novel [FeFe]-hydrogenase Genes[1]

[1]Initial degenerate primer PCR conditions were determined, in part, by Saundra Mason.

INTRODUCTION

The use of hydrogenases to produce H_2 has great potential to supplement existing energy technologies and expand the availability of renewable, clean fuels (1, 2). In particular, [FeFe]-hydrogenases have been investigated for industrial-scale H_2 production, as the catalytic turnover of these proteins is the highest measured among H_2-evolving enzymes (3, 4). For industrial use of these hydrogenases, additional properties would be required for an ideal enzyme, such as: oxygen-insensitivity, a broad pH range, salt tolerance, and thermostability (5, 6, 7). A relatively small number of [FeFe]-hydrogenases have been characterized that possess these properties, and there remains potential for discovery of enzymes with unique qualities.

Degenerate primer-based PCR is one method which could be used to discover new [FeFe]-hydrogenase genes. This technique involves designing primers that utilize nucleotide degeneracy of regions within a gene which are conserved at the amino acid level. Using this approach, homologous protein-encoding genes can be identified, even when large amounts of variability exist elsewhere in the gene. In addition, the efficacy of this method was recently illustrated as degenerate primer-based PCR was used to identify new [FeFe]-hydrogenase genes from a variety of genomic samples (8, 9, 10).

Two primary genomic DNA sources were of interest during our search for new hydrogenase genes. *Geoglobus ahangari* 234 is a hyperthermophilic archaeon that grows anaerobically and is able to oxidize H_2 as an electron source (11). To date, no archaeal genome has been found to contain a gene homolog encoding a functional [FeFe]-hydrogenase. However, the availability of *G. ahangari* 234 genomic DNA, the

greater thermostability of proteins isolated from similar hyperthermophiles, and the noted H_2-oxidizing activity of the organism piqued our interest. Genomic samples from Yellowstone National Park (YNP) were also of interest, as a number of hot springs in the park contain great microbial biodiversity (12, 13). Colonizing and associating with microbial mats in these springs are a variety of auto-, hetero-, and mixotrophic organisms. In addition to high temperatures, these microorganisms often have to deal with both high salinity and extremes in pH, and many are predicted to participate in H_2 metabolism, providing excellent rationale for investigating environmental genomic samples from YNP.

After performing a phylogenetic analysis of known [FeFe]-hydrogenase genes, we identified key regions that were highly conserved between homologs. Using designed primers, ideal PCR conditions were established. No gene fragments homologous to [FeFe]-hydrogenase were identified from *G. ahangari* 234, but 9 gene fragments were found from environmental samples isolated at YNP. Although we extended our knowledge of the fragments, we did not establish the full-length sequence of any one gene fragment and continuing work will focus on this effort.

METHODS

Phylogenetic Tree Construction—The phylogenetic tree used to identify specific clades of organisms was generated using the PHYlongeny Inference Package (PHYLIP) (14). The NCBI database was used to collect 148 annotated and putative [FeFe]-hydrogenase amino acid sequences and these were aligned using ClustalX (15). A protein distance matrix based on the sequences was calculated with the "protdist" algorithm and the tree assembly was carried out using the "Fitch-Margoliash" method. No outgroup was selected and 1,000 bootstrap replicates were performed.

To compare the translated sequences of the identified gene fragments, the alignment software MEGA5 (16) was used to generate a phylogenetic tree comparing 98 [FeFe]-hydrogenase homolog amino acid sequences and the translated gene fragment sequences. [FeFe]-hydrogenase sequences were collected as described previously and the sequences were aligned using MUSCLE (17) with opening gap and gap extension penalties of 13 and 0.05, respectively. Pairwise distances were calculated from the alignment and sequences with a distance <0.1 were eliminated. The remaining 64 sequences were aligned as stated previously, and the alignment was trimmed to isolate only the representative H-cluster-binding domain from HydA. The phylogram was generated by the Neighbor-Joining method (18) and the evolutionary distances calculated by the p-distance method (19). The *Homo sapiens* NARFL protein and *Saccharomyces cerevisiae* Nar1p amino acid sequences were used as outgroups and 2,000 bootstrap replicates performed.

Mulitple Sequence Analysis—Sequences were aligned using the TCOFFEE software tool available at http://igs-server.cnrs-mrs.fr/Tcoffee/tcoffee_cgi/index.cgi.

Degenerate Primer-Based PCR Amplification—Basic PCR amplification was performed as described in section 8.18 of Molecular Cloning (20), using GoTaq Green Master Mix (Promega) and 40 pmol of each primer in a total of 25.0 µL reaction buffer. No BSA was added to the Fe4A reactions, while 200 ng of BSA was added to the Fe9 reactions. Using an Eppendorf Mastercycler, the initial denaturation step was at 95°C for 5 min, followed by 40 cycles composed of (a) 30 s of denaturation at 95°C, (b) 30 s of annealing at 49 °C for Fe9 and 57 °C for Fe4A, and (c) 1 min of elongation at 72 °C. The PCR reaction was finished with an elongation step of 72 °C for 5 min.

Cloning of Gene Fragments—Gene fragments generated during degenerate primer-based PCR were run on a 0.8 % agarose TAE gel (section 5.4 of Molecular Cloning) (20) at 80 V for 30 min. Bands were observed by ethidium bromide-staining and UV illumination. Amplified products were cut from the gel using a clean razor blade and isolated using the QIAGEN Gel Extraction Kit. The isolated amplicons were ligated into the pGEM-T Easy vector (Promega) as described by the kit protocol. The recombinant plasmid was transformed into DH5α *Escherichia coli* chemically-competent cells as described in section 1.116 of Molecular Cloning (20), and selected for resistance to 50 µg/mL ampicillin. Further selection was based on appearance of white transformant colonies in the presence of 20 µg/mL 5-bromo-4-chloro-indolyl-β-D-galactopyranoside (X-gal), denoting β-galactosidase gene interruption by insertion of a gene fragment.

Gene Fragment Identification—White transformant colonies were individually picked with a toothpick and first dipped into a PCR tube containing 11.5 µL sterile water before being streaked onto an LB plate containing 50 µg/mL ampicillin and allowed to grow overnight at 37˚C. Reactions for colony PCR were prepared by adding 12.5 µL of GoTaq Green Master Mix (Promega) and 0.5 µL each of 25 µM forward and reverse M13 primers (5'-GTAAAACGACGGCCAG-3' and 5'-CAGGAAACAGCTATGAC-3', respectively) to each PCR tube. Using a thermocycler, the initial denaturation step was at 94 ˚C for 5 min followed by 30 cycles composed of (a) 30 s of denaturation at 94 ˚C, (b) 30 s of annealing at 48˚C, and (c) 2 min of elongation at 72 ˚C. The PCR reaction was finished with an elongation step of ˚72 for 2 min. The PCR products were analyzed on a 0.8% agarose TAE gel and clones that generated DNA fragments >200bp were flagged for DNA isolation and sequencing. Bacterial cultures were started using flagged transformants in 5 mL of 50 µg/mL ampicillin-supplemented LB and shaken overnight at 37˚C. DNA was isolated from these cultures using the QIAGEN Miniprep DNA Kit, and DNA samples were sent for sequencing to the Michigan State University Research Technology Support facility (http://rtsf.msu.edu/). Resulting sequences were translated, BLASTed against the NCBI database, and flagged for further investigation if they matched an [FeFe]-hydrogenase gene with >55% query coverage and had a <0.001 e-value.

Whole Genome Amplification—To amplify the entirety of the environmental genomic DNA samples, the REPLI-g Mini Kit was used (QIAGEN). The reaction was carried out as recommended by the kit protocol, aliquoting 2.5 µL of template DNA to 50 µL of

reaction and incubating at 30C for 16 h . After amplification, the enzyme was inactivated at 65 ˚C for 3 min.

Sequence Extension—The known sequence of each gene fragment was extended in a sequential process. A 23.5 µL aliquot of REPLI-g amplified genomic sample was mixed with 2.5 µL of 10X restriction digest buffer, 2.5 µL of 10X BSA, and 1.0 µL of desired restriction enzyme (New England Biolabs) and incubated at 37C for two h. The digestion reaction was inactivated at 80 ˚C for 15 min. The digested sample was ligated using T4 DNA ligase (New England Biolabs) overnight at room temperature. The ligated samples were amplified via PCR using GoTaq Green Master Mix with a primer pair specific to the gene fragment of interest. Resulting PCR products were cloned into the pGEM-T Easy vector and sequenced as described above. The new sequence was then compared to the gene fragment of interest. If significant overlap existed, the gene fragment sequence was extended by adding the newly sequenced fragment to either the 5'- or 3'-terminus.

RESULTS

Targeted Degenerate Primer Design—In an effort to design targeted degenerate primers, a phylogenetic tree of 148 [FeFe]-hydrogenases was constructed and individual clades were classified (data not shown). To identify conserved sequences unique to each clade, multiple sequence alignments were generated (TCOFFEE) using clade-specific amino acid sequences. Four clades contained regions of conserved residues unique to those individual clades and degenerate primers of 15-20 bp in length were designed using these regions (Table S1.1, Figure S1.1abcd). Regions of strictly conserved residues among all [FeFe]-hydrogenases were not considered in this analysis.

Table S1.1. **Table of Clade-Specific [FeFe]-hydrogenase Degenerate Primers.** Strictly conserved amino acid (AA) residues are in **bold**. Moderately conserved AA residues are denoted as X/Y, where "X" and "Y" are the residues most commonly observed.

Primer	Clade	Strand	Sequence	Degenerate Primer Sequence
EH295	Green Algae	Sense	H/Q**LE**Q/A**HP**	CAYYTNGARSVNCAYCCNMA
EH296	Green Algae	Anti	**NAKKLI**	NATNAGYTTYTTNGCRTG
EH297	Cellulolytes	Sense	**LC**G/RD/R**C**	CTNTGYGGNGAYTGYG
EH298	Fungi	Sense	**VENPI**	GTNGARAAYCCNATHCC
EH299	Fungi	Anti	**PKSAD**	RTCNGCNGAYTTNGG
EH300	Thermophiles	Anti	**IY**T/S/E**IDE**	YTCRTCDATNKHRTADAT

Figure S1.1. **Multiple sequence analysis of both clade-specific and general hydrogenase proteins.** Using TCOFFEE, amino acid sequences from either clade-specific proteins or from the *Clostridium pasteurianum* HydA protein were aligned. Degenerate primer design was based on regions of high conservation, which are highlighted in the each of the alignments. A) Green algal clades sequences. B) Fungi clade sequences. C) Hyperthermophilic bacteria clade sequences. D) Cellulolytic bacterial clade sequences. E) Various sequences from each mentioned clade and the *C. pasteurianum* HydA sequence.

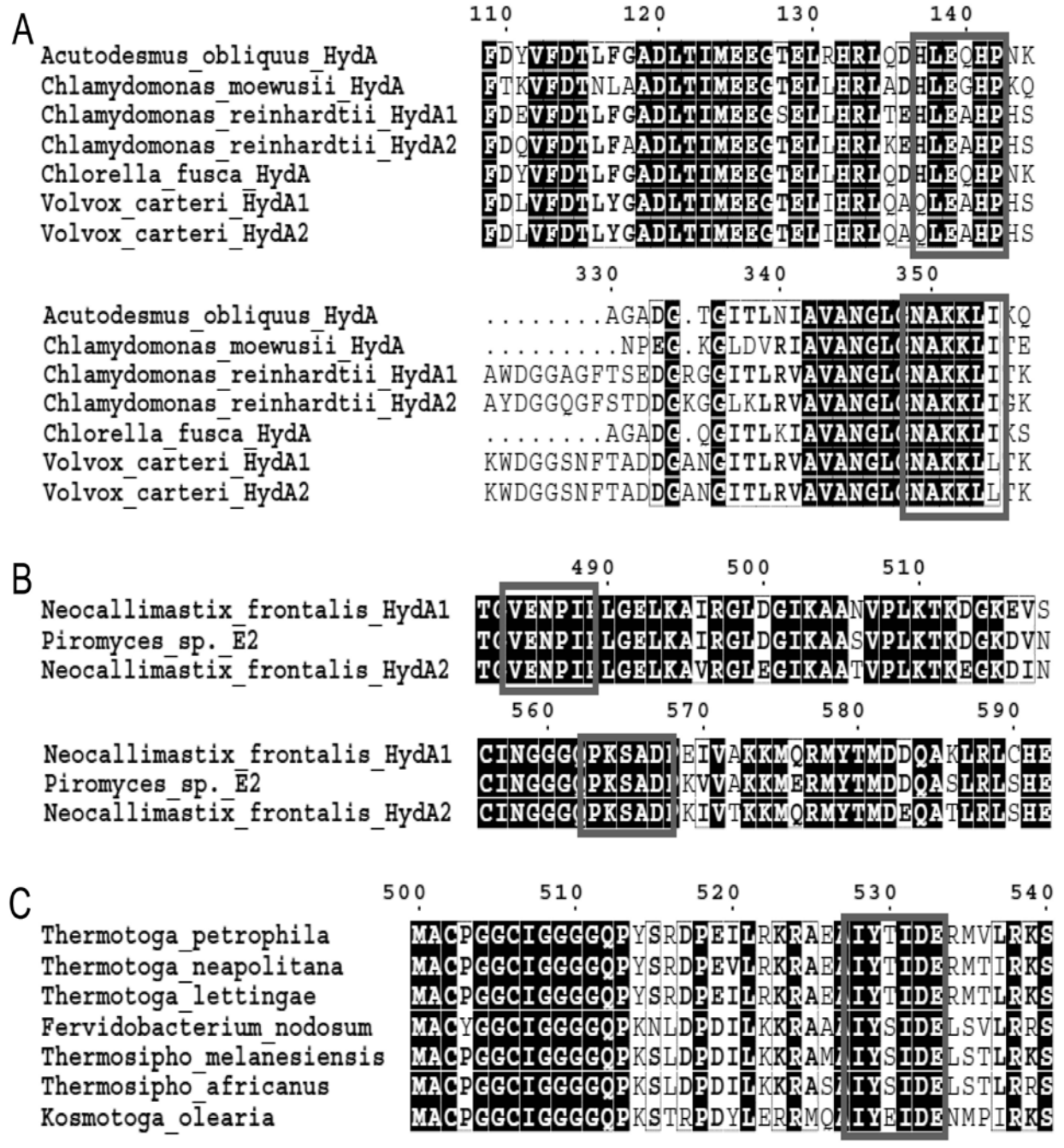

Figure S1.1 (cont'd)

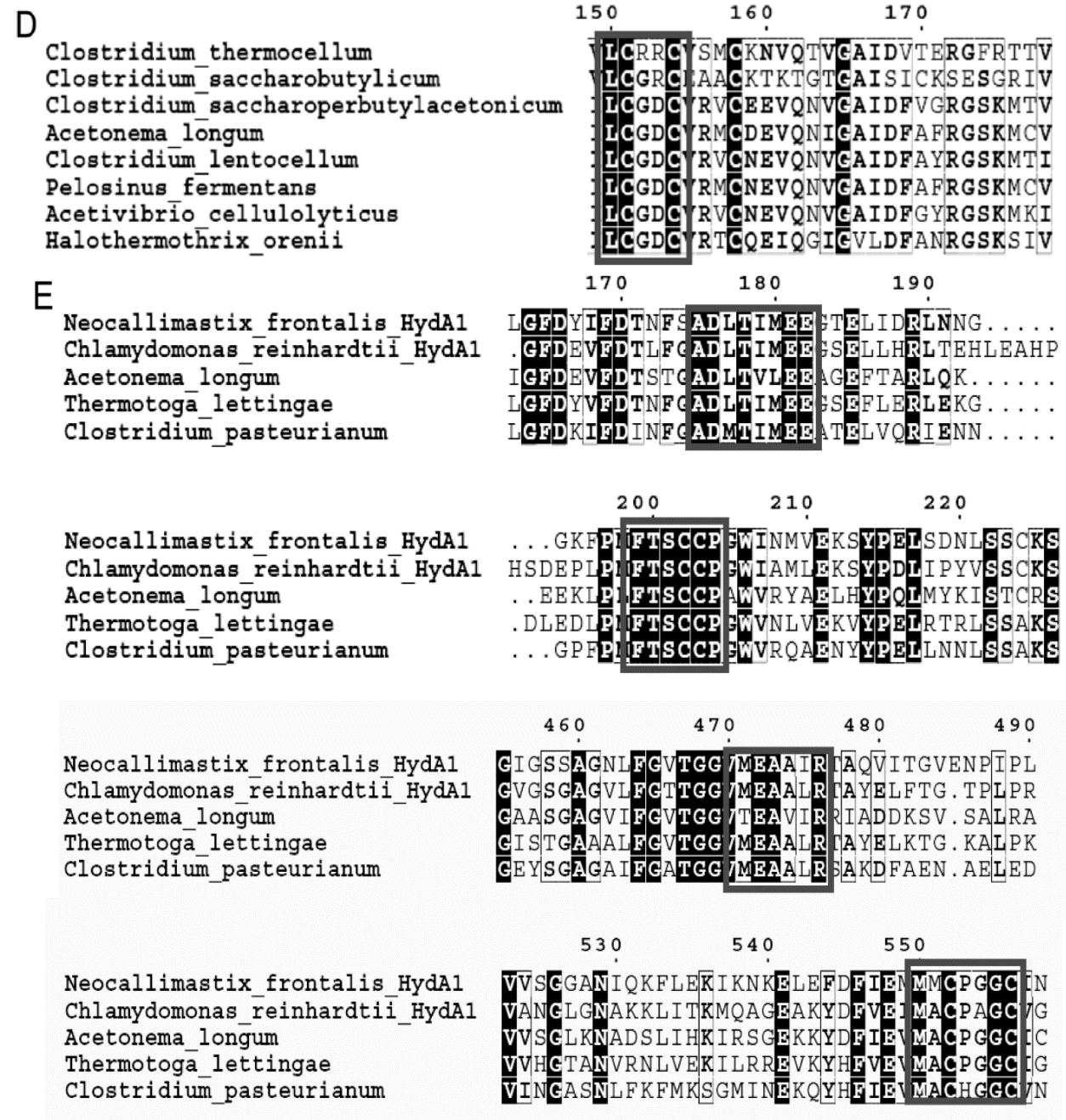

General Degenerate Primer Pair Design and Testing—The degenerate primers described above were designed to amplify specific regions that are not ubiquitous to all [FeFe]-hydrogenase genes. To discover new genes from a wide variety of organisms, however, general primers which apply to all hydrogenase genes were required. Previously, Zac Stephens and Pamela Smith from the Hegg lab designed three sets of degenerate primer pairs which target several regions of high conservation among [FeFe]-hydrogenase genes (Table S1.2, Figure S1.1e). To optimize PCR conditions with the general degenerate primers, *S. oneidensis* MR-1 genomic DNA, which encodes an [FeFe]-hydrogenase, was used to ascertain the best conditions and degenerate primer pair combinations for amplification of a valid gene fragment from the DNA. Ideal PCR conditions were established and are described in the Methods section. The primer pairs best suited to isolate the *S. oneidensis* [FeFe]-hydrogenase gene were pair Fe4A (Fe_4F, Fe_6R) and Fe9 (Fe_9F, Fe_9R) and were used for subsequent degenerate primer-based PCR amplification reactions.

Investigation of G. ahangari *234 Genomic DNA*—Genomic DNA from the hyperthermophilic archeon *G. ahangari* 234 was supplied by Dr. Kazem Kashsefi from the Department of Microbiology and Molecular Genetics at Michigan State University. This DNA was amplified by PCR with both the Fe4A and Fe9 primer pairs under a variety of conditions (i.e. varying [Mg^{2+}] and annealing temperatures). Out of 20 PCR products initially identified and sequence, no amplified products demonstrated significant homology to known [FeFe]-hydrogenase sequences.

Table S1.2. **Table of General [FeFe]-hydrogenase Degenerate Primers.** Strictly conserved amino acid (AA) residues are in **bold**. Moderately conserved AA residues are denoted as X/Y, where "X" and "Y" are the residues most commonly observed.

Primer	Strand	AA Sequence	Degenerate Primer Sequence
Fe_6F	Sense	**AD**L/M**T**I/VM/L**EE**	GAYYTNACNATHATGGARGAR
Fe_1F	Sense	**P**M/L**FTSCCP**	CANTCNTGYTGYCCNG
Fe_4F	Sense	**P**M/L**FTSCCP**	CCNATGTTYACNAGYTGYTGY
Fe_9F	Sense	**P**M/L**FTSCCP**	CCICARTTYACNWSNTGYTGY
Fe_4R	Anti	M/T**EA**V/AL/I**R**	CKNTCNGCYTCNHMYTTYTT
Fe_9R	Anti	M/T**EA**V/AL/I**R**	KWNCKNARNGCNGCYTCCAT
Fe_1R	Anti	**M**M/A**C**P/HG/A**GC**	RTNNCCNGGRCANGCCAT
Fe_6R	Anti	**M**M/A**C**P/HG/A**GC**	RCANCCNCCNGGRCANGCCAT

Investigation of Environmental Genomic DNA Samples from YNP—A relatively small amount of environmental genomic DNA samples from YNP was available for experimentation. To generate more DNA sample, each environmental DNA sample was amplified using REPLI-g, a whole genome amplification kit. The products of the REPLI-g reaction were then used in further experiments.

Environmental genomic DNA samples isolated from 10 distinct sites in the YNP were kindly donated by the Lucigen Corporation (http://www.lucigen.com/). DNA from these samples was amplified by PCR using both the Fe4A and Fe9 primer pairs and performed under the idealized conditions established previously. Nine gene fragments, out of a total of 60 that were isolated and sequenced, were found to have similarity to [FeFe]-hydrogenase genes. Of these 9 fragments, 5 were determined to be distinct from one another and were used for further experiments (Table S1.3). A multiple sequence alignment of these 5 fragments can be seen in Figure S1.2.

Table S1.3. **Table of Gene Fragment DNA Sequences**

Gene Fragment	Length	Sequence
5sisN3.1	453 bp	ATTCCGCAGTTTACGTGGTGTTGTCCAGCCTGG GTTCGGTAAAAACCTATGGTGCAAAAGAGGTTTG GAAAGTAAACCCTGAAGACATGTATATGGTTGGC GTTATGCCCTGTACTGCCAAGAAGTTTGAAGCTT CGCGTCCAGAGTTCCAAAGTGCTGCCCATTATTG GCAGACCCAGGGTAGATCAGGCAGCTATCCAGA TATTGATGTAGTTCTTACTACCAGAGATTTAGCCC GTCTGTTCAAGAAACTAAACATCGACATCAAAAC AGTCGCTGAATTTAGCGACAAAGATAATCCGCTA GCCCAATACAGTGGGGCAGGTACTATTTTTGCCA ACACCGGCGGTGTAATGGAAGCCGCCTTCCGCT CA
AZTEC.1	777 bp	GCGCAAACAGCTCCATCTGTCAGGGTTGCAATA GGTGAAGAATTTGGCATGGAACCCGGAAGCATAA GCACAGGGAAGATGGTTGCTGCACTTAGAAGACT TGGTTTCGACTATGTATTTGACACAAACTTCGCAG CTGACCTTACAATTATGGAAGAGGGTTACGAACT GATTGGAAGGCTCCAAAACGGCGGTAAGTTCCC AATGTTTACGAGGTGTTGTCCTGGTTGGGTAAACG AAATGGAGAAAGAATGGCCCGAACTCAGAGAAC ACCTTTCAACGGCAAAGTCCCCACAACAGATGAT GAGTAGTCTTGTCAAAACATACTTTGCACAAAAGA TAGGTGTGAAACCTGAAGATATAGTTATGGTATCA ATTATGCCATGTACAGCTAAGAAAGACGAAATAA CAAGACCACAACAATTGGTCGACGGTATCAAAGT AACGGATTACGTCATTACAACAAGAGAACTCGGA AAGCTCATTAAACTCAAAGGTATACCATTCGTAAA TCTTCCAGAAGAACAGTATGATAGCCCACTTGGA ACATCAACAGGTGCTGCTGCGCTCTTTGGTGTGA CTGGCGGTGTTATGGAAGCAGCTCTCAGAACAGC TTACGAAGTTTTGACAGGCGAGAAATTACCGAAA CTTGTGTTCGAAAGCGTACGAGGCCTGGATGGTG TAAGAGAAGCAGAAATTGATATCAATGGAAGATG CTAAACAGCAAGGAACCCTAATTCTTCACCTATT GCAACGGACAAGACTACTCATCATCTA-3'
AZTEC.2	786 bp	CATGGCGGCCGCGGGAATTCGATTCCAATGTTTA CGAGCTGCTGTCCGGGCTGGATTGCGATGCTGG AAAAAAGCTATCCGGATCTGATTCCGTATGTGAG CAGCTGCAAAAGCCCGCAGATGATGCTGGCGGC GATGGTGAAAAGCTATCTGGCAGAAAAAAAAGG

Table S1.3 (cont'd)

		CATTGCGCCGAAAGATATGGTGATGGTGAGCATT ATGCCGTGCACCCGTAAACAGAGCGAAGCGGAT CGTGATTGGTTCTGCGTGGATGCGGATCCGACCC TGCGTCAGCTGGATCATGTGATTACCACCGTGGA ACTGGGCAACATTTTTAAAGAACGTGGCATTAAC CTGGCGGAACTGCCGGAAGGCGAATGGGATAAC CCGATGGGCGTGGGCAGCGGCGCGGGCGTGCT GTTCGGCACCACCGGCGGCGTGATGGAAGCGG CGCTGCGTACCGCGTATGAACTGTTTACCGGCAC CCCGCTGCCGCGTCTGAGCCTGAGCGAGGTGCG TGGCATGGATGGCATTAAAGAGACCAACATTACC ATGGTGCCGGCGCCGGGCAGCAAATTTGAAGAA CTGCTGAAACATCGTGCGGCGGCGCGTGCGGAA GCGGCGGCGCATGGCACCCCGGGCCCGCTGG CGTGGGATGGCGGCGCGGGCTTTACCAGCGAAG ATGGCCGTGGCGGCATTACCCTGCGTGTGGGCG TGGCGAACGGCCTGGGGCACGCGAAAAACTGAT TACCAAATGCAGGCGGGCGAAGCGAATATGATTT GTGGGAATATGCATGTCCCGCG
MNDWOOD.1	796 bp	TCCGATGTTCACGAGTTGCTGTCCCAGCTGGGTG AAGTTTGCCGAACAGTATTACCCCGAGCTGTTGC CCAATTTGTCCACCTGCAAGTCGCCCCAGCAGA TGTTTGGCAGCGTGGCCCGCGAGGTTCTTCCTAA ATTGCTCAATATCAAGCCCGAAAACCTTGTCATTG TGTCAATTATGCCTTGCACGGCCAAAAAGTATGA GGCCAAACGCGATGAGTTTATCCATGATGGCCTT GCCGAGGTTGACCATGTGCTCACTACGGAAGGT CTTGGCCGCATGATACACGAAACCGGATTACAGT TCAATAAGCTGAAGCCCGAGTCGTTCGATATGCC ATTGGGCTTTAAGACCGGAGCAGGGGTAATATTC GGTAACACTGGCGGAGTGAGCGAAGCAGTATTG CGTTTCGCCTACGAAAAGATTACCGGTGAAACCC TGATCGACACCGACATCCGGCAGACCCGTGGTA TGGAAGGTATTCGCACAGTGGAGATGCAACTCGG CGAAACCAGAATTAAGCTCGGGATTGCGCATACC CTCTCGAATGCCCGCAAACTGTGCGATGCCATAG TGAAAGGCGAAGCCGATTACGACCTTGTGGAAGT GATGGCCTGCCCGGGCGGCTGTATTGCAGGTGG CGGACAACCAGTGAGCTTCGACCCCGAATTCAG ACAAAAGCGAATTCAAGGGATCTACAATGCCGAT AAACAGCTCGAACTGCACAAATCGCAGGACAATC

Table S1.3 (cont'd)

		CTTATGTTAAGGAGTTGTATCAGAATATTTTAGGCG GAAATAGGCGGACACAG
MNDWOOD.2	910bp	CATTGCCGGAGGAGGACAGCCTTATCACCATGG CAATGATGAGATTGTTAAAAAACGCAGGGAAGCC ATATTTGAAGAGGATAGGAACAAAAAGATAAGAA AATCCCATGAGAACAAAGAAATATTGGAACTATA GCAAAAACCTACTATGCTGAAAAGATGGGAATTG ACCCCGACAATATTGTTATGGTATCTGTCATGCC CTGCATAGCAAAGAAAGGCTGAAGCCAAACGTC CCGAGCTGACAAAGGACGAACACAACAATGTAG ACATATCAATAACCACCTCCGGGAGCTTGGTGCC ATGATACATGAAGCGGGAATAGAATTTGCAAAGC TGCCCGACAGTGAATTTGACAGTCCGCTTGGTGA ATCCTCGGGGGCAGCCGTAATGTTCGGTACTGCC GGAGGCGTTATTGAGGCGGCTCTGCGTACAGCC TCAGAATGGCTGACAGGTGAACCTCTTAAGAAAA TAGAATTTGAAGATTTAAGGGGTATGGAGGGAGTT CGCAGAGCTGCTGTCAAAATAGGAGACAAGGAA CTCAAAATAGGTATTACAAACGGTCTGGGCAATG CACGGCATATATTGGAGGATATCCGCGACGGAA AGGCGGACTACCATGCTATTGAGATAATGGCTTG TCCCGGAGGCTGCATTGCCGGAGGAGGACAGC CTTATCACCATGGCAATGATGAGATTGTTAAAAA ACGCAGGGAAGCCATATTTGAAGAGGATAGGAA CATGAAGATAAGAAAATCCCATGACAACAAAGAA ATATTGGAATTATATAAAACTTATCTGGGTGAACC TTTTAACAAAATAGAATTTGAAGATTTAAAGGGTAT GGAGGGAGTTCTCAGAGCTGCTGTCATACTATGA TACCAGGAACTCAAAATCACTAATGAATTCT

Figure S1.2. **Multiple sequence analysis of gene fragment and [FeFe]-hydrogenase sequences.** Using TCOFFEE, amino acid sequences of the translated gene fragments were compared with known [FeFe]-hydrogenase protein sequences by sequence alignment, as well as the homolog Nar1p from *S. cerevisiae.*

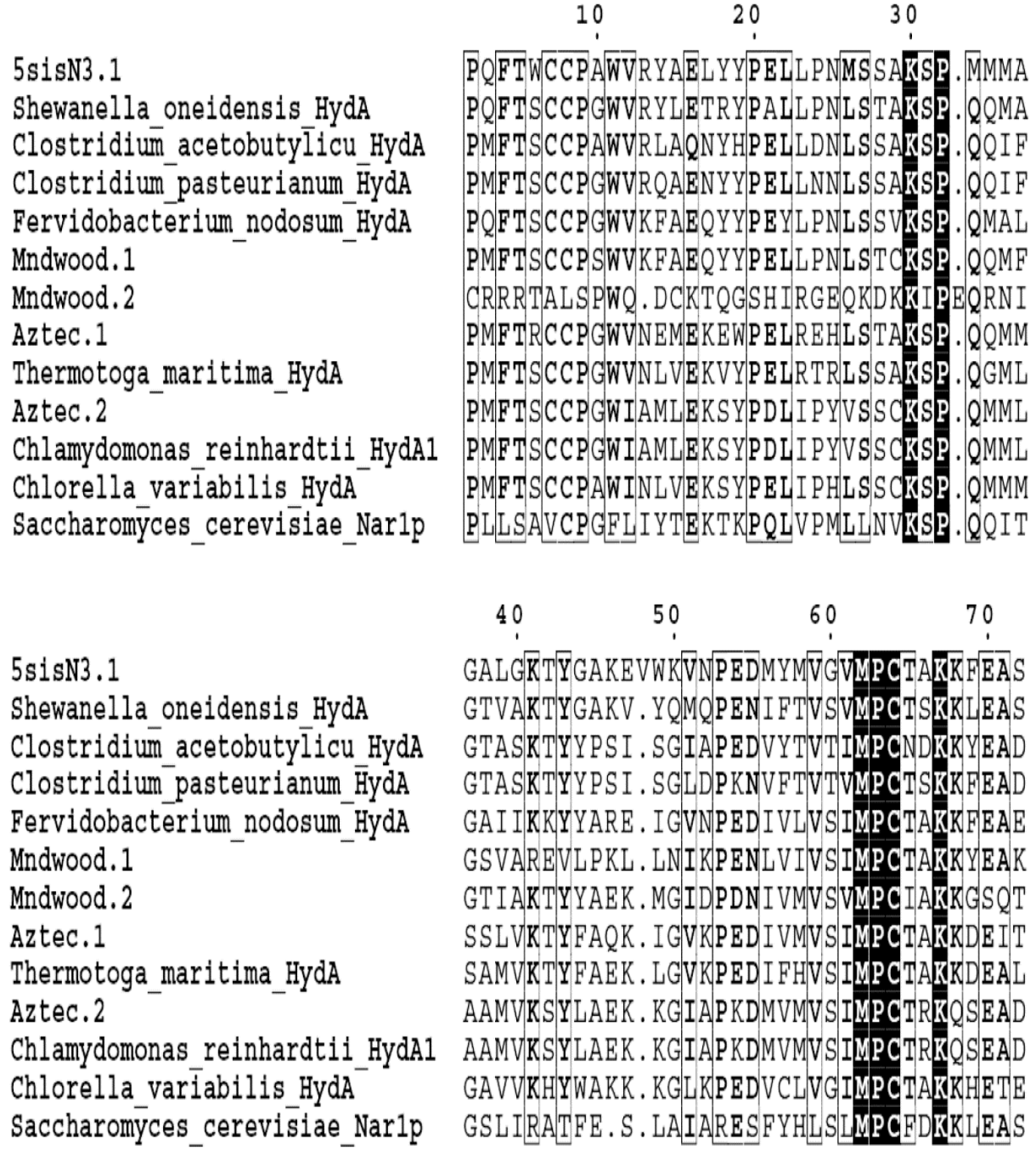

Full-Length Gene Sequence Determination—To determine the full-length gene sequence from the identified fragments, a common restriction site was found within each gene fragment and genomic samples were digested with the desired restriction enzyme. After inactivating the restriction enzyme, ligase was added to each sample to ligate digested fragments within the reaction, essentially generating a variety of circular DNA molecules, some containing the gene fragment of interest. Next, primer pairs were designed at the 5'- and 3'-ends of the fragment, as well as near the restriction cut-site, to amplify *away* from the fragment and into "unknown" gene sequence. The ligation products were then amplified by PCR using the newly-designed primers (Figure S1.3, Sequence Extension Method). The resulting PCR products were sequenced, thereby extending the sequence coverage of the unknown gene.

This method was applied to each of the 5 gene fragments, extending the fragment gene sequence of each except 5sisN3.1 and AZTEC.2 (Table S1.3). At the time of this report, none of the full-length genes had been completely sequenced.

Figure S1.3. **Gene sequence extension methodology.** Graphic representation of the Sequence Extension Method. The gene fragment of interest is light gray, while the "unknown" sequence is dark gray. A common four-base restriction site (HhaI, GTAC) which occurs once in the gene fragment is marked by "┐└". Arrows represent primers designed to amplify away from the gene fragment and into unknown sequence.

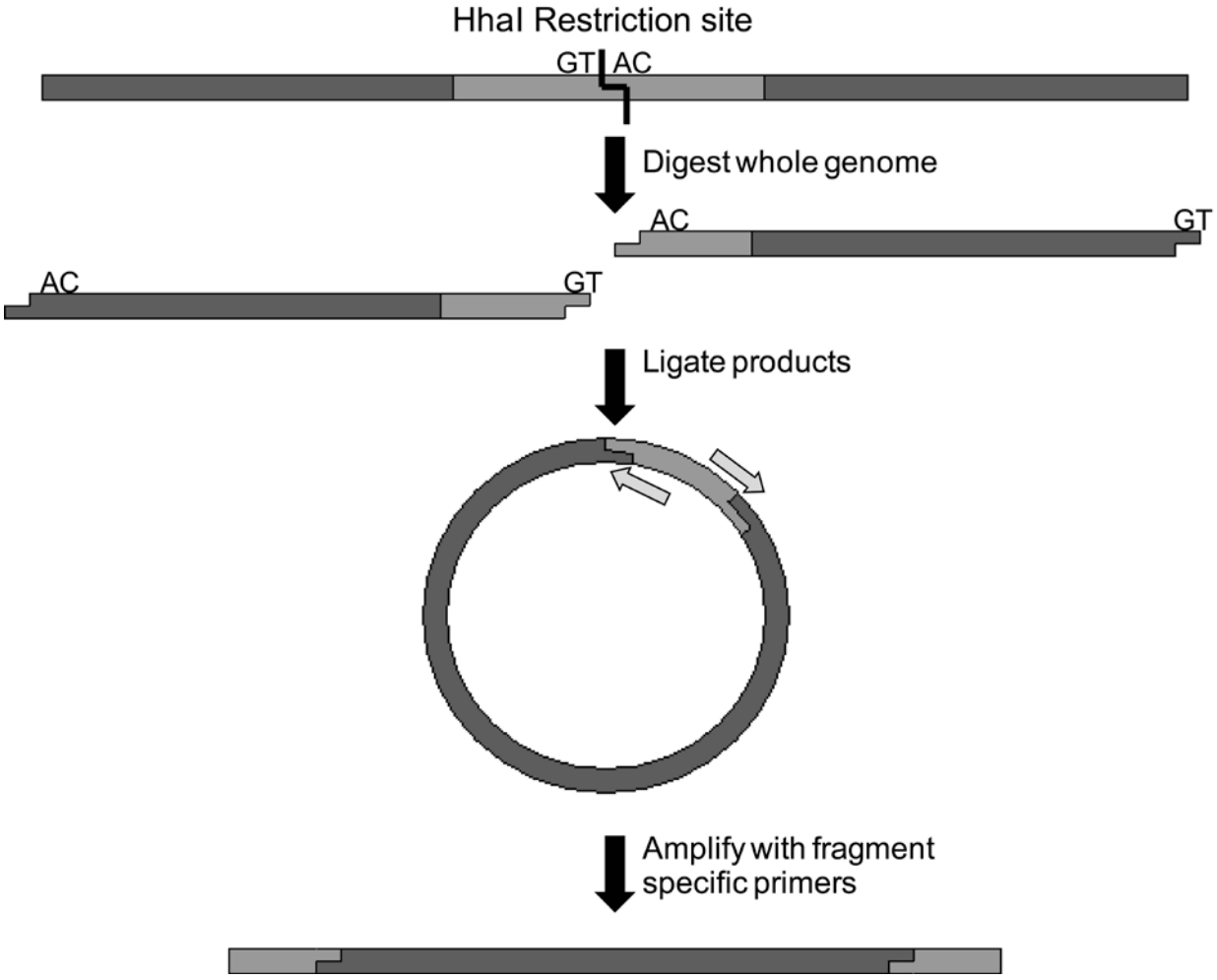

Phylogenetic Analysis of Gene Fragments—To determine a relationship between the identified fragments and known [FeFe]-hydrogenases, a phylogenetic analysis was performed (Figure S1.4). The 5sisN3.1 fragment grouped mostly closely with the *S. oneidensis* MR-1 *hydA* gene, but also groups with genes from *Desulfovibrio* species. The AZTEC.2 fragment groups well with green algal genes and mostly likely comes from a a member of this species, whereas the AZTEC.1 fragment demonstrates a strong relationship to both *Fervidobacterium* and *Thermosipho* species' hydrogenase genes. The MndWood.1 gene demonstrates a relationship only with the *Ruminococcus gnavus hydA* gene. The MndWood.2 fragment was found to associate with *Desulfotomaculum* species and grouped loosely with *Alkaliphilus metalliredigens* and *Clostridium ljungdahlii*, species which are obligate anaerobes.

Figure S1.4. **Evolutionary relationship of translated gene fragments and [FeFe]-hydrogenases.** Phylogenetic analysis of 64 [FeFe]-hydrogenase amino acid sequences and translated gene fragments using the MEGA5 software program. Evolutionary relationships are inferred by the Neighbor-Joining method and 2,000 bootstrap replicates were performed. Evolutionary distances were calculated by the p-distance method and the branch lengths are equal to the number of amino acid substitutions per site. The tree was rooted using Nar1 sequences from *H. sapiens and S. cerevisiae*.

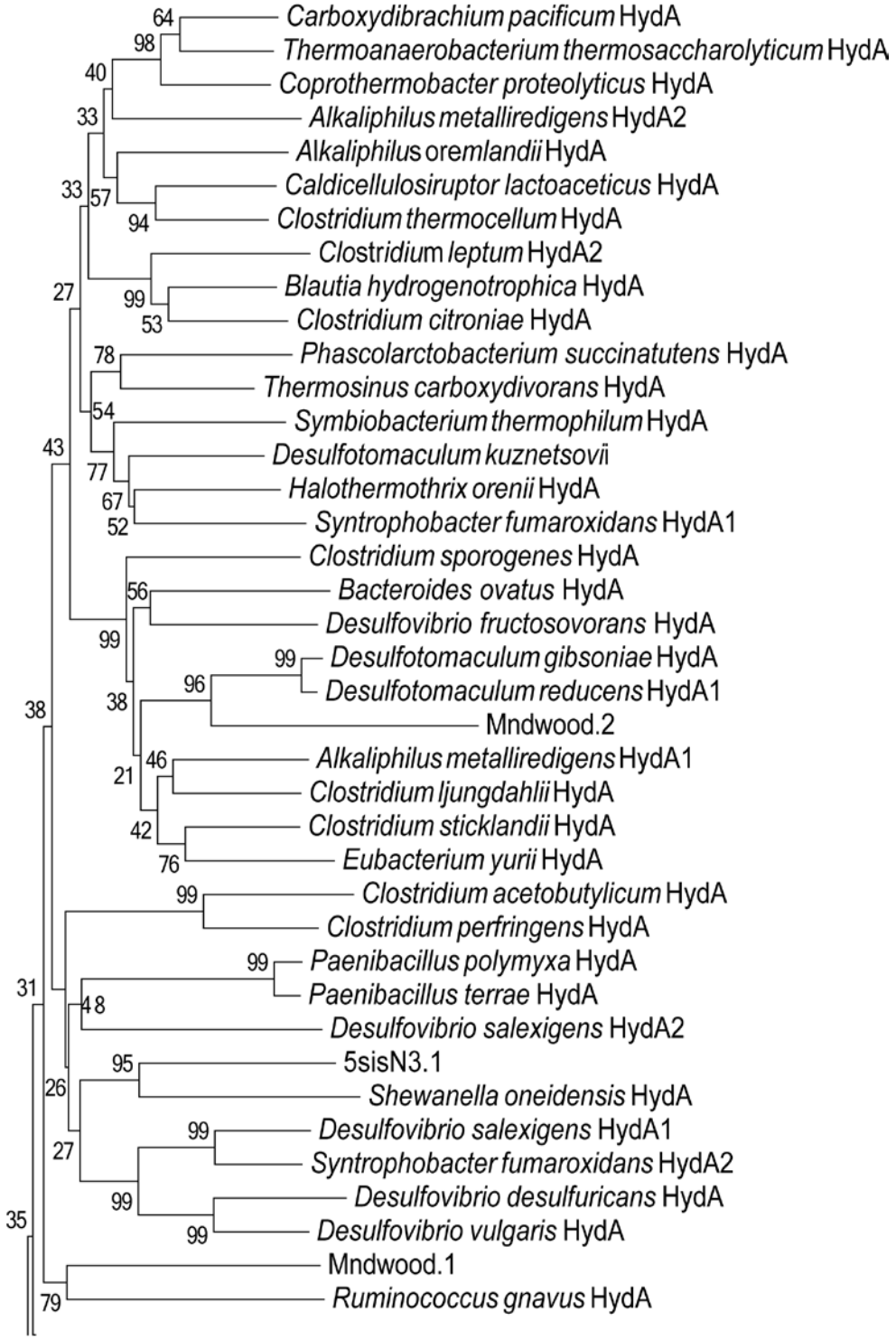

Figure S1.4. (cont'd)

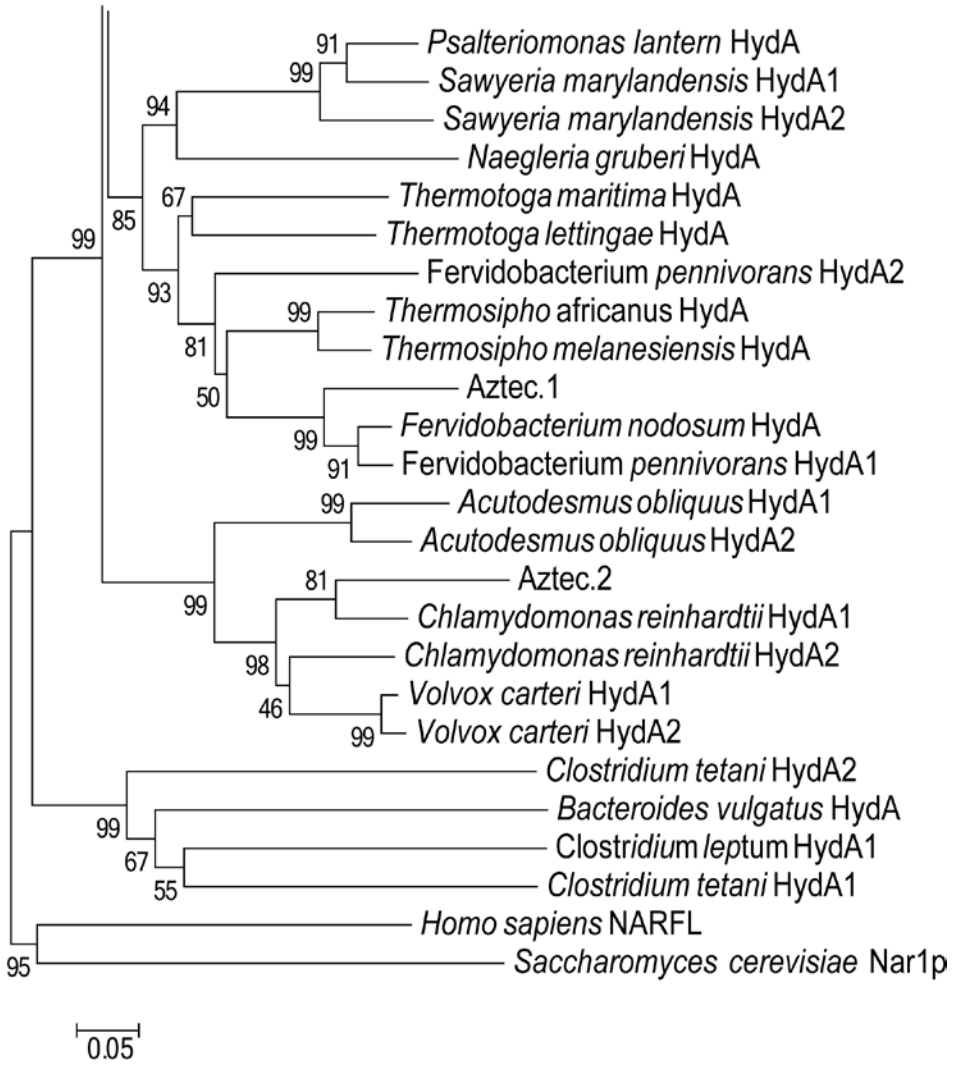

DISCUSSION

Current Results and Interpretation—In an effort to discover new and potentially novel [FeFe]-hydrogenases, degenerate primers were used to amplify genomic DNA samples. In particular, primer pairs that are specific to [FeFe]-hydrogenase-conserved amino acid sequences were used for this amplification. Uniquely conserved regions can be observed within several clades identified via phylogenetic analysis, and these regions were used to design clade-specific degenerate primers. Currently, no experiments have been performed utilizing these clade-specific primers, principally due to the samples available to us. *G. ahangari* 234 is an archeon and does not match any clade identified on the phylogram, thereby greatly decreasing the utility of clade-specific primer pairs for this organism. Additionally, the YNP environmental samples were composed of unknown genomic DNA and likely contain DNA from many organisms that are not targets of the clade-specific primers. Thus, our studies utilized primer pairs specific to strictly conserved amino acid regions (Fe4A and Fe9) in order to isolate the maximum number of gene fragments available. In future experiments, the clade-specific primers could be used to target hydrogenase genes in genomic DNA from individual organisms.

G. ahangari 234 genomic DNA was amplified using optimized PCR conditions with both the Fe4A and Fe9 degenerate primer pairs, and the resulting PCR fragments were sequenced. None of the resulting PCR fragments were homologous to known [FeFe]-hydrogenases. This result is not surprising because all characterized H_2-producing enzymes found in archaea are [NiFe]-hydrogenases. Although an unidentified [FeFe]-hydrogenase could be responsible for the noted H_2 metabolism of *G. ahangari* 234,

based on the data collected here, a different enzyme is likely responsible for this metabolism.

Genomic DNA samples from YNP were amplified utilizing the Fe4A and Fe9 degenerate primer pairs and 9 gene fragments were identified. Utilizing multiple sequence analysis, 4 of the fragments were found to be highly homologous to the AZTEC.2 gene fragment and, as the purpose of this work was to find novel genes, full-length determination of these fragments was not pursued. Taking advantage of restriction sites commonly found in DNA (specifically, short recognition sequences), the environmental genome samples were digested with restriction enzymes, re-ligated to form small DNA molecules, and amplified using primers specific to the gene fragments. The amplified products were sequenced, examined for overlap with the gene fragments, and added to the fragment sequences when positive overlap was determined (Figure S1.3). The AZTEC.1, MndWood.1, and MndWood.2 sequences were all extended by 200-700 bp using this method, but unfortunately no new sequence was added to the 5sisN3.1 or AZTEC.2 sequences.

A number of interesting aspects were noted when examining each of the gene fragments. First, all of the fragments contained canonical [FeFe]-hydrogenase motifs: “VXXMPTC” and “GGVXMEAAXR”. Second, the well-conserved motif “TSCCP” matched exactly with the MndWood.1 and AZTEC.2 gene fragment sequences, but was not observed in the MndWood.2 sequence. This may be due to inaccuracies in amplification during extension of the gene fragment or to the presence of “filler” sequence not normally observed in this region of HydA protein sequence. Intriguingly, in the amino acid sequence of the 5sisN3.1 and AZTEC.1 fragments the serine residue of

the “TSCCP” motif is replaced by tryptophan and arginine, respectively. A role for this serine in hydrogenase activity has yet to be determined, but this residue is strictly conserved among all known HydA proteins. Although this may be a novel finding, it is more likely due to errors in amplification and sequencing, as a small change in the triplet codon for serine (TCN and AGY) can easily lead to tryptophan (TGG) or arginine (AGG).

A phylogenetic analysis was performed to provide insight into the evolutionary relationship between each of the gene fragments and known *hydA* genes. Little information could be gleaned from the MndWood.1 fragment, which only showed a relationship to the HydA protein from *R. gnavus*, a gut microbe that is unlikely to be closely-related to YNP hot springs microbes. The MndWood.2 fragment showed similarity to several strict anaerobes, but more information on the complete gene sequence is needed for further identification. The 5sisN3.1 fragment clustered with genes from bacteria commonly involved in sulfate-reduction, indicating that this fragment may originate from similar organisms. Relationships between the AZTEC fragments were among the most interesting, clustering well with green algal (AZTEC.2) and hyperthermophilic bacterial proteins (AZTEC.1). As seen in Figure S1.4 and discussed previously in relation to *Volvox carteri* (Chapter 4), green algal [FeFe]-hydrogenase genes were presumably acquired via horizontal gene transfer, and the two clades discussed previously are hypothesized to share a common ancestor gene. Because these gene fragments were isolated from the same environmental genomic DNA sample, this strongly suggests that organisms with homologous genes to these fragments currently coexist in YNP hot springs. Assuming that AZTEC.2 and AZTEC.1

are green algal and hyperthermophilic bacterial in origin, respectively, this further suggests that green algae acquired [FeFe]-hydrogenases via horizontal gene transfer, and this event may have occurred in a YNP hot spring-like environment. Additional evidence, such as determining the full-length sequence of the AZTEC fragments would be required to lend more support to this claim.

Due to a change in focus of the thesis project, no additional experiments or analyses were undertaken.

Future Directions—Several gene fragments have been isolated from YNP environmental genomic samples and the translated sequences show strong similarity to known HydA proteins. The full-length sequence of these fragments remains to be determined and this can be accomplished using the Sequence Extension method described previously. Additionally, using knowledge gained from the phylogenetic analysis, clade-specific degenerate primers could be used to extend sequence knowledge of the AZTEC fragments, which demonstrated clustering with both the green algal and the hyperthermophilic bacterial clades. Once the full-length sequences are determined, the genes can be amplified, cloned into the pAC-BAD expression vector, and transformed into the *S. oneidensis* MR-1 *ΔhydAΔhyaB* overexpression system. The expressed and purified gene products can then be characterized on the basis of H_2 evolution activity, thermostability, salt tolerance, pH stability, and resistance to O_2-induced inactivation. In addition, the full-length sequences of the putative genes can be directly compared to known *hydA* sequences, and a more definitive evolutionary analysis conducted by phlyogram.

Conclusions—Using a phylogenetic tree of HydA homologs, we designed several clade-specific degenerate primers, concentrating on regions of residues with high conservation between HydA proteins within that clade. Degenerate primer pairs designed to target highly-conserved regions of all HydA genes were utilized to optimize conditions for PCR amplification of *S. oneidensis* MR-1 genomic DNA. These conditions were used to PCR amplify putative *hydA* gene fragments from *G. ahangari* 234 genomic DNA and YNP environmental genomic DNA. Under the conditions tested, 0 and 9 amplicons with homology to *hydA* genes were identified from *G. ahangari* 234 and the YNP samples, respectively. Extension of the YNP gene fragment sequences was attempted for 5 of the 9 YNP fragments, meeting with moderate success. Future work will focus on determining the full-length sequence of these fragments and characterizing the gene products.

REFERENCES

REFERENCES

1. Ghirardi M. L., Dubini A., Yu J., Maness P. C. (2009). Photobiological hydrogen-producing systems. *Chem. Soc. Rev.* 38(1), 52-61.

2. McKinlay J. B., Harwood C. S. (2010). Photobiological production of hydrogen gas as a biofuel. *Curr. Opin. Biotechnol.* 21(3), 244-251.

3. Adams M. W. (1990). The structure and mechanism of iron-hydrogenases. *Biochim. Biophys. Acta.* 1020(2), 115-145.

4. Frey M. (2002). Hydrogenases: hydrogen-activating enzymes. *Chembiochem* 3(2-3), 153-160.

5. Lee H. S., Vermaas W. F., Rittmann B. E. (2010). Biological hydrogen production: prospects and challenges. *Trends Biotechnol.* 28(5), 262-271.

6. Eberly J. O., Ely R. L. (2008). Thermotolerant hydrogenases: biological diversity, properties, and biotechnological applications. *Crit. Rev. Microbiol.* 34(3-4), 117-130.

7. Maeda T., Sanchez-Torres V., Wood T. K. (2008). Protein engineering of hydrogenase 3 to enhance hydrogen production. *Appl. Microbiol. Biotechnol.* 79(1), 77-86.

8. Ballor N. R., Leadbetter J. R. (2012). Patterns of [FeFe] hydrogenase diversity in the gut microbial communities of lignocellulose-feeding higher termites. *Appl. Environ. Microbiol.* 78(15), 5368-5374.

9. Calusinska M., Joris B., Wilmotte A. (2011). Genetic diversity and amplification of different clostridial [FeFe] hydrogenases by group-specific degenerate primers. *Lett. Appl. Microbiol.* 53(4), 473-480.

10. Boyd E. S., Spear J. R., Peters J. W. (2009). [FeFe] hydrogenase genetic diversity provides insight into molecular adaptation in a saline microbial mat community. *Appl. Environ. Microbiol.* 75(13), 4620-4623.

11. Kashefi K., Tor J. M., Holmes D. E., Gaw Van Praagh C. V., Reysenbach A. L., Lovley D. R. (2002). *Geoglobus ahangari* gen. nov., sp. nov., a novel hyperthermophilic archaeon capable of oxidizing organic acids and growing autotrophically on hydrogen with Fe(III) serving as the sole electron acceptor. *Int. J. Syst. Evol. Microbiol.* 52(Pt 3), 719-728.

12. Klatt C. G., Wood J. M., Rusch D. B., Bateson M. M., Hamamura N., Heidelberg J. F., Grossman A. R., Bhaya D., Cohan F. M., Kuhl M., Bryant D. A., Ward D. M. (2011). Community ecology of hot spring cyanobacterial mats: predominant populations and their functional potential. *ISME J.* 5(8), 1262-1278.

13. Ross K. A., Feazel L. M., Robertson C. E., Fathepure B. Z., Wright K. E., Turk-Macleod R. M., Chan M. M., Held N. L., Spear J. R., Pace N. R. (2012). Phototrophic phylotypes dominate mesothermal microbial mats associated with hot springs in Yellowstone National Park. *Microb. Ecol.* 64(1), 162-170.

14. Felsenstein J. (1981). Evolutionary trees from DNA sequences: a maximum likelihood approach. *J. Mol. Evol.* 17(6), 368-376.

15. Larkin M. A., Blackshields G., Brown N. P., Chenna R., McGettigan P. A., McWilliam H., Valentin F., Wallace I. M., Wilm A., Lopez R., Thompson J. D., Gibson T. J., Higgins D. G. (2007). Clustal W and Clustal X version 2.0. *Bioinformatics* 23(21), 2947-2948.

16. Tamura K., Peterson D., Peterson N., Stecher G., Nei M., Kumar S. (2011). MEGA5: molecular evolutionary genetics analysis using maximum likelihood, evolutionary distance, and maximum parsimony methods. *Mol. Biol. Evol.* 28(10), 2731-2739.

17. Edgar R. C. (2004). MUSCLE: multiple sequence alignment with high accuracy and high throughput. *Nucleic Acids Res.* 32(5), 1792-1797.

18. Saitou N., Nei M. (1987). The neighbor-joining method: a new method for reconstructing phylogenetic trees. *Mol. Biol. Evol.* 4(4), 406-425.

19. Nei M., Kumar S. (2000). Molecular Evolution and Phylogenetics. Oxford University Press, New York.

20. Sambrook J., Russell D. (2001). Molecular Cloning: A Laboratory Manual. Cold Spring Harbor Laboratory Press.

SUPPLEMENTAL CHAPTER 2

Genome Annotation and Investigation of H_2 Metabolism of *Nannochloropsis oceanica* CCMP1779[1]

[1] This chapter is adapted and contains data from Vieler A., Wu G., Tsai C.-H., Bullard B., Cornish A. J., Harvey C., Reca I.-B., Thornburg C., Achawanantakun R., Buehl C. J., Campbell M. S., Cavalier D., Childs K. L., Clark T. J., Deshpande R., Erickson E., Ferguson A. A., Handee W., Kong Q., Li X., Liu B., Lundback S., Peng C., Roston R. L., Sanjaya, Simpson J. P., TerBush A., Warakanont J., Zäuner S., Farre E. M., Hegg E. L., Jiang N., Kuo M.-H., Lu Y., Niyogi K. K., Ohlrogge J., Osteryoung K. W., Shachar-Hill Y., Sears B. B., Sun Y., Takahashi H., Yandell M., Shiu S.-H., Benning C. (2012). Genome, functional gene annotation, and nuclear transformation of the heterokont oleaginous alga Nannochloropsis oceanica CCMP1779. PLoS Genet. **Published Online Ahead of Print**.

INTRODUCTION

In recent years, microalgae have shown promise as sustainable sources of renewable fuels, such as biodiesel, bioethanol, and biohydrogen (1, 2, 3, 4). To date, only a handful of microalgal species have been characterized with appropriate depth for biofuel production, especially at the industrial scale (5). Among well-characterized microalgae, few of these organisms have properties ideal for the targeted engineering required in high-volume fuel production (e.g., efficient knock-out/knock-down of specific genes and optimized expression of transgenes).

Nannochloropsis oceanica CCMP1779 is a photoautotrophic microalga that lies within the class Eustigmatophyceae of Heterokontophyta (6). Organisms in the genus *Nannochloropsis* have been targeted for biofuel production due to lipid accumulation under stress and ease of both gene deletion and expression (7, 8, 9). In addition, *N. oceanica* CCMP1779 can utilize sugars from the media, is sensitive to a range of antibiotics, and can integrate selectable markers into its nuclear genome (10).

Recently, the *N. oceanica* CCMP1779 genome was sequenced by Drs. Christoph Benning and Shin-Han Shiu (Michigan State University) in an effort to characterize the putative metabolism further and investigate unique properties at the genomic level (10). The genome was found to be 28.7 Mb in size and a total of 11,973 genes were identified from RNA sequencing data. Although automated annotation programs were utilized, specific sets of genes were manually annotated to improve identification accuracy and to incorporate the genes into a larger biochemical perspective (10).

Due to our knowledge in respiration, intracellular electron transfer, and hydrogen metabolism, our research group manually annotated genes in the *N. oceanica* CCMP1779 genome. We identified several suites of genes required for the described processes and, based on the presence of hydrogenase genes, we also tested for and measured H_2 production from *N. oceanica* CCMP1779.

METHODS

Manual Annotation of Genome—Nucleic acid sequences for genes of interest were collected from the *Chlamydomonas reinhardtii*, *Ectocarpus siliculosus*, and *Phytophthora infestans* genomes using the NCBI database (http://www.ncbi.nlm.nih.gov/). Homologous sequences in the *N. oceanica* CCMP1779 genome were discovered using TBLASTX with a threshold of <0.001 and ≥55% query coverage. Putative genes were confirmed by BLASTX against the NCBI database, again with a threshold of <0.001 and ≥55% query coverage required for confirmation. The genes were then assigned a putative identity, and the designation and location in the genome noted.

Growth Conditions—*N. oceanica* CCMP1779 strains were grown in 250 mL Erlenmeyer flasks containing 50 mL F/2 Nutrient Media (17 g/L Tropic Marine Salt enriched with f/2 nutrients, trace elements and vitamins (11), and 40 mM bicarbonate and 15 mM Tris buffer [pH 7.6] to prevent carbon limitation). The cultures were shaken at 105 rpm in continuous light (85 µmol photons m^{-2} s^{-1}) and kept at 22 °C (12).

Hydrogen Evolution Assay—To acclimate the cells to anaerobiosis, a culture was concentrated to 75 µg chlorophyll/mL in 2 mL of anaerobic F/2 nutrient media, sealed in a 10 mL serum vial (Wheaton), and shaken at 100 rpm at 22°C in the dark for 4 h. "Aerobic" cells were treated similarly, except that they were exposed to the atmosphere during the 4 h acclimation. To measure H_2 evolution, 0.1 mL of aerobically- or anaerobically-acclimated cells were added to 1.9 mL of H_2 evolution assay buffer (F/2

nutrient media, 100 mM sodium dithionite, 10 mM methyl viologen) in a 10 mL serum vial and incubated with shaking in the dark. H_2 accumulation was measured over time by injecting 10 µL of gas from the headspace into a TRACE GC Ultra Gas Chromatograph (Thermo Scientific) using a 100 µL syringe. Absolute amounts of H_2 were determined by comparison of the peak area against a standard curve.

RESULTS

Manual Gene Annotation—The *N. oceanica* CCMP1779 nuclear genome was sequenced by 454 and Illumina technology. RNA-sequencing was utilized to generate a *de novo* assembly of 65,321 gene transcripts, of which 35,756 were then mapped onto the final genome assembly (10).

Oxidative phosphorylation is ubiquitous among aerobically-grown organisms. Genes were found within the *N. oceanica* CCMP1779 genome encoding key subunits of NADH dehydrogenase (complex I), succinate dehydrogenase (complex II), cytochrome *c* reductase (complex III), cytochrome *c* oxidase (complex IV), and F_oF_1 ATP synthase (complex V), as well as numerous accessory proteins required for the proper folding and the insertion of cofactors into these protein complexes (Table S2.1). In addition, three genes were identified with strong homology to alternative oxidases, proteins which allow for the reduction of O_2 without the concomitant synthesis of ATP (13). Together, the presence of these genes strongly implies a typical respiratory electron transfer chain used to couple O_2 reduction to ATP synthesis.

Reactive oxygen species (ROS) are unavoidable byproducts of cellular respiration and photosynthesis and are able to cause cellular damage (14). Examining the genome, 4 genes with homology to ROS scavenging genes which are typically targeted to both the cytosol and mitochondria were identified (Table S2.1), suggesting a functional ROS scavenging system is present in *N. oceanica* CCMP1779.

Table S2.1. **Manually annotated genes in *N. oceanica* CCMP1779**

Description	Name	ID
HYDROGEN		
[FeFe]-hydrogenase	HydA1	CCMP1779_5967-mRNA-1
[FeFe]-hydrogenase maturation factor	HydG	augustus_masked-nanno_856-abinit-gene-0.2-mRNA-1*
[FeFe]-hydrogenase maturation factor	HydF	CCMP1779_5970-mRNA-1
[FeFe]-hydrogenase maturation factor	HydE	augustus_masked-nanno_856-abinit-gene-0.1-mRNA-1*
RESPIRATION		
succinate dehydrogenase flavoprotein	Sdh2	CCMP1779_10056-mRNA-1
succinate dehydrogenase subunit A	Sdh1	CCMP1779_10769-mRNA-1
succinate dehydrogenase cytochrome *b* subunit	Sdh3	CCMP1779_9122-mRNA-1
succinate dehydrogenase subunit D	Sdh4	CCMP1779_3454-mRNA-1
heme O synthase	Cox10	augustus_masked-nanno1077-abinit-gene-1.10-mRNA-1*
cytochrome *c* oxidase subunit 6b	Cox12	augustus_masked-nanno604-abinit-gene-0.21-mRNA-1*
heme A synthase	Cox15	CCMP1779_925-mRNA-1
cytochrome *c* oxidase assembly	Cox11	CCMP1779_4145-mRNA-1
cytochrome *c* oxidase assembly	Shy1	CCMP1779_22-mRNA-1
cytochrome *c* oxidase assembly	Sco1	CCMP1779_6751-mRNA-1
cytochrome *c* oxidase Cu chaperone	Cox17	CCMP1779_9640-mRNA-1
cytochrome *c* oxidase chaperone	Ssc1	CCMP1779_8242-mRNA-1
cytochrome *c* oxidase subunit II	Cox2	CUFF.84573.1+**
cytochrome *c* oxidase subunit I	Cox1	CUFF.95393.1+**
cytochrome *c* oxidase subunit III	Cox3	CUFF.95359.1+**
alternative oxidase 2	Aox2	augustus_masked-nanno2785-abinit-gene-0.2-mRNA-1*

*This gene model is from augustus or snap gene annotation and was found superior to the final maker annotation after manual examination.

Transcript from expressed sequence tag data, as no final gene model was available.

Table S2.1 (cont'd)

Description	Name	ID
alternative oxidase 2	Aox1	augustus_masked-nanno1051 -abinit-gene-0.9-mRNA-1*
alternative oxidase 3	Aox3	augustus_masked-nanno3659 -abinit-gene-0.0-mRNA-1*
NADH:ubiquinone oxidoreductase subunit 10	Nuo10	CCMP1779_10235-mRNA-1
NADH:ubiquinone oxidoreductase subunit 17	Nuo17	CCMP1779_11866-mRNA-1
NADH:ubiquinone oxidoreductase subunit E	NuoE	CCMP1779_9179-mRNA-1
NADH:ubiquinone oxidoreductase subunit F	NuoF	CCMP1779_4574-mRNA-1
NADH:ubiquinone oxidoreductase subunit I	NuoI	CCMP1779_7640-mRNA-1
NADH:ubiquinone oxidoreductase subunit 9	Nuo9	CCMP1779_6889-mRNA-1
NADH:ubiquinone oxidoreductase 18 kDa subunit	Nuo18k	CCMP1779_11055-mRNA-1
NADH:ubiquinone oxidoreductase subunit B14	NuoB14	CCMP1779_6453-mRNA-1
NADH:ubiquinone oxidoreductase subunit B16	NuoB16	CCMP1779_9016-mRNA-1
NADH:ubiquinone oxidoreductase subunit B18	NuoB18	CCMP1779_211-mRNA-1
NADH:ubiquinone oxidoreductase subunit 11	Nuo11	augustus_masked-nanno_224-abinit-gene-1.7-mRNA-1
NADH:ubiquinone oxidoreductase subunit S4	NuoS4	CCMP1779_2896-mRNA-1
NADH:ubiquinone oxidoreductase subunit S5	NuoS5	CCMP1779_10934-mRNA-1
NADH dehydrogenase subunit 4	Nuo4	CUFF.95343.1+**

*This gene model is from augustus or snap gene annotation and was found superior to the final maker annotation after manual examination.

**Transcript from expressed sequence tag data, as no final gene model was available.

Table S2.1 (cont'd)

Description	Name	ID
NADH dehydrogenase subunit 5	Nuo5	CUFF.84531.1+**
NADH dehydrogenase subunit 1	Nuo1	CUFF.95403.1+**
NADH:ubiquinone oxidoreductase subunit 7	Nuo7	CUFF.95391.1+**
NADH dehydrogenase subunit 2	Nuo2	CUFF.95399.1+**
NADH dehydrogenase subunit 3	Nuo3	CUFF.95361.1+**
F1F0 ATP synthase gamma subunit	Atp3	augustus_masked-nanno_5442-abinit-gene0.2-mRNA-1*
ATP synthase O subunit	Atp5C1	CCMP1779_10955-mRNA-1
F_0F_1 ATP synthase subunit alpha	Atp5A1	CCMP1779_10718-mRNA-1
F-type H-ATPase beta subunit	Atp5B	CCMP1779_9984-mRNA-1
ATP synthase F_0 subunit 6	Atp6	CUFF.95401.1+**
ATP synthase mitochondrial F_1 assembly factor 2	AtpAF2	CCMP1779_10134-mRNA-1
ATP synthase mitochondrial F_1 assembly factor 2	AtpAF1	CCMP1779_6914-mRNA-1
ubiquinol cytochrome *c* cytochrome c_1	CytC1	CCMP1779_9301-mRNA-1
ubiquinol cytochrome *c* reductase 14kDa subunit	Qcr7	CCMP1779_9021-mRNA-1
cytochrome *b*-c_1 complex subunit Rieske	RipI	CCMP1779_8327-mRNA-1
cytochrome *b*-c_1 complex 50 kDa subunit 1	Qcr1	CCMP1779_635-mRNA-1
ubiquinol-cytochrome *c* reductase iron-sulfur subunit 1	Risp1	CCMP1779_8327-mRNA-1
cytochrome *b*	CytB	CUFF.95357.1+**

*This gene model is from augustus or snap gene annotation and was found superior to the final maker annotation after manual examination.

**Transcript from expressed sequence tag data, as no final gene model was available.

Table S2.1 (cont'd)

Description	Name	ID
FERREDOXINS		
[2Fe2S] ferredoxin	Fdx	CCMP1779_688-mRNA-1
ferredoxin, adrenodoxin-like protein	Mfdx1	CCMP1779_10471-mRNA-1
putative chloroplast ferredoxin 1	Fdx1	CCMP1779_7894-mRNA-1
putative chloroplast ferredoxin 6	Fdx6	CCMP1779_3054-mRNA-1
Rieske [2Fe2S] ferredoxin 1	rFDX1	CCMP1779_7488-mRNA-1
Rieske [2Fe2S] ferredoxin 2	rFDX2	CCMP1779_4457-mRNA-1
putative chloroplast ferredoxin 2	Fdx2	CCMP1779_2103-mRNA-1
putative chloroplast ferredoxin 5	Fdx5	CCMP1779_7881-mRNA-1
putative chloroplast ferredoxin 3	Fdx3	CCMP1779_1904-mRNA-1
IRON SULFUL CLUSTER BIOSYNTHESIS		
iron-sulfur cluster assembly protein	IscA1	CCMP1779_11149-mRNA-1
iron-sulfur cluster assembly protein	IscA2	CCMP1779_6581-mRNA-1
iron-sulfur cluster biosynthesis protein	Nar1	CCMP1779_4004-mRNA-1
ROS SCAVENGING		
glutathione synthase	GST	CCMP1779_1871-mRNA-1
microsomal glutathione S-transferase	mGST	CCMP1779_9028-mRNA-1
superoxide dismutase	SOD	CCMP1779_6610-mRNA-1
glutathione peroxidase	GPX	CCMP1779_10092-mRNA-1

A number of photosynthetic microorganisms are capable of H_2 production or oxidation under anaerobic conditions. The genome was investigated for genes involved in H_2 metabolism and a single gene was identified to encode a putative [FeFe]-hydrogenase (*hydA*), as well as three genes coding for proteins required in hydrogenase maturation (*hydE*, *hydF*, *hydG*) (Table S2.1). In addition, these genes are organized in an operon-like gene cluster (Figure S2.1) similar to the cluster seen in *V. carteri* (Chapter 4).

Ferredoxins are proteins integral to much of intracellular electron transport within an organism, especially for delivery of electrons during photosynthesis, H_2 production, and $NAD(P)^+$ reduction (15, 16, 17). Ferredoxins require iron-sulfur clusters for electron transfer activity, and iron-sulfur cluster biosynthesis enzymes are responsible for the assembly and insertion of these clusters in a variety of proteins (18). Within the genome, 9 genes were found with homology to ferredoxins, while 3 putative iron-sulfur cluster biosynthesis genes were identified (Table S2.1).

Figure S2.1. **[FeFe]-hydrogenase operon-like gene cluster in *N. oceanica* CCMP1779.** Four genes with sequence similarity to *hydA*, *hydE*, *hydF*, and *hydG* are arranged within 14 kb of one another.

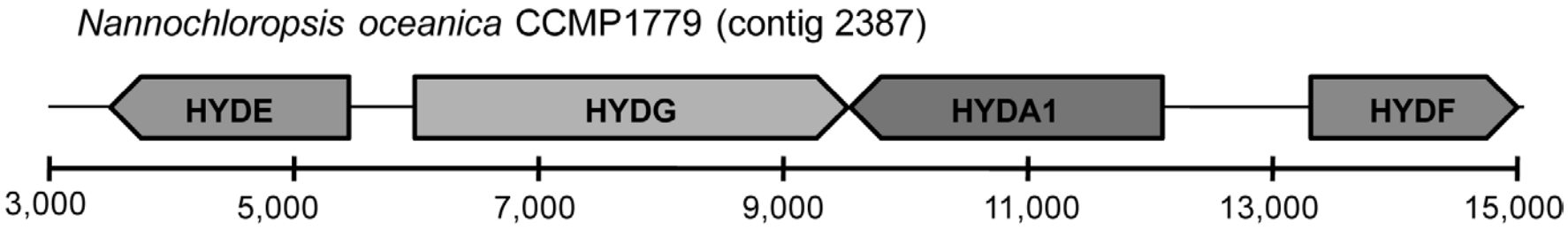

Hydrogen Evolution—To test for its ability to evolve H_2, anaerobically-acclimated *N. oceanica* CCMP1779 was incubated both with and without an abiotic electron donor system and accumulation of H_2 in the headspace was then measured. Headspace H_2 accumulation could be observed when an electron donor was supplied, whereas unsupplemented culture did not accumulate H_2 even 48 s after the beginning of the assay (Figure S2.2). Cells that were acclimated to aerobiosis produced considerably less H_2 in the headspace over the same 48 hour-time period, which was likely due to an initial lack of proteins required for H_2 production until anaerobiosis was established during the assay.

Figure S2.2. **H_2 evolution rate of aerobically- or anaerobically-acclimated *N. oceanica* CCMP1779 cells.** Following a 4 h acclimation period, cells were incubated in F/2 media with and without an abiotic electron donor system. H_2 accumulation in the headspace was measured at 3, 24, and 48 h time-points and normalized on a per mg chlorophyll basis. Error bars denote S.D. (n ≥ 3).

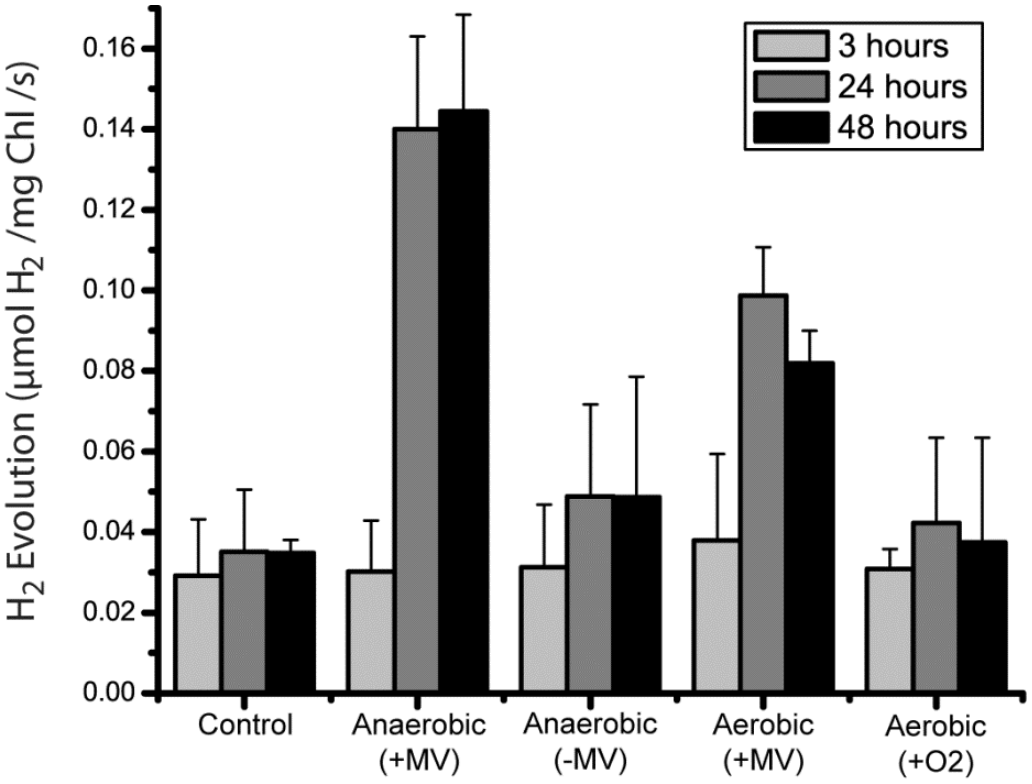

DISCUSSION

N. oceanica CCMP1779 is a photoautotrophic microalga that accumulates high concentrations of lipids and fatty acids under a variety of conditions. To gain a greater perspective on this organism, the genome was sequenced as a joint venture between Drs. Benning and Shiu at Michigan State University. Manual annotation of the genome was accomplished through collaboration with various experts in metabolic processes, including the Hegg lab.

Before the results detailed in this report were published, a manuscript detailing the genomic sequence of *Nannochloropsis gaditana* CCMP526, a close relative of *N. oceanica* CCMP1779, was released (19). When compared, the two genomes were found to be similar in sequence length, although the *N. oceanica* CCMP1779 genome contained more predicted protein models. The *N. oceanica* CCMP1779 genome was also found to contain ~6,500 species-specific genes in comparison to *N. gaditana* CCMP526, using defined orthologous group comparisons (10). These results further affirm the differences that exist between the species and provide a rationale for studying both organisms.

To help confirm gene identity during annotation, putative genes were BLASTed against the NCBI database. The majority of highly homologous genes were encoded by the genomes of two organisms, *Ectocarpus siliculosus* and *Phytophthora infestans*. Both of these organisms are classified as heterokonts. *E. siliculosus* is a filamentous brown alga that forms large colonies on water plants, whereas *P. infestans* is an infectious oocyte that colonizes potatoes and tomatoes. Because of the similarity

between the noted homologs, genes from these organisms were utilized to target genes in *N. oceanica* CCMP1779 that were difficult to identify using typical gene sequences.

The *N. oceanica* CCMP1779 genome was examined for genes important in cellular respiration, ROS scavenging, H_2 metabolism, electron transport, and iron-sulfur cluster biosynthesis. A majority of the genes examined were positively identified, implying that these metabolic processes and pathways are present in the organism. Several mitochondrial genes required for respiration (*Cox1*, *Cox2* and others) could only be identified from expressed transcripts, as the mitochondrial genome was not sequenced. This suggests that the annotation process may have missed genes encoded by the chloroplast and mitochondrial genomes that were not expressed under the tested conditions.

The *N. oceanica* CCMP1779 hydrogenase genes are within a 12 kb sequence of the genome, organized in an operon-like gene cluster (Figure S2.1), similar to a cluster observed in the *V. carteri* genome. Unlike *V. carteri*, the maturation proteins *hydE* and *hydF* have not fused to form the atypical green algal *HYDEF* (green algal nomenclature). Also unlike green algae, *hydA* more closely resembles bacterial [FeFe]-hydrogenase genes, containing F-domains that ligate additional iron-sulfur clusters. When BLASTed against the NCBI database, three of the genes had the most similarity to green algal sequences, in contrast to *hydF*, which shared the most sequence identity to a gene in *Nagleria gruberi*, a non-photosynthetic amoeba. Together, these results may suggest that this hydrogenase cluster in *N. oceanica* CCMP1179 shares ancestry with the genes acquired in green algae and that comparatively less genetic drift has occurred since this acquisition. Finally, measured rates of H_2 production and the

presence of putative [FeFe]-hydrogenase genes within the genome suggest that *N. oceanica* CCMP1779 has functional hydrogenase genes that allow for H_2 metabolism under anaerobiosis.

In summary, the *N. oceanica* CCMP1779 genome contains putative genes involved in a variety of basic metabolic processes. Of particular interest were several genes required for H_2 production. A putative role for these genes in H_2 metabolism was strengthened by experiments performed under dark anaerobiosis with an electron donor system, as *N. oceanica* CCMP1779 generated appreciable amounts of H_2 under these conditions.

REFERENCES

REFERENCES

1. Georgianna D. R., Mayfield S. P. (2012). Exploiting diversity and synthetic biology for the production of algal biofuels. *Nature* 488(7411), 329-335.

2. Jones C. S., Mayfield S. P. (2012). Algae biofuels: versatility for the future of bioenergy. *Curr. Opin. Biotechnol.* 23(3), 346-351.

3. Branyikova I., Marsalkova B., Doucha J., Branyik T., Bisova K., Zachleder V., Vitova M. (2011). Microalgae--novel highly efficient starch producers. *Biotechnol. Bioeng.* 108(4), 766-776.

4. Beer L. L., Boyd E. S., Peters J. W., Posewitz M. C. (2009). Engineering algae for biohydrogen and biofuel production. *Curr. Opin. Biotechnol.* 20(3), 264-271.

5. Menetrez M. Y. (2012). An overview of algae biofuel production and potential environmental impact. *Environ. Sci. Technol.* 46(13), 7073-7085.

6. Suda S., Atsumi M., Miyashita H. (2002). Taxonomic characterization of a marine Nannochloropsis species, *N. oceanica* sp. nov. (Eustigmatophyceae). *Phycologia* 41(3), 273-279.

7. Quinn J. C., Yates T., Douglas N., Weyer K., Butler J., Bradley T. H., Lammers P. J. (2012). *Nannochloropsis* production metrics in a scalable outdoor photobioreactor for commercial applications. *Bioresour. Technol.* 117, 164-171.

8. Pal D., Khozin-Goldberg I., Cohen Z., Boussiba S. (2011). The effect of light, salinity, and nitrogen availability on lipid production by *Nannochloropsis* sp. *Appl. Microbiol. Biotechnol.* 90(4), 1429-1441.

9. Weeks D. P. (2011). Homologous recombination in *Nannochloropsis*: a powerful tool in an industrially relevant alga. *Proc. Natl. Acad. Sci. U.S.A.* 108(52), 20859-20860.

10. Vieler A., Wu G., Tsai C.-H., Bullard B., Cornish A. J., Harvey C., Reca I.-B., Thornburg C., Achawanantakun R., Buehl C. J., Campbell M. S., Cavalier D., Childs K. L., Clark T. J., Deshpande R., Erickson E., Ferguson A. A., Handee W., Kong Q., Li X., Liu B., Lundback S., Peng C., Roston R. L., Sanjaya, Simpson J. P., TerBush A., Warakanont J., Zäuner S., Farre E. M., Hegg E. L., Jiang N., Kuo M.-H., Lu Y., Niyogi K. K., Ohlrogge J., Osteryoung K. W., Shachar-Hill Y., Sears B. B., Sun Y., Takahashi H., Yandell M., Shiu S.-H., Benning C. (2012). Genome, functional gene annotation, and nuclear transformation of the heterokont oleaginous alga *Nannochloropsis oceanica* CCMP1779. *PLoS Genet.* Accepted.

11. Andersen R. A., Berges J. A., Harrison P. J., Watanabe M. M. (2005). Appendix A, p. 429-538, Algal culturing techniques, 1 ed. Elsevier Academic Press, San Diego.

12. Vieler A., Brubaker S. B., Vick B., Benning C. (2012). A lipid droplet protein of *Nannochloropsis* with functions partially analogous to plant oleosins. *Plant Physiol.* 158(4), 1562-1569.

13. Gupta K. J., Zabalza A., van Dongen J. T. (2009). Regulation of respiration when the oxygen availability changes. *Physiol. Plant* 137(4), 383-391.

14. Apel K., Hirt H. (2004). Reactive oxygen species: metabolism, oxidative stress, and signal transduction. *Annu. Rev. Plant Biol.* 55, 373-399.

15. Arakaki A. K., Ceccarelli E. A., Carrillo N. (1997). Plant-type ferredoxin-$NADP^+$ reductases: a basal structural framework and a multiplicity of functions. *FASEB J.* 11(2), 133-140.

16. Fukuyama K. (2004). Structure and function of plant-type ferredoxins. *Photosynth. Res.* 81(3), 289-301.

17. Yacoby I., Pochekailov S., Toporik H., Ghirardi M. L., King P. W., Zhang S. (2011). Photosynthetic electron partitioning between [FeFe]-hydrogenase and ferredoxin:$NADP^+$-oxidoreductase (FNR) enzymes in vitro. *Proc. Natl. Acad. Sci. U.S.A.* 108(23), 9396-9401.

18. Bandyopadhyay S., Chandramouli K., Johnson M. K. (2008). Iron-sulfur cluster biosynthesis. *Biochem. Soc. Trans.* 36(Pt 6), 1112-1119.

19. Radakovits R., Jinkerson R. E., Fuerstenberg S. I., Tae H., Settlage R. E., Boore J. L., Posewitz M. C. (2012). Draft genome sequence and genetic transformation of the oleaginous alga *Nannochloropis gaditana*. *Nat. Commun.* 3, 686.